

Thermodynamic based prediction Model for NO_x and CO Emissions from a Gasoline Direct Injection Engine

Dissertation

zur

Erlangung des akademischen Grades

Doktor-Ingenieur (Dr.-Ing.)

der Fakultät für Maschinenbau und Schiffstechnik

der Universität Rostock

vorgelegt von

M. Eng. Nataporn Chindaprasert, geb. am 22. November 1977 in Bangkok

aus Bangkok

Rostock, 12. August 2007

Gutachter: 1. Prof. Dr.-Ing. habil. Egon Hassel
2. Prof. Dr.-Ing. Horst Harndorf
3. Dr.-Ing. Olaf Magnor

Tag der Verteidigung: 25 Juni 2008

This work is dedicated to my parents,
Winyoo and Sopit Chindaprasert.

Preface

This thesis is based on my research performed at the Institute for Technical Thermodynamics, University of Rostock in Germany between 2003 and 2007. The work was funded by IAV GmbH, Germany.

I would like to thank my advisor, Prof. Dr.-Ing. habil. E. Hassel, who gave me a great educational chance in Germany, for the initiation of the project and the supports throughout the course of my work.

I wish to thank Dr.-Ing. J. Nocke for the good advice, supports and many helps. Thanks are further due to project colleagues for their most valuable supports and discussions. I would like to thank all of the colleagues in both LTT and LKV for the supports, friendship and my great working time in Rostock. Special thanks go to Ms. D. Nautsch and Ms. S. Worbs for supports and helps in documents and business contacts.

Further more, I would like to thank Prof. Dr.-Ing. H. Harndorf and Dr.-Ing. O. Magnor for being the thesis committee.

Nataporn Chindaprasert
Rostock, 12 August 2007

Abstract

Concerns about global warming are increasing the demands on modern engines, which are expected to operate at high efficiency and at the same time have minimal emissions. Emission models to predict the level of engine exhaust gas have become increasingly important in the automobile industry. In this dissertation a two-zone thermodynamic model is implemented and combined with extended Zeldovich mechanism to calculate nitrogen oxides (NO_x) from a gasoline direct injection engine. Furthermore, a chemical kinetic model has been combined with the two-zone model to predict the carbon monoxide (CO) emission. For a better CO prediction over the operating range of lambda from lean to rich mixture, a new zone has been introduced into the combustion chamber. This enables the integration of the thermal boundary layer into the emissions model. The mixture in this zone is oxidized at a lower temperature than the majority of the gas in the combustion chamber and therefore modelled with a reduced chemical mechanism.

The model was validated by experimental data from a gasoline direct injection 1.6 litre engine. The results show satisfactory NO_x- and CO-predictions.

Keywords: nitrogen oxides, carbon monoxide, chemical kinetics, direct injection, exhaust emissions, gasoline, spark ignition engines, thermodynamics.

Zusammenfassung

Die aktuellen Erkenntnisse und Diskussionen zur globalen Erwärmung haben die Anforderungen an modernen Motoren verschärft, von denen neben hohen Wirkungsgraden auch niedrige Abgasemissionen erwartet werden. In diesem Kontext werden Emissionsmodelle zur Vorhersage des motorischen Abgasverhaltens in der Automobilindustrie weiter an Bedeutung gewinnen. Im Rahmen dieser Arbeit wird ein 2-Zonen-Modell entwickelt und mit einem auf dem erweiterten Zeldovich-Mechanismus basierten reaktionskinetischen Modell kombiniert, um die NO_x-Emissionen direkteinspritzender Otto-Motoren zu berechnen. Ein zusätzliches reaktionskinetisches Modell erlaubt aufbauend auf dem 2-Zonen-Modell die Vorhersage der CO-Emissionen. Um über den gesamten, von unter- bis überstöchiometrischer Verbrennung reichenden Betriebsbereich des Motors eine bessere CO-Vorhersage zu ermöglichen, wurde eine zusätzliche Zone im Brennraum eingeführt. Das erlaubt die gesonderte Berücksichtigung der thermischen Grenzschicht im Emissionsmodell. Das Gemisch in dieser Zone oxidiert bei geringeren Temperaturen als der Hauptteil der Gasmasse im Brennraum und wird daher mit einem reduzierten Kinetik-Ansatz modelliert.

Zur Validierung des Modells werden experimentelle Daten eines 1,6 Liter Otto-Motors mit Benzin-Direkteinspritzung herangezogen. Die mit Hilfe des Emissionsmodell vorhergesagten Abgasemissionen zeigen eine zufrieden stellende Übereinstimmungen mit den experimentell bestimmten Werten.

Schlüsselworte/Stichworte: Stickoxide - NO_x, Kohlenmonoxid - CO, Reaktionskinetik, Benzin-Direkteinspritzung BDE, Abgasemissionen, Benzin, Otto-Motoren, Thermodynamik, 2-Zonen-Modell

Contents

Nomenclature

VIII

1. Introduction.....	1
1.1 Emissions from Vehicles.....	1
1.2 Emissions Model.....	2
1.3 Purpose and Content of the Work.....	3
2. Literature Review.....	4
2.1 NO Model.....	4
2.2 CO Model.....	6
2.3 Post Oxidation of UHC.....	7
2.4 Summary.....	9
3. The NO and CO Model.....	10
3.1 One-zone Thermodynamic Model.....	10
3.2 Two-zone Thermodynamic Model.....	13
3.2.1 Unburned Gas Composition.....	19
3.2.2 Burned Gas Composition.....	21
3.2.3 Thermodynamic Properties of Gases.....	23
3.3 NO Model.....	24
3.4 CO Model.....	26
3.4.1 Gasoline and its Oxidation.....	26
3.4.2 CO Formation.....	28
3.4.3 Chemical Kinetics.....	30
3.4.4 CO Kinetic Model.....	32
3.4.4.1 Implementation of CO Kinetic Model	33
3.4.4.2 Chemical Kinetic Mechanisms.....	34
4. Engine Measurement.....	38
4.1 Engine Specification.....	38
4.2 Exhaust Gas Analyzer.....	39

4.3 Operating Condition.....	40
5. NO Model Result.....	42
5.1 NO Model Result.....	42
5.2 Improved NO Model.....	44
5.3 Sensitivity Analysis of NO Model.....	52
5.4 Summary.....	58
6. CO Model Result.....	60
6.1 CO Model Result Using Chemical Equilibrium.....	60
6.2 CO Model Result Using Kinetic Model.....	62
6.3 Improved CO Model.....	67
6.3.1 Thermal Boundary Layer Thickness.....	69
6.3.2 Thermal Boundary Layer Temperature.....	73
6.3.3 New Chemical Model for Thermal Boundary Layer.....	74
6.4 Improved CO Model Result.....	76
6.4.1 Thermal Boundary Layer Temperature Result.....	76
6.4.2 Thermal Boundary Layer Thickness Result.....	77
6.4.3 CO Result Using Oxidation Factor.....	79
6.4.4 CO Result Using Chemical Kinetic Model.....	82
6.5 Sensitivity Analysis of CO Model.....	94
6.6 Summary.....	97
7. Summary and Conclusion.....	99
7.1 Summary.....	99
7.2 Conclusion.....	100
References.....	101
Appendix A.....	108
Erklärung.....	110
Curriculum Vitae.....	111
List of Publications.....	112

Nomenclature

Symbols

a_s :[/]	Stoichiometric molar air/fuel ratio
A :[m ²]	Area across which heat transfer occurs
C :[/]	Constant
C_n :[kJ/kgK]	Specific heat
C_p :[kJ/kgK]	Specific heat capacity at constant pressure
C_v :[kJ/kgK]	Specific heat capacity at constant volume
f : [/]	Residual mass fraction
G :[kJ]	Gibbs function (free energy)
h_q :[kW/m ² K]	Heat transfer coefficient
H :[kJ]	Enthalpy
H_u :[kJ/kg]	Lower heating value
k :[cm, mol, s]	Rate coefficient of the reaction
K :[/]	Equilibrium constant
m :[kg]	Mass of the system
M :[kg/kmol]	Molecular weight
N_{total} :[/]	Total number of moles
n : [/]	Polytropic index of the process
p :[Pa]	Pressure of the charge
q :[W/m ²]	Heat flux (in section 6.3.1)
Q :[kJ]	Total heat
R :[kJkg/K]	Gas constant
R :[/]	Hydrocarbon radical
S :[kJ/K]	Entropy
t :[sec]	Time
T :[K]	Temperature
T_w :[K]	Assumed temperature of the surroundings of the charge
u :[m/s]	Stream velocity in x direction

U :[kJ]	Internal energy
v :[/]	Coefficient
v :[m/s]	Stream velocity in y direction
V :[m ³]	Volume
x :[m]	Coordinate length in x direction
x :[/]	Mass fraction
y :[m]	Coordinate length in y direction
y :[/]	Mole fraction
δ :[m]	Boundary layer thickness
α :[W/m ² K]	Convection heat transfer coefficient
λ :[W/mK]	Conduction heat transfer coefficient
λ , lambda :[/]	Relative air/fuel ratio
κ :[/]	Ratio of specific heat capacities (C_p/C_v)
ρ :[kg/m ³]	Density
ϑ :[K]	Temperature
τ :[N/ m ²]	Sheer stress

Subscripts

b	Indicates properties or value for the burned products zone
$conv$	Convective
e	Equilibrium
f	Fuel
g	Gas
ht	Heat transfer
i	Indicates the i^{th} data point
i	Inlet
le	Leakage
m	mean
th	thermal boundary layer
u	Indicates properties or value for the unburned reactants zone
r	residual
s	stream

w	wall
z	Indicates values applicable to the zone under consideration

Notations

[]	Concentration, moles/ m^3
-----	------------------------------------

Abbreviations

a.u.	Arbitrary unit
BC, ABC, BBC	Bottom-center crank position, after BC, before BC
CFD	Computational fluid dynamics
CO	Carbon monoxide
ECU	Engine control unit
EGR	Exhaust gas recirculation
EZM	Extended Zeldovich mechanism
HC	Hydrocarbons
MFB	Mass fraction burned
NO	Nitric oxide
NO _x	Nitrogen oxides
RPM	Revolution per minute
SEZM	Super extended Zeldovich mechanism
SI	Spark ignition
UHC	Unburned hydrocarbons
TC, ATC, BTC	Top-center crank position, after TC, before TC

1. Introduction

Motor vehicles have become one of the major sources of atmospheric pollutants worldwide. The legislative exhaust emission limits are continually tightened e.g. the European emission standards 5 (Euro 5) planned for the year 2009, to ensure constantly decreasing exhaust limit values. With present technology the new emissions standards are difficult to meet. This in turn compels car manufactures to develop advanced technologies to obtain better engine performance with lower emissions. The main emissions from gasoline engines are nitrogen (N_2), water (H_2O), carbon dioxide (CO_2), hydrocarbons (HC), nitrogen oxides (NO_x) and carbon monoxide (CO). Modern gasoline engines are operated with nearly stoichiometric air/fuel ratio to minimize NO_x , but they produce higher CO than with the lean mixture.

1.1 Emissions from Vehicles

The emissions produced by a vehicle fall into three basic categories: tailpipe emissions, evaporative emissions and life cycle emissions. Tailpipe emissions are the main emissions which come direct from engine through the exhaust pipe and the catalytic converter. Evaporative emissions are produced from the evaporation of fuel for example, gas tank venting and refuelling losses. Life cycle emissions are produced in activities associated with the manufacturing, maintenance, and the disposal of automobiles.

Crucial emissions from engine are CO, NO_x , HC and CO_2 . NO_x are mainly formed inside engine's combustion chamber due to the reactions of atomic oxygen (O), atomic nitrogen (N), atomic hydrogen (H), nitrogen (N_2), oxygen (O_2) and hydroxyl (OH), described by extended-Zeldovich mechanism, under high temperature and pressure during the combustion process. NO_x emissions contribute to both smog and acid rain. CO, a toxic gas, is a product from incomplete combustion. It reduces the blood's ability to carry oxygen and is dangerous to human which may lead to heart disease. HC is unburned or partially burned fuel, and is a major contributor to urban smog, as well as to be toxic. They can cause liver damage and even cancer.

CO₂ is a product from combustion of hydrocarbons and plentiful in the atmosphere which is non-toxic gas. However carbon dioxide is considered as a significant greenhouse gas, increasing its level in the atmosphere will further contribute to global warming. The European emission standards for gasoline passenger car have been set up to control emissions from vehicles and are summarized in table 1.1.

Table 1.1: Acceptable limits for exhaust emissions of new vehicles sold in EU member states in gram per kilometer.

Unit in g/km	Euro 1	Euro 2	Euro 3	Euro 4	Euro 5
Start from	1992	1996	2000	2005	2009
CO	3.16	2.20	2.30	1.0	1.0
HC	-	-	0.20	0.10	0.075
HC+NO _x	1.13	0.5	(0.35)	(0.18)	(0.135)
NO _x	-	-	0.15	0.08	0.06

1.2 Emissions Model

Many models have been designed to improve internal combustion engine performance and achieve better understanding of the engines. The type of internal combustion engine models to predict emissions within the engine cylinder can be considered into two main types, zero-dimensional model and dimensional model. Zero-dimensional models which based on energy and mass conservation within the engine cycle are called zero-dimensional thermodynamic model. One- and multi- dimensional thermodynamic models are based on mass, momentum, energy conservation and detail analysis of fluid flow within the cylinder. The fluid flow is typically determined by computational fluid dynamics (CFD). The most complex model is three dimensional comprehensive computational fluid dynamics (3D-CFD) with thermodynamics which is normally used for prediction of fluid flow and flame propagation. Using the 3D-CFD with thermodynamics for combustion in cylinder problem is extremely complicated for many reasons. It is hard to define the exact boundary conditions and to properly solve the physical

processes at low computational requirements. Zero-dimensional thermodynamic modelling is simpler, faster and its results are also very satisfactory.

1.3 Purpose and Content of the Work

Gasoline direct injection technology had been introduced to improve the engine efficiency and reduce exhaust gas emissions. However, the reduction of emissions from the engine alone cannot make a car reach the emission standards then catalytic converter is needed to treat exhaust gas. It is necessary to know the emissions from the engine that go into the catalytic converter. The purpose of the work was to predict NO_x and CO emissions from combustion chamber of a gasoline direct injection engine with low calculation time. The model should be compact, fast and supposed to be embedded in the engine control unit. The cylinder pressure-time data from the engine is used as the main input. The model should also be able to combine with combustion cycle simulation (incl. HC model). Results from the predictions of model can be used to reduce test rig time for engine map data creation and engine emissions.

A zero-dimensional two-zone thermodynamic model which is simple to use and gives good result is introduced. It divides the combustion chamber into two zones; burned zone and unburned zone. The gas mixture in each zone is undergoing a different series of continuously varying polytropic processes. Combustion products are calculated by using chemical equilibrium. NO model based on extended-Zeldovich mechanism is integrated in the two-zone model. For better results, NO model is improved with multi- burned zone calculation. CO model is a kinetic model with complex reaction mechanism. It is found that at lean mixture conditions or lambda more than 1, the model results are lower than measurements. The two-zone model is improved to three-zone model to overcome this problem. This new zone based on thermal boundary layer theory. Oxidation in this zone is low temperature combustion which using chemical kinetic to solve the problem. The validation of the model is done by comparing with measured values.

2. Literature Review

NO_x mechanism is usually well known as extended-Zeldovich mechanism and slightly improved and widely used. On the other hand, there are limited literatures dealing with CO formation in spark ignition engines. Due to post oxidation of unburned hydrocarbon (UHC) in cylinder and exhaust gas pipe have effects on CO concentration, literatures of UHC oxidation are reviewed.

2.1 NO Model

Nitric oxide is the predominant oxide of nitrogen produced in a spark ignition engine. NO_x are formed throughout the combustion chamber during combustion and expansion process due to the oxidation of molecular nitrogen. Zeldovich [1] was first to suggest in 1946 the importance of reactions



Zeldovich or thermal mechanism is well known and generally understood. In year 1970 Lavoie, Heywood and Keck [2] suggested the reaction



can also contribute to NO production, especially in near stoichiometric and rich fuel-air mixture. Equation (2.1) to (2.3) is called extended-Zeldovich mechanism (EZM). Heywood [3, 4] showed results of two-zone thermodynamic model and EZM in a S.I. engine. The results show that the EZM, a rate controlled model, delivers better results compared to equilibrium concentration during the combustion and expansion process. The EZM is often and widely used with different rates which have been summarized in [5].

Raine, Stone and Gould [5] used multi-zone thermodynamic model, which was the extension of two-zone model, and EZM to predict NO. The results showed that the use of multiple burned gas zones was likely to be important for the accurate prediction of NO emissions. It was also shown that 5 or 10 burned zones were likely to be efficient for most purposes.

Rublewski and Heywood [6] studied sensitivity of NO concentration in a 2.0 liter spark ignition engine. A thermodynamic based cycle simulation which used a thermal boundary layer, either a fully mixed or layered adiabatic core, and a crevice combustion inefficiency routine had been used to explore the sensitivity of NO concentration predictions to critical physical modeling assumptions. It was reconfirmed that the simple three equations of EZM were capable of predicting NO concentration. Sensitivity analysis showed NO predictions to be relatively insensitive to changes in overall heat loss and size of crevice volume used on model combustion inefficiency. It was also confirmed that residual fraction and burn rate were the most critical engine variables for making NO predictions.

Miller et al. at Ford motor company [7, 8] made a new reaction scheme for NO_x production which was incorporated into a steady state quasi-dimensional engine combustion simulation. The reaction kinetics includes 67 reactions and 13 chemical species, and assumed equilibrium concentration for all other chemical species. The General Engine SIMulation (GESIM) was used to model the engine cycle. The new reaction scheme was called a super-extended Zeldovich mechanism (SEZM). The rate constant of equation (2.1) had been adjusted by the factor of 0.7-1.3 for calibration. The results showed the prediction of NO at lambda 1 to 1.4. It can be summarized that SEZM results were much better than EZM when fuel-air mixtures were leaner, but no different result was found when lambda was equal 1.

Stone, Wyszynski and Raine [9] showed the prediction of NO emissions from a stratified charge spark ignition engine. Thermodynamic model with multiple burned gas zones had been extended to permit the different burned gas zones to have different mixture strengths. The NO formation was predicted in each burned gas zone using the EZM. The model had been used for study of stratified charge spark ignition engine combustion, in order to investigate the influence of overall equivalence ratio and degree of stratification on the NO emissions and the engine brake specific fuel consumption.

2.2 CO Model

The CO emissions from internal combustion engines depend primarily on fuel-air ratio. The CO formed in the combustion process is oxidized to CO₂ at a rate which is relatively slow compared to the CO formation rate. The principal CO oxidation reaction in hydrocarbon flames presented by Bowman [10] was



Newhall [11] showed theoretical analysis of chemical kinetics of the internal combustion engine expansion process. The chemical kinetic model result had been compared with chemical equilibrium result and experiment data. It was found that CO concentration predicted by chemical kinetic model was close to equilibrium concentration, only at the later stages of the expansion stroke the predicted CO concentration departed from equilibrium concentration. Newhall obtained a good match with experiment data from kinetic model, the kinetically controlled aspects of the CO emissions had thus been confirmed [3].

Arsie et al. [12] presented a thermodynamic model for simulation of performance and emissions in a spark ignition engine. The main model was based on the classical two-zone approach. For a proper evaluation of temperature gradient in the burned gas region, a multi-zone model was then derived from the two-zone calculation. Emissions of HC, CO and NO_x were then predicted by three sub-models. The CO model used reaction (equation 2.4) from Bowman [10] and added reaction



into CO sub-model. The CO concentrations predicted by the model were lower than the measured values, but higher than the equilibrium concentrations at the exhaust conditions. It was also concluded that the number of zones, boundary thickness and air/fuel ratio strongly influenced on the CO formation process.

Raggi and Sodr  [13] developed a numerical model to calculate the kinetic formation rate of CO in spark ignition engines. The CO sub-model that uses the same method as Arsie et al. [12], was added to a computer program that simulated the cycle of spark ignition engines to calculate CO

concentration in the exhaust gas. The model was validated through experimental data from a single-cylinder research engine. Comparing the model result with the calculated equilibrium concentration of carbon monoxide confirmed that for a better understanding of the measured exhaust values, especially in the rich mixture region. This pollutant should be modeled according to the theory of kinetic formation. However, the model results were under estimated in lean mixture region.

A 1D fluid dynamic model for predicting pollutants from a spark ignition engine was presented by D'Errico et al. [14]. The combustion process took into account the burned gas stratification and turbulence levels inside the combustion chamber. The pollutant formation process used integration of the thermodynamic module with the CHEMKIN code. The super-extended Zeldovich mechanism (SEZM) was introduced for better NO_x prediction, while separate modules were used to calculate CO and HC. The CO model was based on only two equations used by Arsie et al. [12]. The CO model predictions were compared with predicted equilibrium concentrations and measured exhaust levels. Furthermore, it was concluded that the spark advance had no effect on CO emission.

A more complex model was introduced by D'Errico et al. [15]. The CFD code OpenFOAM and the thermo-fluid dynamic code GASDYN were applied and enhanced. The multi-dimensional combustion model had then been adapted to the quasi-dimensional approach, embedded into a one-dimensional fluid-dynamic code for the simulation of the whole engine system. The combustion model assumed that fuel oxidation to H₂O and CO₂ occurred in two global steps. First, fuel was quickly burned to produce H₂O and CO. Second, CO was slowly oxidized to give CO₂. Predictions of CO with rich fuel-air mixture were accurate, but not for lean mixture since the model results were extremely lower than measured values. The explanation was that in the lean mixture the prompt CO concentration was much higher than the CO equilibrium concentration. This fact had not been taken into account by the model.

2.3 Post Oxidation of UHC

Sources of HC emission from inside the engine cylinder are crevices (in the combustion chamber walls), oil layers (adsorption of the fuel into oil films on the cylinder wall), deposits (build up

over extended mileage and absorb some of the liquid fuel injected), liquid fuel in the cylinder (in port or direct injection engines), flame quenching (quenching of the flame on the walls) and incomplete combustion. These UHC may then oxidize in the combustion chamber [16, 17, 18, 19], exhaust system [20, 21, 22, 23] and catalytic converter. Under lean the mixture condition, incomplete UHC oxidation can result in an increase in CO level [3, 24, 25]. This causes the additional source of CO in the lean mixture. This can be the answer of why most CO models predict CO values too low compared to measured values when λ is close to or more than one. In this part, oxidation of UHC in engines and the relation of UHC & CO will be described.

UHC levels in the exhaust of a S.I. engine under normal operating condition are typically in the range of 1000 to 3000 ppm C_1 . This corresponds to approximate 1 to 2.5 % of fuel flow in the engine [3]. Cheng et al. [26] provided an overview of S.I. engine HC emission mechanism. Using the assumption that 1.8% of fuel for engine-out HC as a starting point, the calculation showed that 9% of the total fuel which came into the cylinder was not burnt and had escaped during the normal combustion process into HC mechanisms. After 0.7% of total fuel loss by blowby, one third of 8.3% was oxidized in cylinder and another one third of 8.3% was still in the cylinder as residual gas, the last one third (2.8% of total fuel) went out of the cylinder as exhaust gases. One third of these 2.8% (exhaust gas) was further oxidized in exhaust system. This result showed 3.7% of total fuel that went through HC mechanisms was oxidized to CO_2 or CO and this value has never been accounted for in any CO models.

Mendillo and Heywood [20] presented an experimental study to determine the fraction of UHC emissions which were oxidized in the exhaust port and runner of a S.I. engine. The technique used was injection of CO_2 quench gas into the exhaust port, at the various planes along the port centerline, to cool down the exhaust gas and freeze the HC oxidation reaction. Results showed that the reduction in HC level due to oxidation in the exhaust port, which was more important than oxidation in the exhaust gas runner, ranges between 2-37%. This particular reduction depended on substantial changes in the gas temperature, port residence time, or oxygen concentration. Stoichiometric engine operation yielded the highest percent UHC oxidized in the exhaust port due to highest exhaust temperature and adequate oxygen in the exhaust gas. Rich operation ($\lambda < 1$) gave the lowest value of UHC conversion due to lower exhaust gas temperature and low oxygen concentration.

The extension work of Mendillo and Heywood [20] was published by Drobot et al. [21]. The purpose was to study the variation of fuel types to both the evolution and the extent of oxidation of HC species in the exhaust port/runner system of a S.I. engine at light load condition. Results showed no significant fuel dependence on the percentage of the cylinder-out HC oxidized in exhaust port/runner system, which ranges from 35% to 45%. Most of the reduction of HC species changed throughout the exhaust system occurred in the port, although the distribution of HC species changed throughout the port/runner system. For gasoline, the reduction of HC occurred in the exhaust port at 41% and 1% in exhaust runner.

2.4 Summary

Extended Zeldovich mechanism which is widely used with multi-zone thermodynamic model to calculate NO_x is simpler and faster compared to complex super extended Zeldovich mechanism. Moreover, both mechanisms predicted nearly the same results when lambda was one which is the usual operating condition for modern engines. Hence, it is unnecessary to use SEZM for this work. CO models were introduced both in thermodynamics model and CFD model. It was agreed that CO formation should be considered to be kinetically controlled. It was found that using complex CFD model had no advantage over thermodynamic model to predict CO from S.I. engines. Nonetheless, the most CO model predicted too low CO value in the stoichiometric and lean mixture condition. The oxidation of UHC in combustion chamber and exhaust system can be an important answer for this problem. The UHC can be oxidized up to 33% in combustion chamber and 45% of the rest in exhaust port and runner. However, there is no published data showing the amount of CO occurred due to UHC post flame oxidation, the information show only amount of UHC that oxidized. Another reason that should be considered is the oxidation of UHC which starts at temperature 600°C but the oxidation of CO starts at temperature 700°C [3]. This means, if the temperature is lower than 700°C, HC will be oxidized to CO but not CO₂. The oxidation of UHC cannot be neglected when predicting CO.

3. The NO and CO Model

This chapter describes the overview of this dissertation. It starts with one-zone thermodynamic model, and then two-zone thermodynamic model. NO model based on extended Zeldovich mechanism is implemented in two-zone model. CO kinetic model received the burned gas temperature data from the two-zone model and then predicted the CO emission. It should be noted that this work only calculates NO and CO emissions until the end of expansion process which is the end of the work focus.

3.1 One-zone Thermodynamic Model

The one-zone thermodynamic model is the simplest way to study combustion characteristics in combustion chambers. The system boundary is combustion chamber walls. There are mass, heat and work transfer over the system boundary. Gas mixture is assumed to be homogeneous of concentration, temperature and pressure.

Principal equations of one-zone model are the conservation of mass, energy or first law of thermodynamics. Figure (3.1) shows details of one-zone thermodynamics model. The equation of mass balance result is as follows:

$$\frac{dm}{dt} = \frac{dm_i}{dt} - \frac{dm_e}{dt} - \frac{dm_{le}}{dt} + \frac{dm_f}{dt} \quad (3.1)$$

The change of system mass per unit time results mainly from the mass flowing during the gas exchange, inlet gas m_i , exhaust gas m_e , leakage m_{le} and fuel injected m_f . Leakage or blowby which is lost through the piston rings to the crankcase can usually be neglected. The energy conservation of the system consists of the following terms.

$$\frac{dU}{dt} = \frac{d(m_b H_u)}{dt} - \frac{dQ}{dt} - p \frac{dV}{dt} + h_i \frac{dm_i}{dt} - h_e \frac{dm_e}{dt} - h_{le} \frac{dm_{le}}{dt} + h_f \frac{dm_f}{dt} \quad (3.2)$$

where H_u is the lower heating value or net heating value of the gas mixture, m_b is the mass of burned gas mixture.

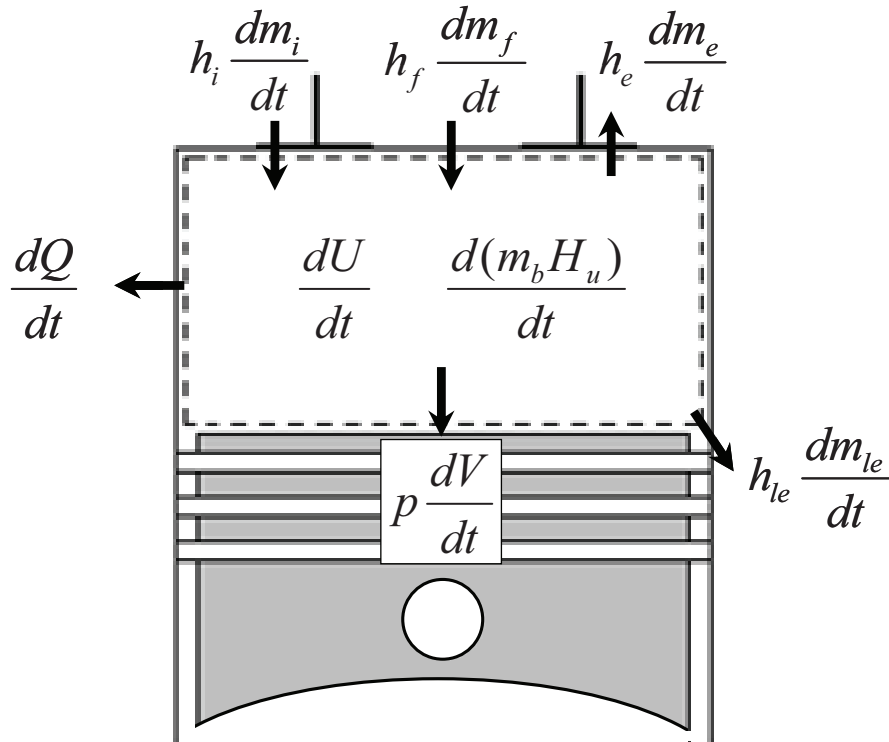


Figure 3.1: Schematic of one-zone model

Equation (3.2) expresses the change of the internal energy. Terms of the left side are heat from chemical energy released by combustion, heat-transfer over the combustion chamber walls and work done by the system. The in and out energy through mass flow over the system boundary is still considered, with the respective enthalpy of the mass. The fuel evaporation enthalpy is relative small compare to the others and can be neglected.

The one-zone model can be modelled by close intake valve until the exhaust valve is opened as a closed system, in both from a homogeneous mixture is proceeded from a homogeneous pressure and temperature distribution. Due to these assumptions, equations are simplified substantially and led on the following set of equations.

$$\frac{dm}{dt} = 0 \quad (3.3)$$

$$\frac{dU}{dt} = \frac{d(m_b H_u)}{dt} - \frac{dQ}{dt} - p \frac{dV}{dt} \quad (3.4)$$

The convective heat-transfer rate to the combustion chamber walls can be calculated from the relation

$$\frac{dQ}{dt} = A\alpha(T - T_w) \quad (3.5)$$

where A is the chamber surface area, T is the mean gas temperature, T_w is the mean wall temperature, and α is the heat-transfer coefficient. α can be estimated by engine heat-transfer correlations of Nusselt, Hohenberg, Eichelberg or Woschni. Hohenberg's correlation has been used because the fuel consumption predicted by one-zone model is best matched with measured value.

The specific internal energy u , the only remaining parameter of equation (3.4), can be computed by using a real gas relation based on Zacharias [27]. The specific internal energy is described in a function of pressure, specific volume and air content.

$$u = f(p, v, R) \quad (3.6)$$

$$\dot{u} = \frac{\partial u}{\partial p} \dot{p} + \frac{\partial u}{\partial v} \dot{v} + \frac{\partial u}{\partial R} \dot{R} \quad (3.7)$$

The real gas relation based on Zacharias is indicated in detail by equation (3.8), which is an empirical approximation function that was set up for stoichiometric air-fuel mixture.

$$u = R[C_1^u p^2 v^2 + C_2^u p v - C_3^u - C_4^u (p - p_0) - C_5^u (p - p_0) p v] \\ + (1 - R)[C_6^u p^2 v^2 + C_7^u p v - C_8^u + C_9^u (p - p_0) - C_{10}^u (p - p_0) p v] \quad (3.8)$$

Table A1 in appendix A shows constants C_i^u . In equation (3.8), R represents the ratio of air mass to the total gas mass and the reference pressure p_0 ($p_0 = 5$ MPa). The cylinder pressure p is defined in [Pa] while the specific volume v in [m^3/kg]. The temperature in the combustion chamber is computed using the real gas approach by Zacharias as follows:

$$T = R[C_1^T + C_2^T p v + C_3^T p^2 v^2 + (p - p_0)(C_4^T - C_5^T p v + C_6^T p^2 v^2)] \\ + (1 - R)[C_7^T + C_8^T p v + C_9^T p^2 v^2 + (p - p_0)(C_{10}^T - C_{11}^T p v + C_{12}^T p^2 v^2)] \quad (3.9)$$

where T is in [K]. R , ν and p_0 have the same unit as equation (3.8). Constants C_i^T are defined in table A2 in appendix A. Figure 3.2 shows measured pressure and temperature calculated by one-zone model.

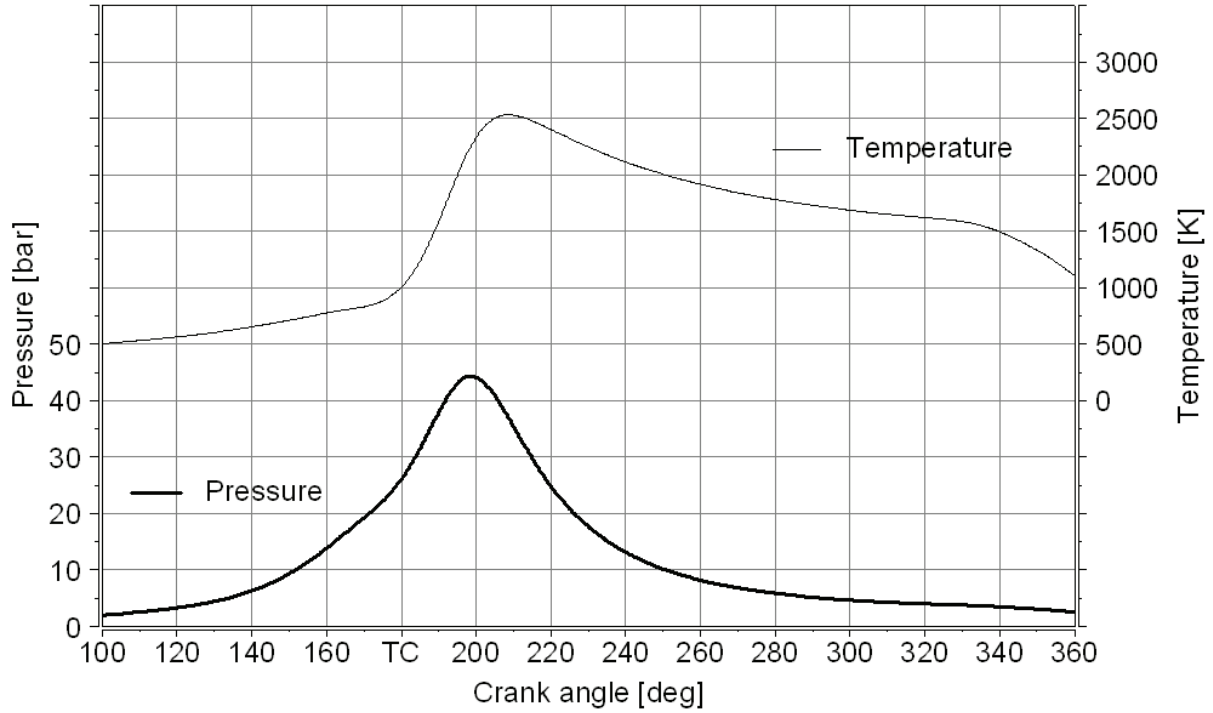


Figure 3.2: Measured pressure and calculated temperature by one-zone model of the gas in the cylinder at an ignition timing of 20 deg BTC and engine rotational speed of 3500 rpm, load 102 Nm, lambda 1.

3.2 Two-zone Thermodynamic Model

The model approach described by Al-Himyary and Karim [28] has been selected for the thermodynamic calculation due to its simple formulation, good computational efficiency and low calculation time. The main function of this model is to use pressure-time data from the experiment as input to calculate the gas temperature in the cylinder and send the result to the emission model.

The two-zone model uses the first law of thermodynamics, mass balance and also chemical equilibrium. The system is considered to be closed and therefore mass loss due to blowby will be ignored. The temperature of the charge is calculated by using the gross polytropic index n , which can be calculated from the observed instantaneous cylinder pressure and the corresponding cylinder volume, as follows:

$$n = -(dp / dV) \cdot (V / p) \quad (3.10)$$

where dp and dV represent the change in the cylinder pressure and volume across a small interval time. Figure (3.3) shows the overall polytropic index of the cylinder charge as derived from the pressure and volume record by equation (3.10). The temperature of the charge can be calculated from the polytropic process relation, as follows:

$$(p_i / p_{i+1})^{n-1} = (T_i / T_{i+1})^n \quad (3.11)$$

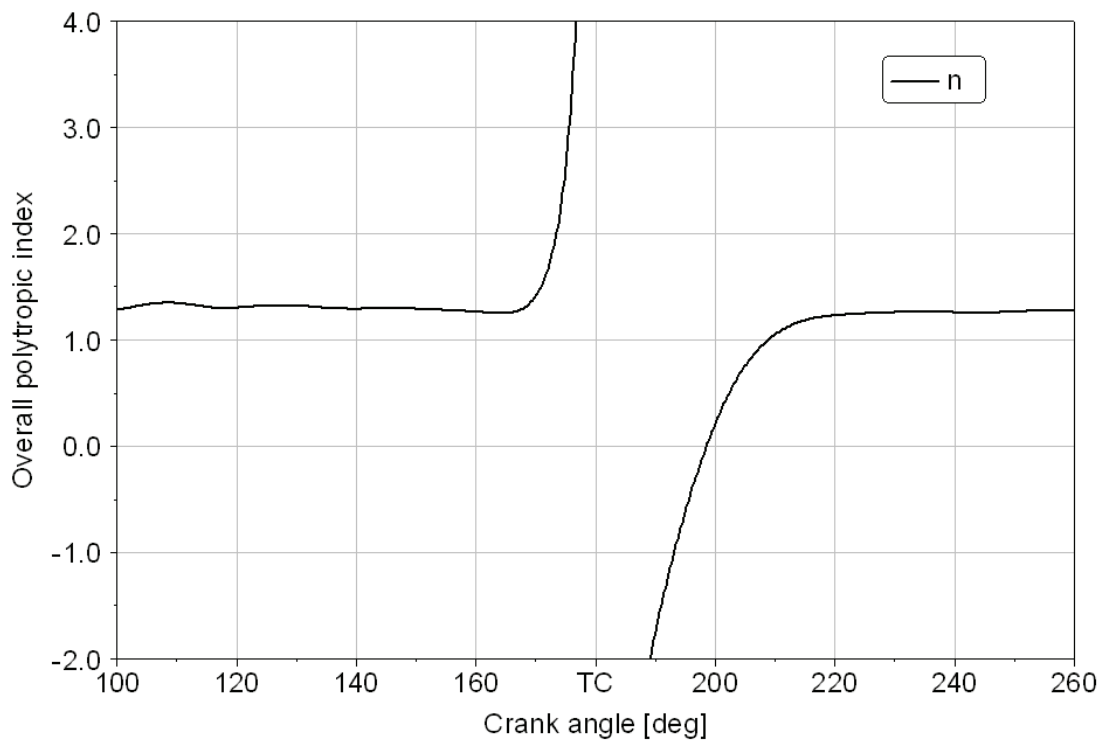


Figure 3.3: Overall polytropic index of the cylinder charge at an ignition timing of 20 deg BTC and rotational speed of 3500 rpm, load 102 Nm, lambda 1.

During the combustion process, the cylinder is divided into two zones, an unburned zone and a burned zone, shown in Figure (3.4). The same in-cylinder pressure data has been used for both

unburned and burned zone. Both zones are separated by an infinitely thin flame front and each zone represents a control volume. Heat transfer only takes place between zones and walls. The ideal gas equation can be written as

$$p \cdot V = m_u \cdot R_u \cdot T_u + m_b \cdot R_b \cdot T_b \quad (3.12)$$

To reduce the amount of variables, the total mass m , $m = m_u + m_b$, is used instead of m_u . Equation (3.12) can then be written as follows:

$$p \cdot V = m \cdot R_u \cdot T_u + m_b \cdot (R_b \cdot T_b - R_u \cdot T_u) \quad (3.13)$$

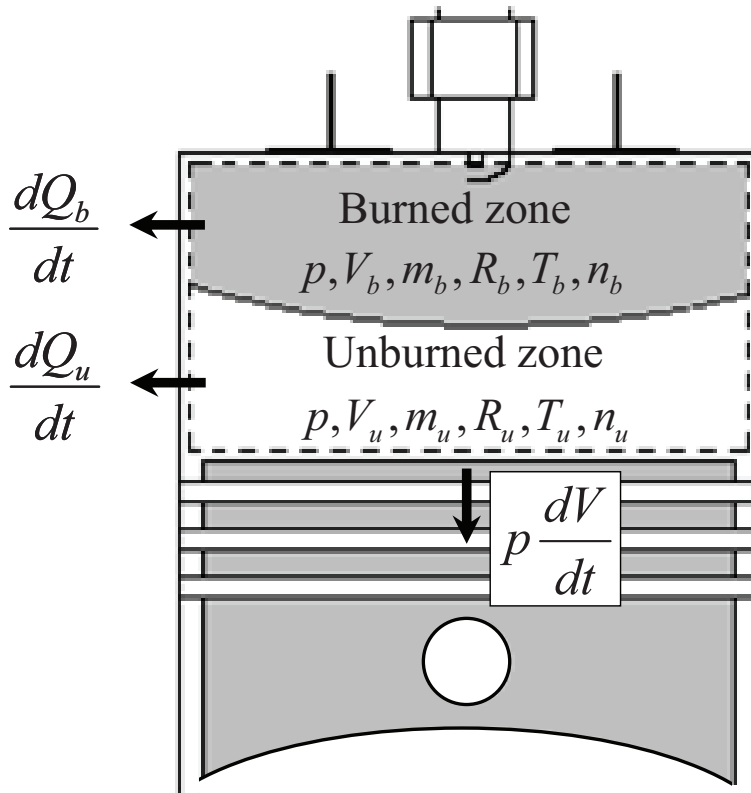


Figure 3.4: Schematic of two-zone model

For a very short interval, it can be assumed that each of the two control volumes is undergoing a polytropic process with a distinct variable polytropic index, which includes the work and heat exchanged between that control volume and its surroundings. For a constant mass closed system in equilibrium undergoing a reversible polytropic process, the following applies [28]

$$dQ = m \cdot C_n \cdot dT \quad (3.14)$$

where

$$C_n = C_v \cdot (\kappa - n) / (1 - n) \quad (3.15)$$

If the heat transfer is assumed to be exchanged through the boundary of the system, with an area A and instantaneous heat transfer coefficient h_q , then

$$dQ = h_q \cdot A \cdot (T - T_w) \cdot dt \quad (3.16)$$

Combination of equations (3.14) and (3.16) yields the following

$$h_q \cdot A \cdot (T - T_w) \cdot dt = m \cdot C_n \cdot dT \quad (3.17)$$

Across a small time interval dt , equation (3.17) can be integrated by the trapezoidal rule to produce equation (3.18).

$$[h_{q,i+1} \cdot A_{i+1} \cdot (T_{i+1} - T_{w,i+1})] / [h_{q,i} \cdot A_i \cdot (T_i - T_{w,i})] = m_{i+1} \cdot C_{n,i+1} / m_i \cdot C_{n,i} \quad (3.18)$$

For a very short interval, the wall temperature can be assumed to be constant and the sum of the change in the value of the heat transfer coefficient and the change in the external heat transfer area is small. It is further suggested that the change in m across the small time interval is also too small compared to the changes of T , κ and C_v . In this case, the following simplified equation applies

$$(T_{z,i+1} - T_w) / (T_{z,i} - T_w) = C_{n_z,i+1} / C_{n_z,i} \quad (3.19)$$

The relationship to link temperature of the zone T_z and its corresponding polytropic index n_z is derived from the assumption that each of the two zones is undergoing a series of a distinct polytropic processes; hence, for any of these zones across the interval of time for which equation (3.19) applies, the following is valid

$$(P_i / P_{i+1})^{n_z - 1} = (T_{z,i} / T_{z,i+1})^{n_z} \quad (3.20)$$

An iteration scheme was developed using equations (3.19) and (3.20) to calculate the temperature and polytropic index histories for each of the zone during the progress of the combustion process.

- 1.) A starting point is needed where the polytropic index, temperature and composition is known.
- 2.) Using equation (3.20) and the known polytropic index, as first approximation, a value for T_{i+1} can be found.
- 3.) Using T_{i+1} , $C_{v,i+1}$ can be calculated; and then equations (3.15) and (3.19) can be used to calculate the polytropic index at the end of the interval studied, n_{i+1} .
- 4.) An average value of the polytropic index over the time interval can now be found. Equation (3.20) can be used again to provide another estimate for T_{i+1} .
- 5.) Another value of $C_{v,i+1}$ can be found; and then equations (3.15) and (3.19) can be used again for a better estimate of n_{i+1} ...etc.

From the iteration scheme, it is needed to know the initial value of n_i , T_i , and $C_{v,i}$ of each zone. These variables are already known for the unburned zone, polytropic index is directed from the pressure and volume history at the ignition point, temperature is calculated using equation (3.11) and $C_{v,i}$ is calculated using temperature and known mixture composition. The iteration scheme of the unburned zone starts from the ignition point until the end of combustion where there is no unburned gas left.

For the burned zone, the polytropic index, temperature and concentration of the gas in the zone at the ignition point are unknown. The calculation is then started at the end of combustion process because at this point, there is only one type of gas left, the burned gas. With the help of one-zone thermodynamic model, the crank angle position and temperature can be found. The polytropic index of burned zone at this point can be found directly from the pressure and volume history. The iteration scheme of the burned zone is then started at the end of combustion and stopped at the ignition point. Figure (3.5) shows the overall polytropic index of the charge and figure (3.6) shows the temperature of gases in cylinder.

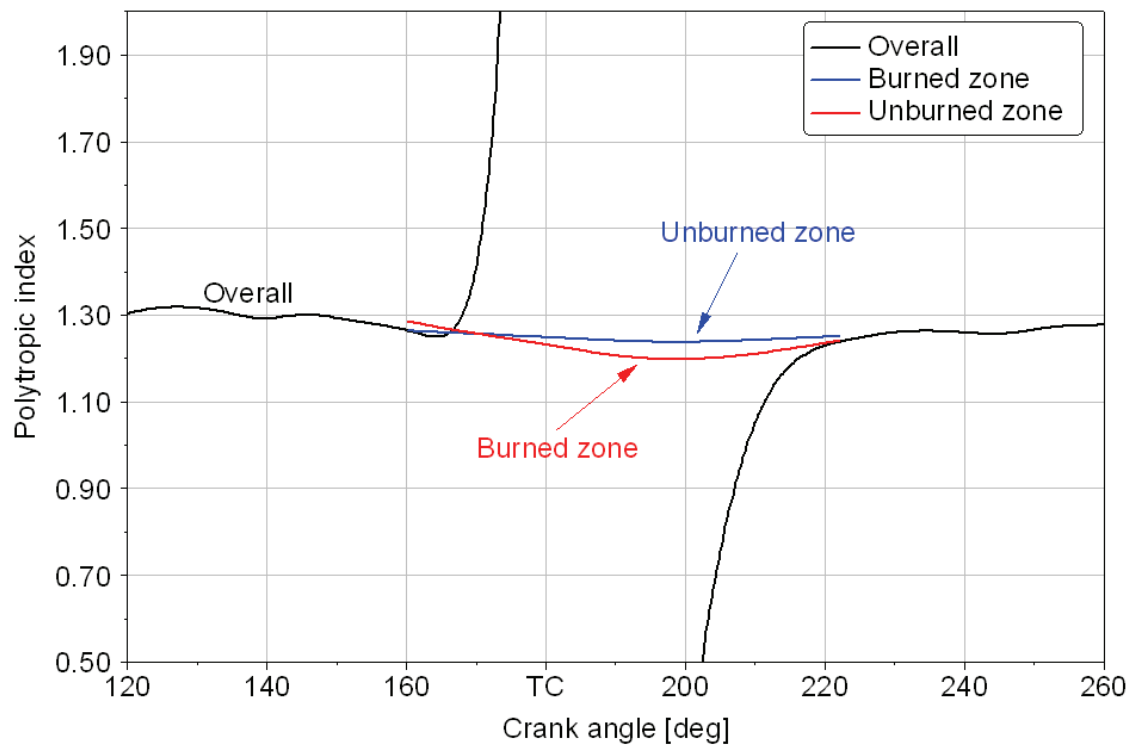


Figure 3.5: The overall polytropic index of the charge as compared to the indices of the burned and unburned zone at an ignition timing of 20 deg BTC and rotational speed of 3500 rpm, load 102 Nm, lambda 1.

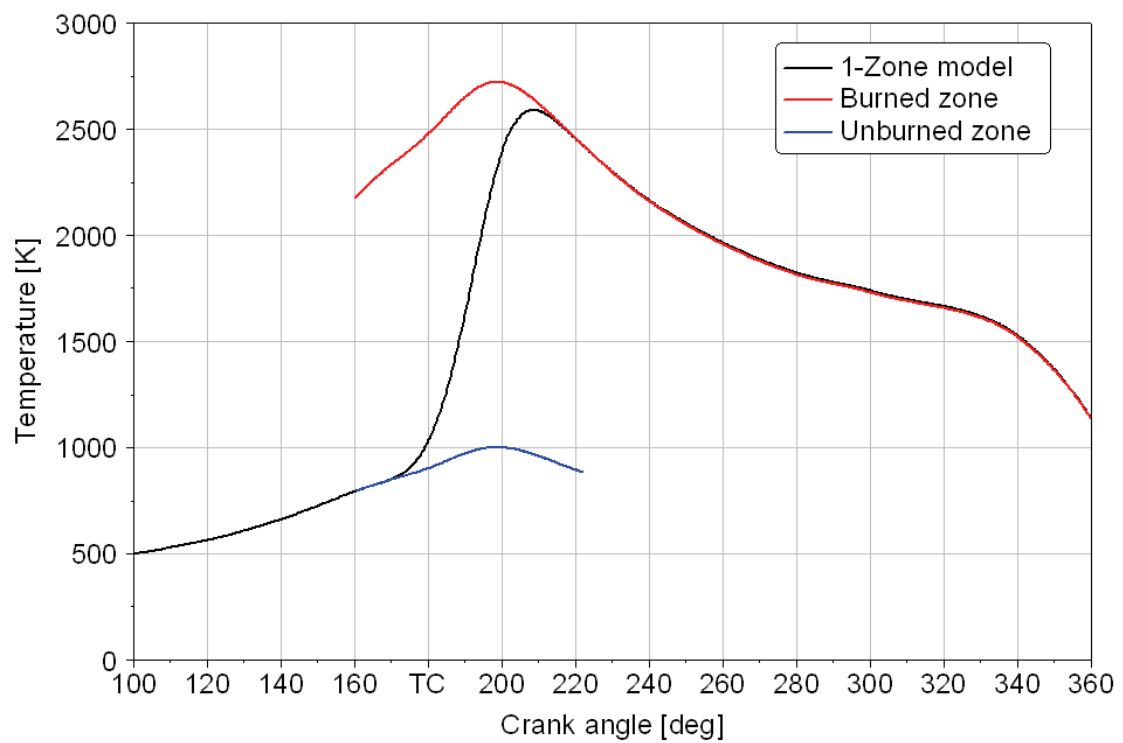
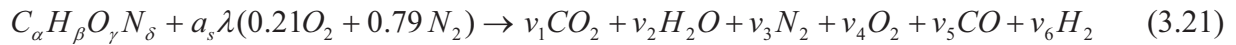


Figure 3.6: Temperature of the gas in the cylinder calculated by one-zone model and two-zone model at an ignition timing of 20 deg BTC and rotational speed of 3500 rpm, load 102 Nm, lambda 1.

3.2.1 Unburned Gas Composition

After the intake air, exhaust gas recirculation, residual gas and gasoline are mixed together, the concentration of gas mixture is unknown. This part describes how to find the mixture composition of the unburned gas in the cylinder. The general fuel chemical formula can be written as $C_\alpha H_\beta O_\gamma N_\delta$. At low temperatures ($T < 1000$ K, such as in the exhaust) and carbon to oxygen ratios less than one, the overall combustion reaction can be written as follows [24]:



where a_s is the stoichiometric molar air-fuel ratio, λ is the air-fuel equivalence ratio, and ν_i (i = 1, 2, 3, 4, 5, 6) are coefficients.

For reactant C/O ratio greater than one, there is solid carbon C(s) and several species occur which is not in the scope. Under the lean and stoichiometric mixture ($\lambda \geq 1$), CO and H₂ can be neglected. Under the rich mixture ($\lambda < 1$), O₂ can be neglected. Convenient approximations for lean and rich combustion are

$$\begin{aligned} \lambda > 1 & \quad \nu_5 = \nu_6 = 0 \\ \lambda \leq 1 & \quad \nu_4 = 0 \end{aligned}$$

For lean or stoichiometric cases, atom-balance equations are sufficient to determine the product composition (four equations and four unknowns using C, H, O N atom conserve). For the rich case, there are not enough equations to solve the problem. Equilibrium consideration between the product species CO₂, H₂O, CO and H₂ is assumed to determine the product composition. This reaction is termed the water-gas reaction



with the equilibrium constant providing the fifth equation

$$K(T) = \frac{\nu_2 \nu_5}{\nu_1 \nu_6} \quad (3.23)$$

The equilibrium constant $K(T)$ equation is a curve fit of the JANAF Table data for $400 < T < 3200$ K

$$\ln K(T) = 2.743 - 1.761 \times 10^3 \cdot T^{-1} - 1.611 \times 10^6 \cdot T^{-2} + 0.2803 \times 10^9 \cdot T^{-3} \quad (3.24)$$

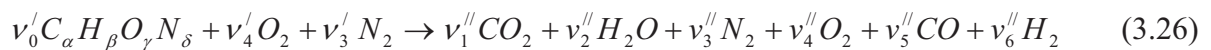
In the rich case, the parameter ν_5 is given by the solution of a quadratic equation

$$\nu_5 = \frac{-b + \sqrt{b^2 - 4ac}}{2a} \quad (3.25)$$

where $a = 1 - K$ $b = 0.5\beta + K\alpha - d(1 - K)$

$$c = -\alpha d K \quad d = 2a_s(1 - \lambda)$$

In modern reciprocating engines, there are exhaust gas recirculation (EGR) and therefore residual gas in the cylinder can be mixed with the fuel and air. It is necessary to determine the composition of such a mixture ahead of the flame. First, the EGR and the residual gas composition should be calculated. The sum of exhaust gas recirculation (external) and residual gas (internal) mass fraction f is a convenient parameter to deal with. By considering 6 species of gas, CO_2 , H_2O , N_2 , O_2 , CO and H_2 , the combustion equation can be written as



where ν'_i reactant coefficient, ν''_i product coefficient

The mass fraction of the gas mixture can be written as

$$x_i = (1 - f)x'_i + fx''_i \quad i = 0 \dots 6 \quad (3.27)$$

The mole fraction is given by

$$y_i = (1 - y_r)y'_i + y_r y''_i \quad (3.28)$$

where the EGR and residual gas mole fraction is

$$y_r = \left[1 + \frac{M''}{M'} \left(\frac{1}{f} - 1 \right) \right]^{-1} \quad (3.29)$$

M is defined as molecular weight of a mixture. With the composition of the fuel-air-residual gas mixture known, the thermodynamic properties of the mixture are found by application of gas mixture relations.

3.2.2 Burned Gas Composition

The combustion products of the burned zone are calculated based on chemical equilibrium which considers 10 gas species CO_2 , H_2O , N_2 , O_2 , CO , H_2 , O , H , OH and NO [24]. The equilibrium combustion products calculation used the temperature, pressure and composition of the reactant as input. The condition for equilibrium is usually stated in term of thermodynamic functions such as the minimization of the Gibbs or Helmholtz free energy or the maximization of entropy. Consider a system of chemically reacting substances undergoing a constant pressure and temperature process, in the absence of shear, gravity and another kind of work, the first law of thermodynamics can be written as [29]

$$\delta Q = dH \quad (3.30)$$

The second law of thermodynamics gives

$$\delta Q \leq T \cdot dS \quad (3.31)$$

Combination of equation (3.30) and (3.31) results as follows:

$$dH - T \cdot dS \leq 0 \quad (3.32)$$

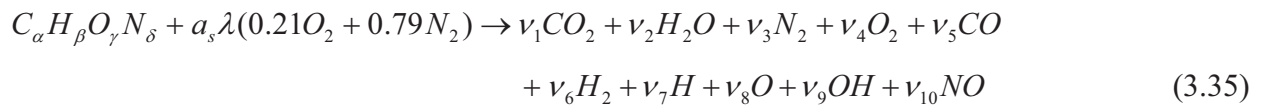
Since the considering process is a constant temperature process, this equation holds for the finite changes

$$\Delta H - T\Delta S = \Delta G \leq 0 \quad (3.33)$$

Thus, reactions can only occur (at constant pressure and temperature) if $G (= H - TS)$ for the products is less than G for the reactants. Hence, at equilibrium

$$(\Delta G)_{p,T} = 0 \quad (3.34)$$

When the temperature, pressure and composition of the gas mixture are given, the chemical equilibrium is available to find out the species of combustion product. The method developed by Olikara and Borman [30], which used six equilibrium constants, has been used to solve for the equilibrium composition. The combustion equation can be written as



Atom balancing yields the following equations

$$C \quad \alpha = (y_1 + y_5) N_{total} \quad (3.36)$$

$$H \quad \beta = (2y_2 + 2y_6 + y_7 + y_9) N_{total} \quad (3.37)$$

$$O \quad \gamma + 2a_s \lambda = (2y_1 + y_2 + 2y_4 + y_5 + y_8 + y_9 + y_{10}) N_{total} \quad (3.38)$$

$$N \quad \delta + 3.76a_s \lambda = (2y_3 + y_{10}) N_{total} \quad (3.39)$$

where $N_{total} = \sum_{i=1}^{10} \nu_i$ is the total number of moles and y_i is the mole fraction. By definition, the sum of mole fraction is equal 1, the mole fraction can be written

$$\sum_{i=1}^{10} y_i - 1 = 0 \quad (3.40)$$

Six equilibrium constants are used to get eleven equations for ten unknown mole fractions y_i and number of moles N_{total} . These equations are

$$\frac{1}{2} H_2 \leftrightarrow H \quad K_1 = \frac{y_7 P^{1/2}}{y_6^{1/2}} \quad (3.41)$$

$$\frac{1}{2}O_2 \leftrightarrow O \quad K_2 = \frac{y_8 P^{1/2}}{y_4^{1/2}} \quad (3.42)$$

$$\frac{1}{2}H_2 + \frac{1}{2}O_2 \leftrightarrow OH \quad K_3 = \frac{y_9}{y_4^{1/2} y_6^{1/2}} \quad (3.43)$$

$$\frac{1}{2}O_2 + \frac{1}{2}N_2 \leftrightarrow NO \quad K_4 = \frac{y_{10}}{y_4^{1/2} y_3^{1/2}} \quad (3.44)$$

$$H_2 + \frac{1}{2}O_2 \leftrightarrow H_2O \quad K_5 = \frac{y_2}{y_4^{1/2} y_6 P^{1/2}} \quad (3.45)$$

$$CO + \frac{1}{2}O_2 \leftrightarrow CO_2 \quad K_6 = \frac{y_1}{y_5 y_4^{1/2} P^{1/2}} \quad (3.46)$$

where K_i is equilibrium constant. The unit of pressure is the atmosphere. Olikara and Borman [30] had curved fitted the equilibrium constants to JANAF Table data of National Aeronautics and Space Administration (NASA). Their expressions were of the form

$$\log K_i(T) = A_i \ln\left(\frac{T}{1000}\right) + \frac{B_i}{T} + C_i + D_i T + E_i T^2 \quad (3.47)$$

Using of equilibrium constant is identical to maximizing the entropy of the gas. This method is simpler when considering restricted species lists such as the present case, where T is in Kelvin. For the range of $600 \leq T \leq 4000$ K their values are summarized in [24]. Equations (3.36) to (3.46) yield 11 equations for 11 unknowns: 10 unknown mole fractions y_i and the unknown total products mole N_{total} . This set of 11 equations is nonlinear and can be solved by Newton-Raphson iteration. With the product mole fraction composition known, one can proceed to compute the thermodynamic properties of interest: enthalpy, entropy, specific volume, and internal energy.

3.2.3 Thermodynamic Properties of Gases

The gas mixture properties depend on composition of the mixture, temperature, and thermodynamic properties of them, such as, enthalpy, entropy and specific heat capacity can be

computed. The accurate and fast way to get thermodynamic properties of the mixture is by using the JANAF Table thermodynamic data. In the model, the polynomial curve fitted is used to fit the JANAF table data and their values are summarized in [24]. For each species i in its standard state at temperature T [K], the specific heat capacity C_p of species i is approximated by equation (3.48), the standard state enthalpy of species i is given by equation (3.49) and the standard state entropy of species i at temperature T [K] and pressure 1 atm is given by equation (3.50).

$$\frac{C_p}{R} = a_1 + a_2 T + a_3 T^2 + a_4 T^3 + a_5 T^4 \quad (3.48)$$

$$\frac{h}{RT} = a_1 + \frac{a_2}{2} T + \frac{a_3}{3} T^2 + \frac{a_4}{4} T^3 + \frac{a_5}{5} T^4 + \frac{a_6}{T} \quad (3.49)$$

$$\frac{s^0}{R} = a_1 \ln T + a_2 T + \frac{a_3}{2} T^2 + \frac{a_4}{3} T^3 + \frac{a_5}{4} T^4 + a_7 \quad (3.50)$$

3.3 NO Model

There are three different paths of the NO formation in internal combustion engines: 1.) Thermal NO formation, 2.) prompt NO formation, and 3.) NO formation from fuel-bound nitrogen. The dominant part of S.I. engine-out NO emission has been assigned to the thermal NO formation [3, 10]. Thermal NO formation depends on in-cylinder gas temperature, availability of oxygen, pressure and residence time. The extended Zeldovich mechanism was adopted to describe the NO formation process as following equations.



Equations (3.51) and (3.52) were identified by Zeldovich [1], equation (3.53) was added by Lavoie et al [2]. The rate of formation of NO via reactions (3.51), (3.52) and (3.53) is given by

$$\frac{d[NO]}{dt} = k_1^+[O][N_2] + k_2^+[N][O_2] + k_3^+[N][OH] - k_1^-[NO][N] - k_2^-[NO][O] - k_3^-[NO][H] \quad (3.54)$$

where $[]$ denotes species concentrations in moles per cubic centimetre when k_i are rate constants.

A similar relation to equation (3.54) can be written for $d[N]/dt$:

$$\frac{d[N]}{dt} = k_1^+[O][N_2] - k_2^+[N][O_2] - k_3^+[N][OH] - k_1^-[NO][N] + k_2^-[NO][O] + k_3^-[NO][H] \quad (3.55)$$

Due to the low concentration level of atomic nitrogen, the steady-state approximation is appropriated: $d[N]/dt$ is set equal to zero and equation (3.55) used to eliminate $[N]$. The NO formation rate leads to equation (3.56) and can be reduced to equation (3.57).

$$\frac{d[NO]}{dt} = 2k_1^+[O][N_2] \frac{1 - [NO]^2 / (K[O_2][N_2])}{1 + k_1^-[NO] / (k_2^+[O_2] + k_3^+[OH])} \quad (3.56)$$

where $K = (k_1^+ / k_1^-)(k_2^+ / k_2^-)$

$$\frac{d[NO]}{dt} = \frac{2R_1 \{1 - ([NO]/[NO]_e)^2\}}{1 + ([NO]/[NO]_e)R_1 / (R_2 + R_3)} \quad (3.57)$$

$$R_1 = k_1^+[O]_e[N_2]_e = k_1^-[NO]_e[N]_e \quad k_1^+ = 7.6 * 10^{13} * \exp(-38000/T)$$

$$R_2 = k_2^+[N]_e[O_2]_e = k_2^-[NO]_e[O]_e \quad k_1^+ = 1.5 * 10^9 * \exp(-19500/T)$$

$$R_3 = k_3^+[N]_e[OH]_e = k_3^-[NO]_e[H]_e \quad k_1^+ = 2.0 * 10^{14} * \exp(-23650/T)$$

$[]_e$ denotes equilibrium concentration.

3.4 CO Model

From literature review, it is clear that CO model is supposed to be a chemical kinetic model, which is complex and need the understanding in chemical kinetics. Furthermore, CO kinetic is related to the hydrogen-containing species. Small quantities of water and hydrogen can have a strong effect on the oxidation rate. This is because the CO oxidation involving hydroxyl radical is faster than the oxidation involving oxygen [31]. Kinetic model and mechanism should be taken extra care when chosen. This part will describe the oxidation of gasoline, formation of CO, chemical kinetics and kinetic model to predict CO.

3.4.1 Gasoline and its Oxidation

Gasoline is blended from many different hydrocarbon compounds, grouped into families of hydrocarbon molecules termed paraffins, olefins, naphthanes and aromatics, obtained by refining petroleum or crude oil. It is predominantly made up by carbon and hydrogen, typically about 86 % carbon and 14 % hydrogen [4]. The information of hydrocarbon compounds will be described briefly for a better understanding of hydrocarbon oxidation.

Paraffins (alkanes) are alkyl compounds, single-bound open-chain saturated hydrocarbon molecules. They are called saturated hydrocarbon because there are no double or triple bounds. The general formula is C_nH_{2n+2} , for larger molecules straight-chain and branched-chain configurations exist. Example of straight chain paraffins are methane, CH_4 , and octane, C_8H_{18} . Isooctane or 2,2,4 trimethylpentane is an isomer of octane. It has the same number of carbon atoms as octane but not in a straight chain.

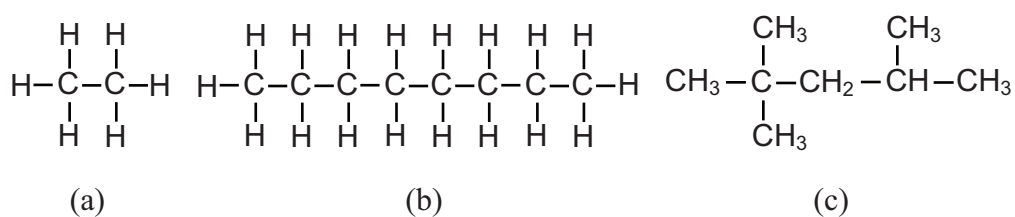


Figure 3.7: (a) Paraffins, (b) Octane and (c) Isooctane, 2,2,4 trimethylpentane

Olefin (alkenes) is alkyl compound, open chain hydrocarbon molecules containing one or more carbon-carbon double bonds. The general formula is C_nH_{2n} . Examples are: C_2H_4 , ethene; C_3H_6 , propene; C_4H_8 , butene. Naphthenes (cycloalkanes) are alkyl compounds, single bound ring hydrocarbon molecules. It has the same general formula as olefins, C_nH_{2n} which is unsaturated, since ring can be broken and additional hydrogen added. Examples: C_3H_6 , cyclopropane; C_4H_8 , cyclobutane; C_5H_{10} , cyclopentane. Aromatics are hydrocarbon with carbon-carbon double bounds internal to a ring structure. The ring structure is very stable so that a greater temperature is required to initiate combustion. The most common aromatic is benzene. The general formula is C_nH_{2n-6} . Examples are: C_7H_8 , toluene; C_8H_{10} , xylene.

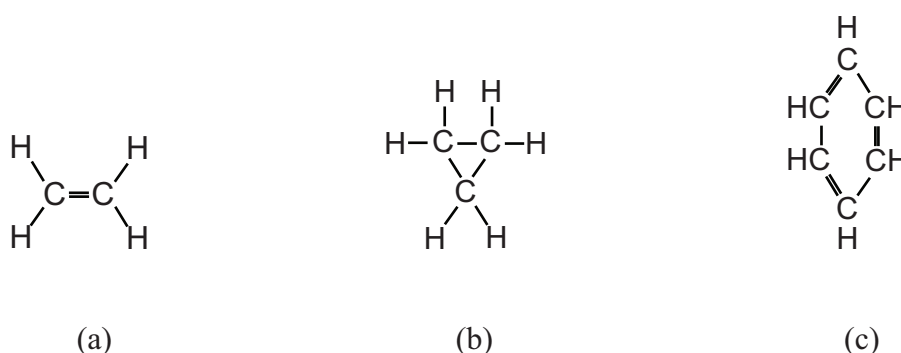


Figure 3.8: (a) Olefin, (b) Naphthenes and (c) Aromatics

The oxidation of large molecules hydrocarbon can be described in the following way [32], in lean and moderately rich flames the hydrocarbon is attacked by O, H, and OH, in the first step. These radicals are produced by the chain-branching steps of the oxyhydrogen reaction. Afterwards, thermal decomposition to smaller alkyl radicals by fast thermal elimination of alkenes turns out to be the only relevant reaction of the higher alkyl radicals (see Figure (3.9) (a) [32]). The three other possible reactions (alkyl radical recombination, alkyl + O_2 to form an alkene and HO_2 and alkyl + O to form an aldehyde and H atoms) are completely unimportant for propyl and the higher alkyl radicals.

The oxidation of C_1/C_2 hydrocarbons are widely studied and well known. Figure (3.9) (b) [32] shows the oxidation of C_1/C_2 hydrocarbons. Methane is attacked exclusively by H, O, and OH. The resulting CH_3 radical reacts only with O atoms to give formaldehyde. The CHO radical is formed then by H atom abstraction. CHO can be decomposed in two ways- 1) thermally yielding CO and H atoms or 2) the H atom can be abstracted by H or O_2 . However, the recombination of CH_3 in stoichiometric and especially rich flames to be C_2H_6 or C_2H_5 occurs and needs bigger and

more complex set of reaction mechanisms to solve this problem, for example, Warnatz [29] used 29 set of reactions or 160 elementary reactions to solve this problem.

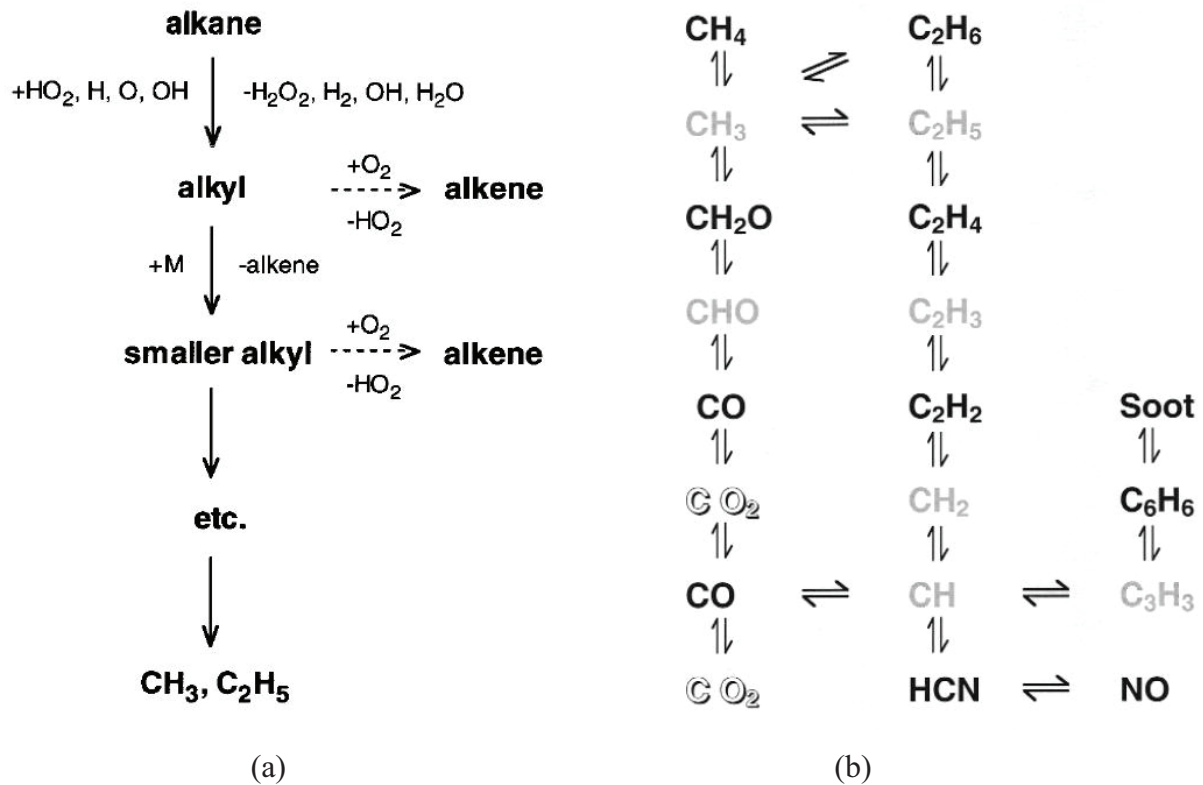
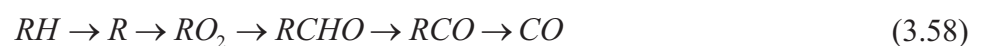


Figure 3.9: (a) Alkyl radical decomposition, (b) oxidation of C_1/C_2 hydrocarbons

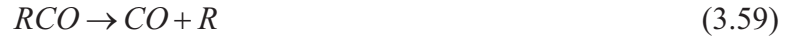
3.4.2 CO Formation

Carbon monoxide emission from spark-ignition engines depend primarily on the fuel/air mixture equivalence ratio. Under the richer mixture, due to lack of oxygen causing incomplete combustion, the level of CO in exhaust gas increased. Levels of CO observed in spark-ignition engine exhaust gases are lower than the maximum value measured within the combustion chamber, but are significantly higher than equilibrium value for the exhaust conditions. The CO formation is considered to be kinetically controlled [4, 10, 24, 33].

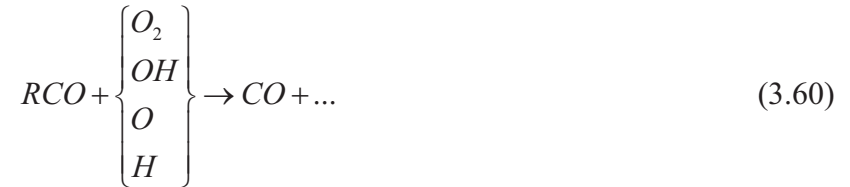
The carbon monoxide formation process is written in the following way [4, 10]



where R signifies a hydrocarbon radical. The reaction of the RCO radical to produce CO may occur via thermal decomposition [10]



or via



At a typical combustion temperature, the reaction of the RCO radical to produce CO occurs via thermal decomposition. The CO formed in the combustion process via reaction (3.59) is then oxidized to CO_2 at a rate relatively slower than the CO formation rate. The governing equations of CO are mainly controlled by the following chemical reactions [4, 10, 12].



The carbon monoxide concentration increases rapidly in the flame front zone, mainly produced by thermal decomposition of partially oxidized hydrocarbon compounds. The partial CO is successively oxidized to CO_2 via a kinetic controlled mechanism. The simple CO model is used [12, 13, 14] considering two equations that derived from equation (3.61) and (3.62). The rate of CO formation via reactions (3.61) and (3.62) is then given by

$$\frac{d[CO]}{dt} = k_1^- [CO_2][H] - k_1^+ [CO][OH] + k_2^+ [CO_2][O] - k_2^- [CO][O_2] \quad (3.63)$$

where $[]$ denotes the species concentration in moles per cubic centimeter when k_i are rate constants, + is forward, - is backward. Parameters in brackets refer to combustion products concentration. If O, O_2 , OH, H and CO_2 are in equilibrium state, the CO formation rate can be expressed as

$$\frac{d[CO]}{dt} = (R_1 + R_2) \left(1 - \frac{[CO]}{[CO]_e} \right) \quad (3.64)$$

$[\]_e$ denotes equilibrium concentration, and the variables R_1, R_2 are defined as

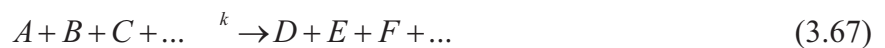
$$R_1 = k_1^+ [CO]_e [OH]_e = k_1^- [CO_2]_e [H]_e \quad (3.65)$$

$$R_2 = k_2^+ [CO_2]_e [O]_e = k_2^- [CO]_e [O_2]_e \quad (3.66)$$

This CO model is a simple empirical model which still based on equilibrium concentration of other species except CO. The equilibrium concentration is good enough to define the value of species only when temperature is high. However, at lower temperature, during late expansion stroke, the equilibrium is not an accurate solution anymore, and the full kinetic model is needed for a better result.

3.4.3 Chemical Kinetics

In section 3.2.2, the chemical equilibrium is described. Since the CO model based on chemical kinetics, this part will describe fundamentals of chemical kinetics [29]. Consider a chemical reaction



where A, B, C, ... denote different species involved in the reaction. A rate law describes an empirical formulation of the reaction rate, the rate of formation or consumption of a species in a chemical reaction. For species A, the reaction rate can be expressed according to

$$\frac{d[A]}{dt} = -k \cdot [A]^a [B]^b [C]^c \dots \quad (3.68)$$

where a, b, c, \dots are reaction orders with respect to species A, B, C, ... and k is the rate coefficient of the reaction. The sum of all exponents is the overall reaction order.

Rate coefficients of the reaction play an important role with combustion process. They are nonlinear and depend considerably on temperature. For this reason the determination of the

temperature, with the help of the two-zone model, is the most importance. This temperature dependence is to be described by a simple formula (Arrhenius law).

$$k = A \cdot \exp\left(\frac{-E_a}{RT}\right) \quad (3.69)$$

where A is the pre-exponential factor or simply the pre-factor, which is usually small in comparison to the exponential dependence. R is the gas constant. The activation energy, E_a corresponds to an energy barrier, has to overcome for execution of a reaction. Its maximum value corresponds to bond energies in the molecule but it can be much smaller (or even zero) if new bonds are formed simultaneously with the breaking of the old bonds. For the backward reaction, the similar rate law applies for the production of A

$$\frac{d[A]}{dt} = k^{(r)} \cdot [D]^d [E]^e [F]^f \dots \quad (3.70)$$

When the system stays in chemical equilibrium, forward and backward reactions have the same rate on a microscopic level. The forward reaction is characterized by superscript (f), the reverse reaction by superscript (r). For the system, the net reaction is observed as none, there is no change in the amount of any species during the time. Equation can be derived as

$$k^{(f)} \cdot [A]^a [B]^b [C]^c \dots = k^{(r)} \cdot [D]^d [E]^e [F]^f \dots \quad (3.71)$$

or

$$\frac{[D]^d [E]^e [F]^f \dots}{[A]^a [B]^b [C]^c \dots} = \frac{k^{(f)}}{k^{(r)}} \quad (3.72)$$

The expression on the left side conforms to the equilibrium constant of the reaction, which can be calculated from thermodynamic data described in section 3.2.2. The important relation between the rate coefficient of forward and reverse reaction can be obtained,

$$K_c = \frac{k^{(f)}}{k^{(r)}} = \exp(-\Delta_R \bar{A}^0 / RT) \quad (3.73)$$

where \bar{A}^0 is free energy corresponding to \bar{G}^0 , superscript “0” refer to the standard pressure and \bar{G} is the partial derivative of the free energy G with respect to the amount of substance (mole number) of compound n_i .

3.4.4 CO Kinetic Model

The prediction of CO concentration in the exhaust gas by equilibrium concentration supplies insufficient results [10, 11, 34]. During the expansion phase, the burned gas cools down very rapidly and thus the chemical equilibrium is not an accurate solution to predict the gas in cylinder. It is well-known and had been proved that the CO in the cylinder is determined by chemical kinetics, for example, the classical kinetic model of Newhall [11]. It is a theoretical analysis of chemical kinetics for the internal combustion engine expansion process. Fourteen couples of non-linear differential equation based on 32 elementary chemical reactions were integrated numerically through use of a Runge-Kutta procedure. The chemical equilibrium concentration was used as the initial concentration of kinetic model and the starting point of the calculation at the maximum pressure point. The fuel used was isooctane, lambda value was 1 and engine speed was 4000 rpm. Figure 3.10 shows the results of CO concentration calculated by kinetic model and equilibrium concentration.

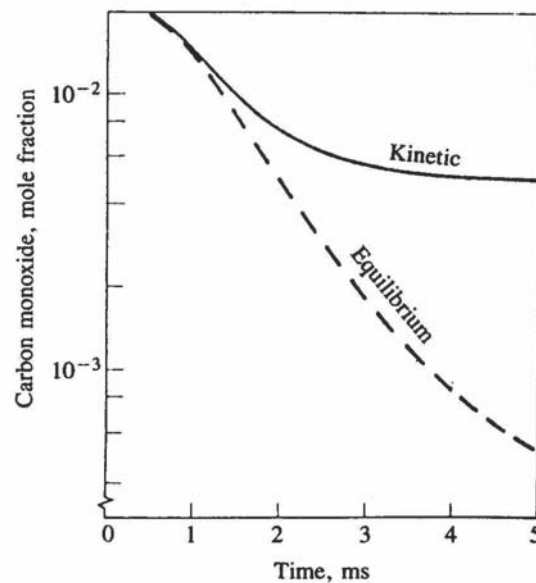


Figure 3.10: Carbon monoxide concentration during expansion [11]

Figure 3.10 shows that the CO concentration predicted by chemical kinetic is close to equilibrium, only at the later stage of the expansion stroke that the CO concentration predicted departs from equilibrium. Newhall showed that the kinetic model delivered the good result compared to the measured value.

3.4.4.1 Implementation of CO Kinetic Model

After the calculation of two-zone model, the kinetic model was started. The starting point was the point that the mass fraction burned equals to 0.90, i.e. 90% of the mixture is burned; shortly after maximum pressure and temperature point. Under these conditions, the mass of the burned zone is so much bigger than the unburned zone, thus the unburned zone can be neglected. Moreover, the burned gas temperature remains high, therefore, the concentration of burned gas can be calculated by using chemical equilibrium [11, 29, 34, 35]. The burned gas was post flame gas, and assumed that there was no gasoline left. If we consider the equilibrium combustion products species as N_2 , CO_2 , H_2O , O_2 , CO , H_2 , O , H , OH , NO , NO_2 , N_2O and N then a complex chemical mechanism of gasoline was unnecessary. This had reduced computational effort and calculation time significantly. Even though there was no methane, ethane or propane as input in kinetic model, their mechanisms were still included in the model because their reformation can occurred and could react with another species. Their inclusion had made the model more comprehensive.

The CHEMKIN software [36] has been chosen as a kinetic model solver due to its high efficiency and ability to solve complex kinetics problems. The internal combustion engine model is an extension of the homogeneous zero dimensional model. It can simulate a combustion cylinder in an internal combustion engine under auto-ignition conditions and homogeneous charge compression ignition engines. However, because of its homogeneous consideration, it can simulate only one zone.

In the beginning when the mass fraction burned equivalent to 0.90, the chemical equilibrium model received the pressure data from pressure sensor and temperature and reactant concentration from the two-zone model to calculate equilibrium concentration. Reactants were gasoline and air. Results from the equilibrium model were sent to the internal combustion engine model.

Inputs of the internal combustion engine model were engine geometry, pressure, temperature, equilibrium combustion products, engine speed and the heat transfer coefficient. When all input data were completed, the kinetic model calculated from the starting point until the end of expansion process. The main results of the kinetic model and internal combustion engine model

were concentration and temperature of the gas in the cylinder during the expansion process. Outputs at the time the exhaust valves open were used as the exhaust gas condition prediction by the model. The predicted temperature and pressure from internal combustion engine model were compared with the two-zone model temperature and measured pressure-time data to verify the heat transfer coefficient.

There is an alternative method to solve the kinetic model using CHEMKIN. This method uses a closed homogeneous batch reactor instead of an internal combustion engine model. The equilibrium combustion products were needed as initial input data. The measured pressure-time and temperature-time data from two-zone model, from the starting point (90% MFB) until the end of expansion process, were directly delivered to kinetic model. Therefore, other parameters such as engine geometry, engine speed and heat transfer coefficient were no longer needed. This reduces time to find the exact engine heat transfer coefficient. Given the engine heat transfer coefficient is correct, results of both methods are the same because both methods calculate chemical kinetic with the same temperature and pressure.

3.4.4.2 Chemical Kinetic Mechanisms

There were different reaction mechanisms for the chemical kinetic model to determine the concentration of the gas with high temperature. In this thesis, one of the mechanisms mentioned had been chosen based on a mechanism that delivers a more accurate result. The four reaction mechanisms, GRI-Mech, Primary Reference Fuel (PRF), H.K. Newhall, and I. Glassman, had been investigated.

GRI-Mech mechanism [37] was developed by the Gas Research Institute. It was a list of elementary chemical reactions and associated rate constant expressions. Most of the reactions listed had been studied one way or another in the laboratory, and so the rate constant parameters mostly had been more or less directly measured. GRI-Mech version 3.0 had been optimized for methane and natural gas oxidation. As such, it included reactions that were involved in the combustion of other hydrocarbon constituents of natural gas (e.g., ethane and propane). However, since the optimization did not include targets relevant to other fuels, it should not be used for model combustion of pure fuels such as methanol, propane, ethylene, and acetylene even though these compounds were on the GRI-Mech species list. GRI-Mech contains 325

reactions with 53 species and had limited operating area from 1000 to 2500 K and 1330 Pa to 1 bar. This high temperature range is satisfied for the in-cylinder gas temperature. However, the indicated pressure range is not suitable for the simulation of the exhaust pollutants of the engine because it lies approximately between 1 and 100 bar.

Lawrence Livermore National Laboratory [38] developed a detailed chemical kinetic mechanism which has been used for the oxidation of primary reference fuels (PRF), isooctane and n-heptane, for gasoline. The mechanism was developed by combining the isooctane and n-heptane mechanisms. This mechanism has been used in the simulation of homogeneous compression ignition engines (HCCI). Currently, the isooctane oxidation mechanism is used in a jet-stirred reactor, flow reactors, shock tubes and in a motored engine. Over a series of experiment investigated, the initial pressure ranged from 1 to 45 atm, the temperature from 550K to 1700K, and the equivalence ratio from 0.3 to 1.5, with nitrogen-argon dilution from 70% to 99%. Because of the temperature limit, this mechanism was not appropriated for this work.

The reaction mechanism of H.K. Newhall based on 13 species and 32 elementary reactions [11]. The 13 most important species for the combustion of any C_xH_y fuels were N, N_2 , O, CO_2 , H, H_2 , OH, H_2O , CO, CO_2 , N_2O , NO_2 and NO. It was specified that the 32 elementary reactions were crucial in the expansion phase. This mechanism is appropriately chosen to be used in the expansion phase and only applies in the expansion phase when the flame front went through the combustion chamber leaving only burned gas in the cylinder. The chemical equilibrium concentrations were used as the initial condition of chemical kinetic model. This method was a good way to vanish the complex combustion mechanism of isooctane. The temperature and pressure range for this reaction mechanism were suitable for the burned gas in cylinder and can be good for the simulation of the carbon monoxide emission. However, this mechanism considered only 13 species which were relatively small. Perhaps the mechanism was implemented in 1969 when the computer power was limited. A proper mechanism for CO kinetic model should be introduced.

The reaction mechanisms collected by I. Glassman [39] were sets of chemical mechanisms for describing high temperature oxidation of various small molecule fuels, which considered 83 species and 516 elementary reactions. The temperature limit (1000 to 3000 K) and pressure limit (1 to 100 bar) were suitable for the gas properties in cylinder during expansion phase. These reactions were organized into 11 sets of chemical mechanisms. The first 6 mechanisms

contained high temperature oxidations of various fuels, increasing in complexity from hydrogen to ethane.

1. H_2/O_2
2. $\text{CO}/\text{H}_2/\text{O}_2$ (original from [40])
3. $\text{CH}_2\text{O}/\text{CO}/\text{H}_2/\text{O}_2$
4. $\text{CH}_3\text{OH}/\text{CH}_2\text{O}/\text{CO}/\text{H}_2/\text{O}_2$
5. $\text{CH}_4/\text{CH}_3\text{OH}/\text{CH}_2\text{O}/\text{CO}/\text{H}_2/\text{O}_2$
6. $\text{C}_2\text{H}_6/\text{CH}_4/\text{CH}_3\text{OH}/\text{CH}_2\text{O}/\text{CO}/\text{H}_2/\text{O}_2$

The mechanism 7 described the more complex oxidation of propane.

7. C_3H_8

The mechanisms 8-11 described the post combustion gases including nitrogen oxides, hydrogen chloride, ozone and sulfur oxides. The SO_x mechanism was optional and could be employed for fuel such as diesel that contained sulfur.

8. $\text{N}_x\text{O}_y/\text{CO}/\text{H}_2/\text{O}_2$
9. $\text{HCl}/\text{N}_x\text{O}_y/\text{CO}/\text{H}_2/\text{O}_2$
10. $\text{O}_3/\text{N}_x\text{O}_y/\text{CO}/\text{H}_2/\text{O}_2$
11. $\text{SO}_x/\text{N}_x\text{O}_y/\text{CO}/\text{H}_2/\text{O}_2$

Before the expansion phase and during the combustion, there still were large molecule hydrocarbons in the combustion chamber, which were not considered by this mechanism. In order to reduce the complex of combustion mechanism, as the Newhall method, the chemical equilibrium concentrations were used as initial conditions of chemical kinetic model. In the post flame gas, according to the equilibrium consideration, there were no gasoline molecule in the burned gas. Hence, this mechanism was capable to be used in this work.

The selection of the mechanism should be done carefully to get the appropriate mechanism. Pressure and temperature range during the kinetics computation are crucial parameters. Therefore the reaction mechanisms must be applicable to the in-cylinder burned gas pressure and temperature. If the wrong mechanism had been chosen, the CO model result would have been too far from the experiment. For example, at a test point, results of kinetic model four mechanisms are compared to the measured value. Results are shown in Figure (3.11).

Figure 3.11 shows clearly the result using Glassman mechanism is closer to the measured value than the other reaction mechanisms. The reason is that the Gri-Mech and PRF mechanisms are

not appropriate mechanism due to limitation in the operating condition. The pressure range exceeded Gri-Mech requirement and the maximum PRF temperature range of 1700 K is too small for the burned gas in the cylinder, which required a range of up to 3000 K.

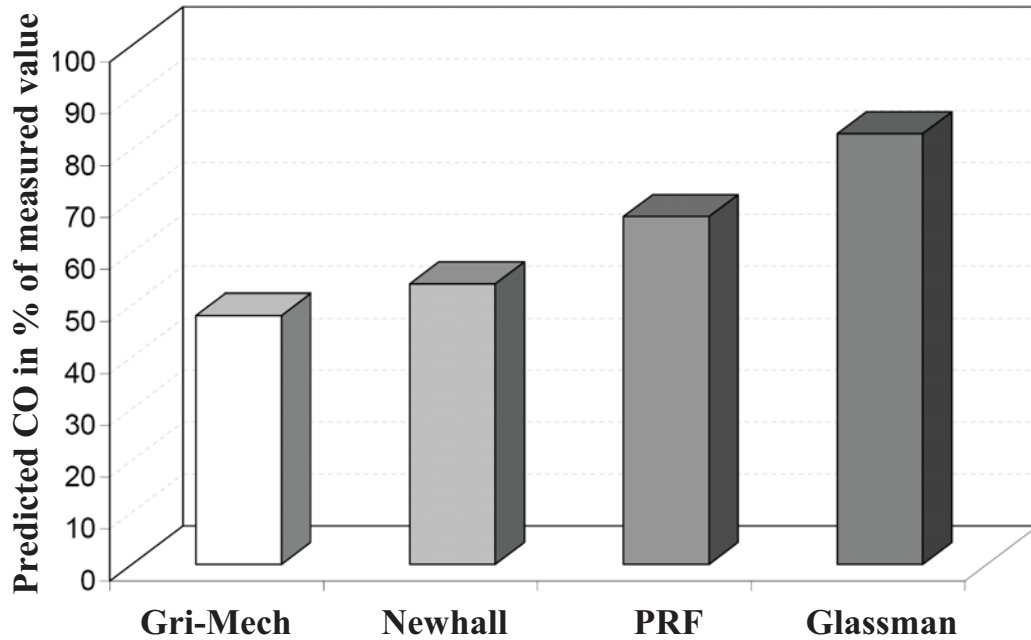


Figure 3.11: Comparison of CO predicted using different mechanisms

If one compares the reaction mechanisms of Newhall and Glassman, the different CO prediction result is due to the fact that Glassman mechanism considers more species and thus more reactions than Newhall, which can take into account additional portions of CO concentration. The Newhall mechanism considered only one CO elementary reaction (equation 3.61) but the Glassman mechanism considered both main reactions (equation 3.61 and 3.62) and two extra equations that CO reacts directly with other species (following equations) and HCO reactions.



Due to the clear advantage of the Glassman mechanism, all following computations were accomplished exclusively with the reaction mechanism by Glassman.

4. Engine Measurement

To validate the model prediction, engine measurement was done at the engine laboratory in University of Rostock. The engine specification, exhaust gas analyser details and engine operating conditions will be described in this chapter.

4.1 Engine Specification

A 1.6-liter gasoline direct injection engine was used for the validation of the model. The engine characteristics are shown in Table 4.1.

Table 4.1: Engine Characteristics

Number of cylinder	4
Bore	76 mm.
Stroke	86 mm.
Swept volume/cylinder	399 cc.
Compression ratio	12
Intake valves/cylinder	2
Exhaust valves/cylinder	2
Fuel injected pressure	~80 bar
Fuel	Gasoline, RON 98

A pressure sensor is installed in each engine combustion chamber, one sensor per cylinder. These cylinder pressure sensors are water cooled quartz type. The pressures in the combustion chambers were measured during 100 consecutive cycles at each test point. The average pressure-time data were used to minimize the calculation time of the two-zone and emissions model.

4.2 Exhaust Gas Analyzer

Figure (4.1) shows the schematic of the engine measurements. The exhaust gas probe position was at the exhaust manifold before the pre-catalyst. The exhaust gas sampling pipe from the engine to the exhaust gas analyzer was heated to 180 °C so that no condensation process occurred. Nevertheless, the exhaust gas temperature was so low that no oxidation reaction can occur. The CO and CO₂ concentrations were measured by non-dispersive infrared detector (NDIR). The HC, NO_x and O₂ concentrations were measured by flame ionization detector (FID), chemiluminescence detector (CLD) and paramagnetic oxygen detector (PMD), respectively. Table 4.2 shows the measuring range of exhaust gas analyzers which have the repeatability <1% FS for all ranges.

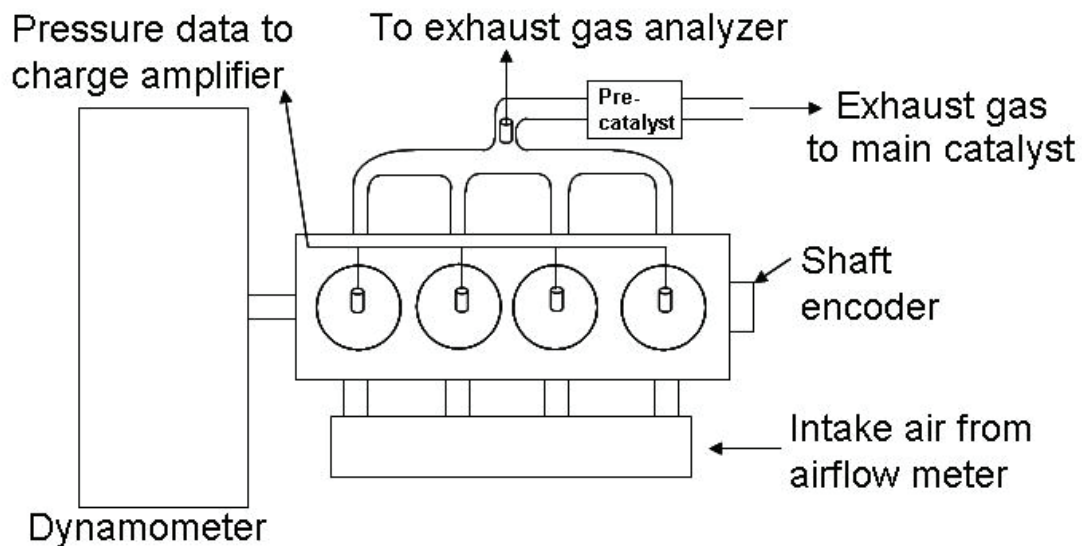


Figure 4.1: Schematic of the engine measurements.

Table 4.2: Exhaust gas analyzer characteristics

Gas type	Measuring range (min, max)
CO	0-2,500 ppm, 0-10%
NO _x	0-50 ppm, 0-10,000 ppm
HC (C1)	0-9 ppm, 0-300,000 ppm
CO ₂	0-0.5%, 0-20%
O ₂	0-1%, 0-100%

4.3 Operating Condition

The operating conditions were controlled to be close to the real engine operating condition. Engine rotational speeds were from 1000-4500 rev/min. Due to technical grounds, the experiments with 3000 rev/min conditions were excluded. Engine loads also vary from low to high load as shown in figure (4.2). There was no exhaust gas recirculation used. Ignition timings were adjusted at maximum brake torque for all engine operations to achieve the optimum efficiency.

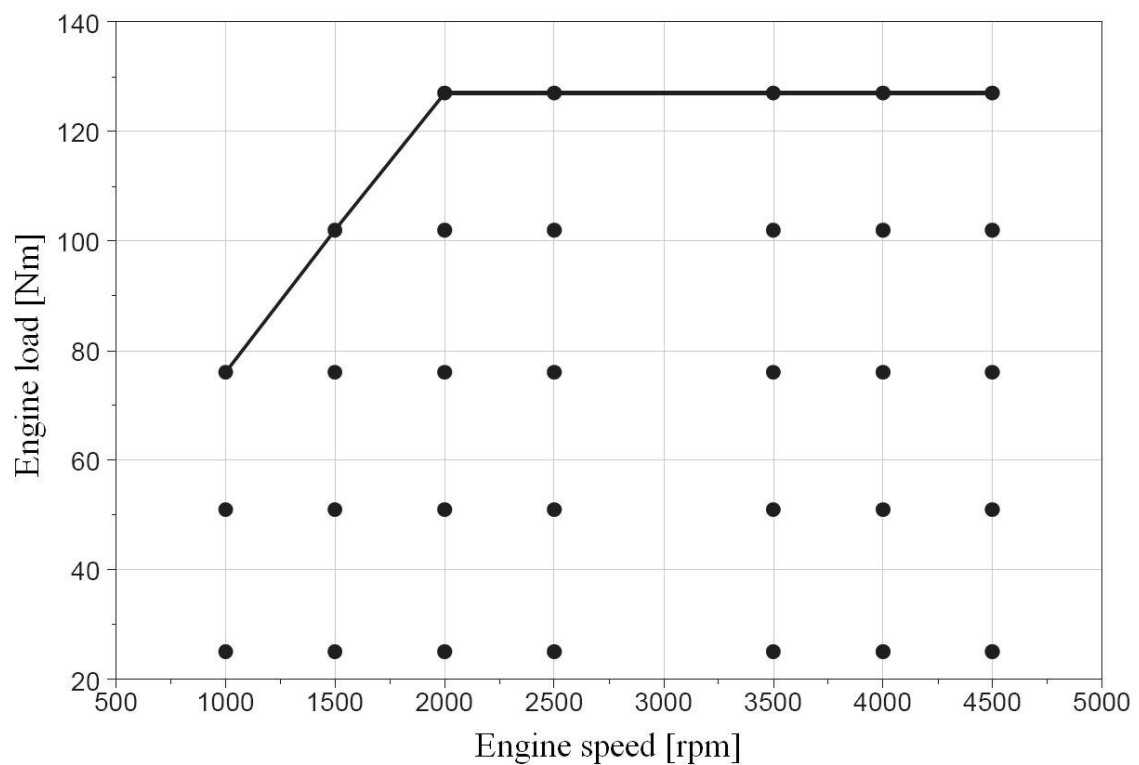


Figure 4.2: The engine operating map.

The fuel/air equivalence ratio (λ) of the engine should be set constantly to one to represent the real value of fuel/air equivalence ratio when the engine is commercially operated. In addition, this engine under normal operation conditions $\lambda = 1$ was running at set-point λ value of 0.98 and 1.02, with amplitude of 2%, (shown in Figure 4.3) for the optimum efficiency of three way catalytic converter. Figure (4.4) shows the real λ value from the λ sensor. One can see that the main λ values are close to set-point λ value. To reduce the calculation time, the λ of the engine were set constantly to 0.98 and 1.02

without amplitude, and then the model can calculate only these two lambda values to represent the real engine operating lambda. This research focus does not consider rich or lean mixtures as they are not used in this modern engine. Please note that, the engine is operated with a homogeneous charge, which is the same as the concept of the two-zone model.

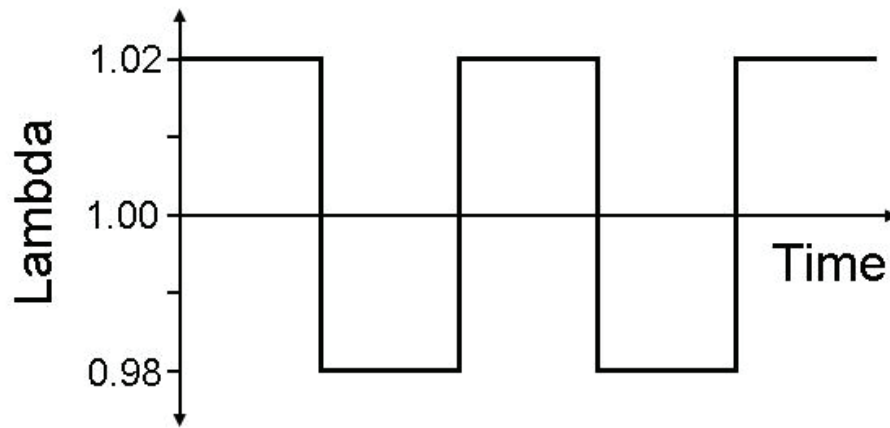


Figure 4.3: Set-point lambda value.

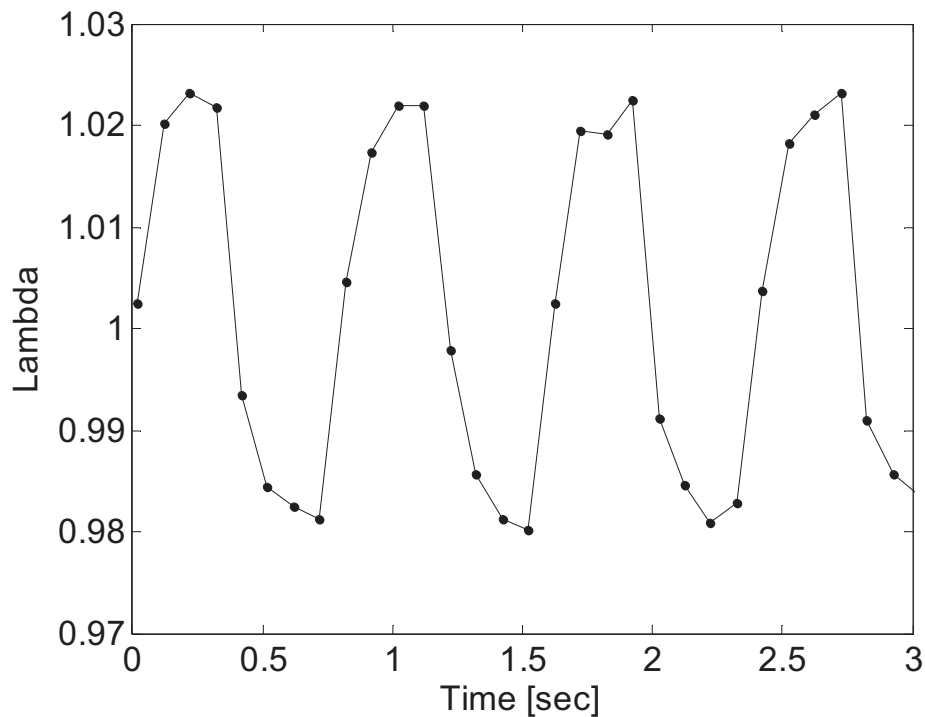


Figure 4.4: Lambda sensor signal.

5. NO Model Result

To validate the model prediction, this chapter shows results of various NO models compared to the engine measurements. The second part shows method to improve the model prediction using multi-zone burned gas to predict NO. The last part shows sensitivity analysis of the model.

5.1 NO Model Result

The two-zone thermodynamics model is used for the calculation of temperature and combustion product of the gas in cylinder. Thereafter, the extended Zeldovich mechanism is introduced to calculate NO using equation (3.57). The pressure, burned gas temperature and NO concentration are shown in figure (5.1).

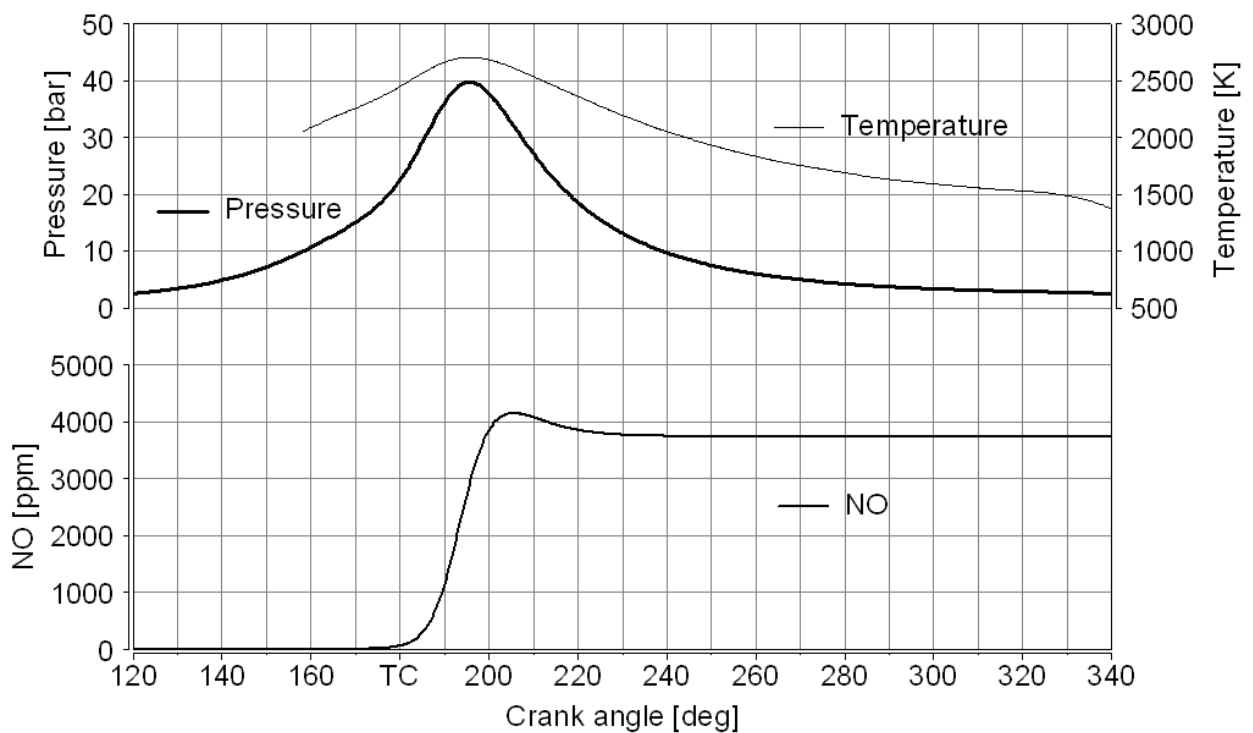
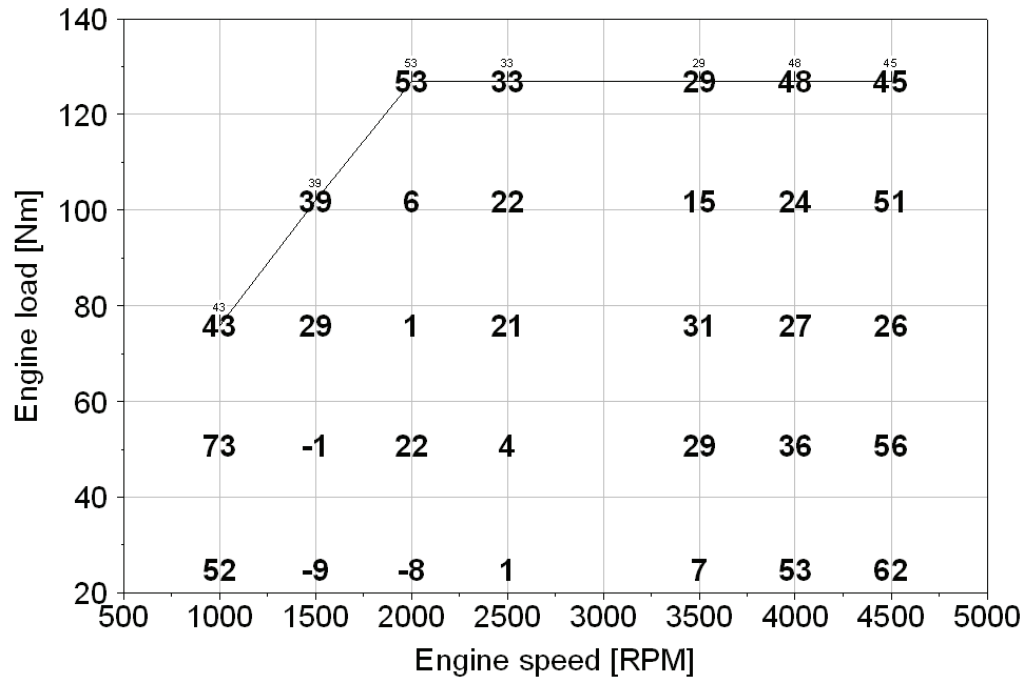
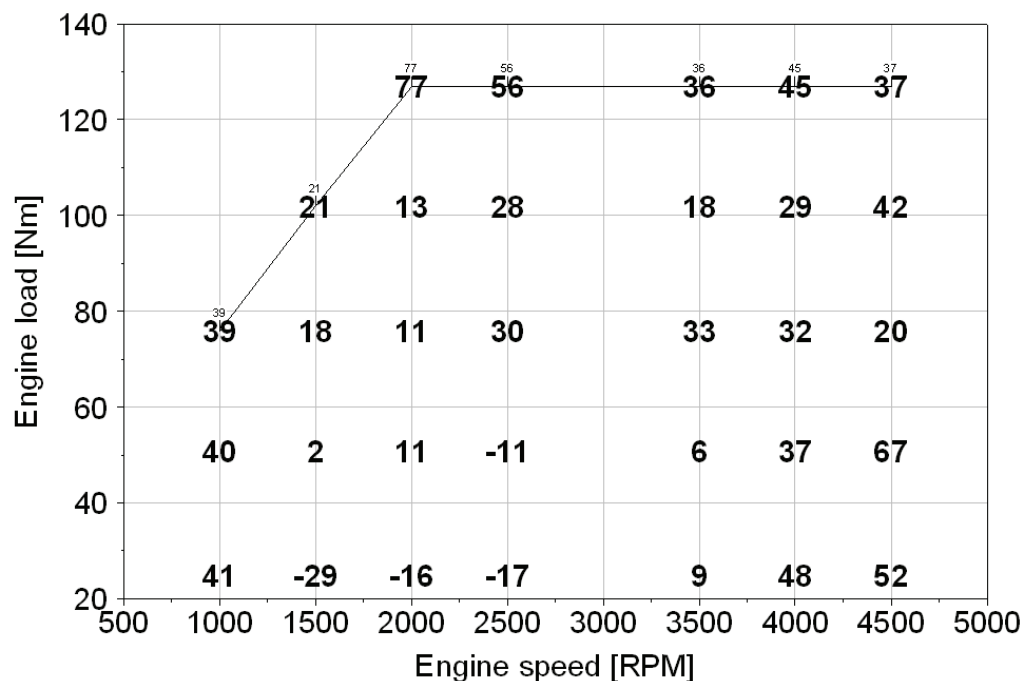


Figure 5.1: Pressure, burned gas temperature and NO concentration of the gas in the cylinder calculated by extended Zeldovich mechanism (Spark at 21.5 deg BTC, engine speed 2500 rpm, load 76 Nm and lambda 0.98).

NO concentrations were taken when crank angle degree is 330 deg because the exhaust valves open about 30 deg BBC. The percentage error of the model compared to measured value over engine operating map is shown as follows:



(a) Lambda 0.98



(b) Lambda 1.02

Figure 5.2: Percentage error of NO prediction calculated by extended Zeldovich mechanism compared to measured value over engine operating map.

The average percentage error from figure (5.2) with lambda 0.98 is 30.0 % and with lambda 1.02 is 30.4 %. Model results are mostly higher than measured values. The reason is that the model calculation based on only one burned gas zone (called early-burning element) and this zone gave the maximum NO prediction compared to the late-burning element [4]. When one physically considers the flame front, during it goes in to the unburned gas, combustion occurs and it produces the burned gas all time during the combustion period. The model prediction will not be accurate if the calculation is done only on early burned gas but not for every small gas element that always occurs during the combustion period. Heywood [4, 6] and Raine [5] showed using the multi-zone model to predict NO and their results were better compared to simply one burned zone NO model.

5.2 Improved NO Model

Raine, Stone and Gould [5] showed multi-zone thermodynamic model, which was the extension of two-zone model based on the routines from Ferguson [24] and using extended Zeldovich mechanism to predict NO. The two-zone model had been extended to multiple burned gas zones because there were evidences that more than one burned gas zone should be considered because of the temperature gradient which was established in the burned gas, due to the consecutive nature of combustion [4]. Typically, temperature difference of approximately 100-200 K had been reported between the first and last burned regions; first burned attaining the highest temperature.

The concept of the multi-zone model is, during the combustion, for every short time interval there is unburned gas that converts to be the burned gas due to combustion. This amount of gas is considered to be one burned zone. Number of zone depends on the time interval or crank angle degree. The gas in each zone which occurred during the combustion has a different temperature and concentration, but they have the same pressure. The gases in the zones are considered homogeneous and not mixed with the other zones. At the end of expansion stroke, the mole fractions in each zone are weighted with the mass fraction burned to calculate the engine fully mixed emissions. They concluded that using 5 or 10 burned zones were likely to be efficient for

most purposes. The result of the model is shown in Figure (5.3). It is clear that the NO concentration in the first zone is significantly higher than the last zone.

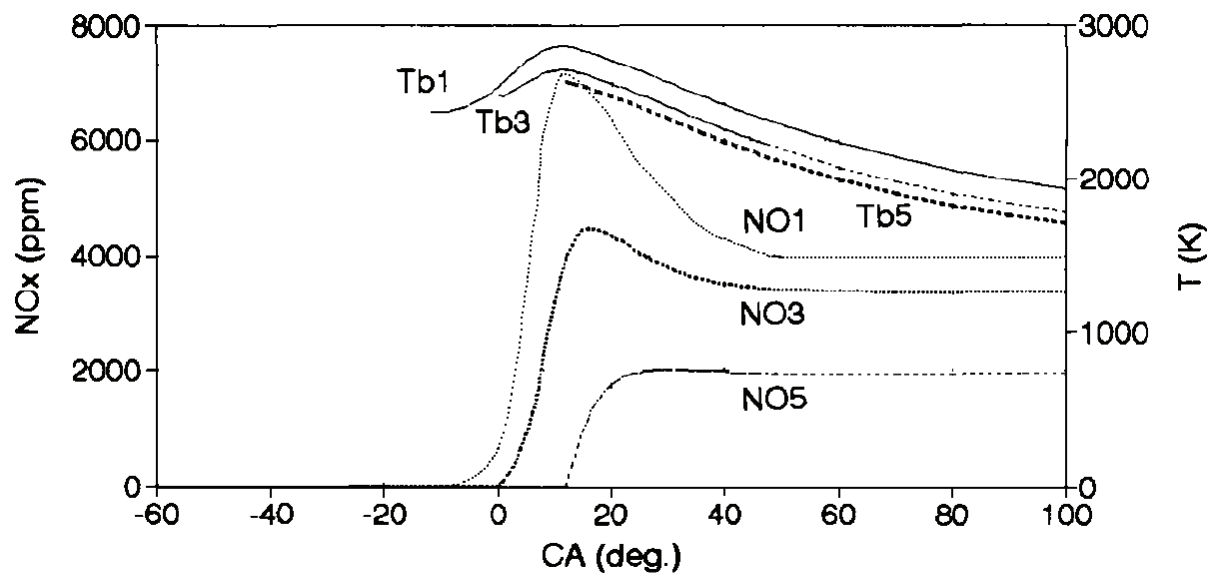


Figure 5.3: Multi-zone model result of Raine [5] (five burned zones), showing burned gas temperatures (Tb), and kinetically determined NO concentrations as a function of crank angle in first, middle and last zones.

To improve the NO result of this thesis, the modification of the NO calculation should be considered. With the minimum calculation time was still concerned. This work still uses the two-zone thermodynamic model but the NO calculation had been modified. The concept of the NO multi-zone calculation is, during the combustion, for every short time interval there is unburned gas that converts to be the burned gas due to combustion. This amount of gas is considered to be one burned zone. The gas in each zone that occurred during the combustion has the same temperature and pressure (as two-zone thermodynamic model). The assumption is when the unburned mixture converted to be the burned gas; the temperature is suddenly changed to be the same as the temperature of two-zone model. This method should be roughly accurate enough comparing to the result of figure (5.3), where the maximum temperature difference between the first and last zone was about 230 K or 12 % but between the other zones were lower.

Gases in the zones are considered homogeneous and not mixed with another zone. Because the gas in any burned zone has the same temperature and pressure; equilibrium concentration of them are the same, only kinetically NO concentrations are different between various zones. This is the advantage to keep the minimum calculation time. The extended Zeldovich mechanism was

used to predict the NO concentration of each zone. Considering figure (5.3), each zone started with the zero NO concentration, because NO did not occur when the flame just past. At the end of expansion stroke, the mole fractions in each zone were weighted with the mass fraction burned to calculate the engine fully mixed emissions as follows:

$$NO_{overall} = \sum_i MFB_i [NO]_i \quad (5.1)$$

Figure (5.4) shows result of NO multi-zone calculation. The first zone contained burned gas that combust from spark to 2.5 crank angle degrees later. The new zone occurred every 2.5 crank angle degree until the end of combustion. Then total number of the zones depends on the combustion duration (20 zones in figure (5.4)). It is clear that NO concentration in the first zone is about 3.5 times compared to the last zone.

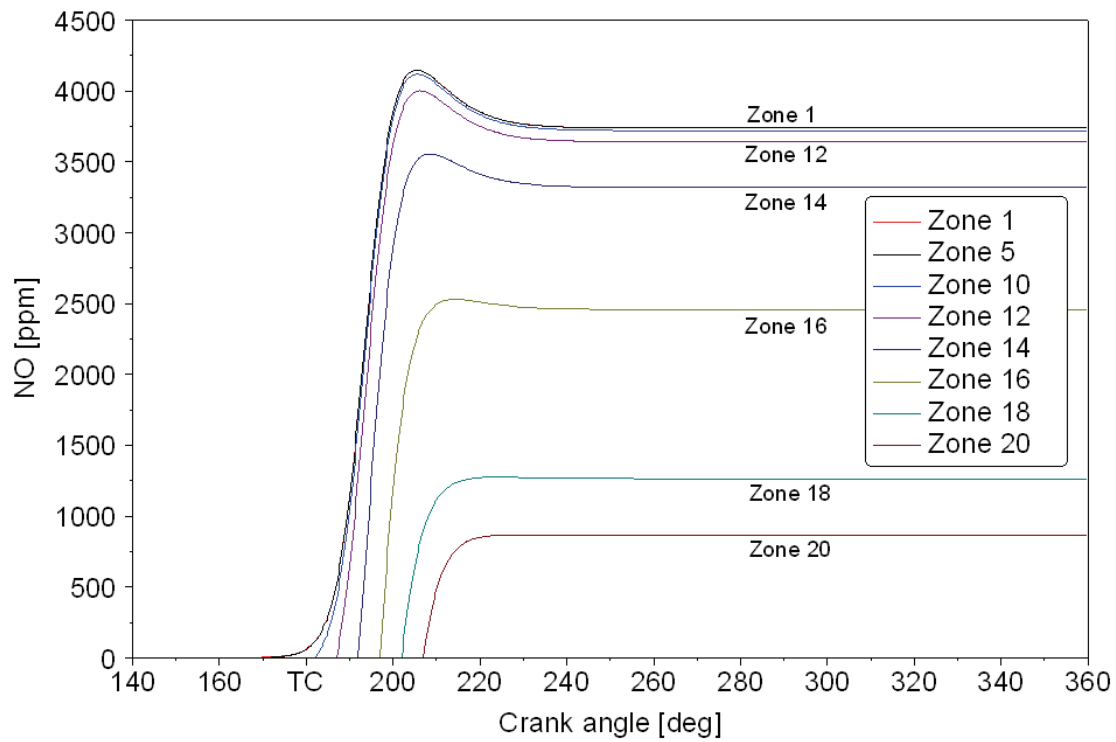


Figure 5.4: NO concentrations of the gas in the cylinder calculated by multi-zone NO calculation using extended Zeldovich mechanism (Spark at 21.5 deg BTC, engine speed 2500 rpm, load 76 Nm and lambda 0.98).

Figure (5.5) shows accumulated NO concentration of the multi-zone NO calculation compare to the simply one burned zone NO calculation. The NO value of multi-zone NO calculation is about 12% lower than one burned zone NO value for this operating point; and about 10-40% or average value 26% lower than one burned zone NO value for all operating point.

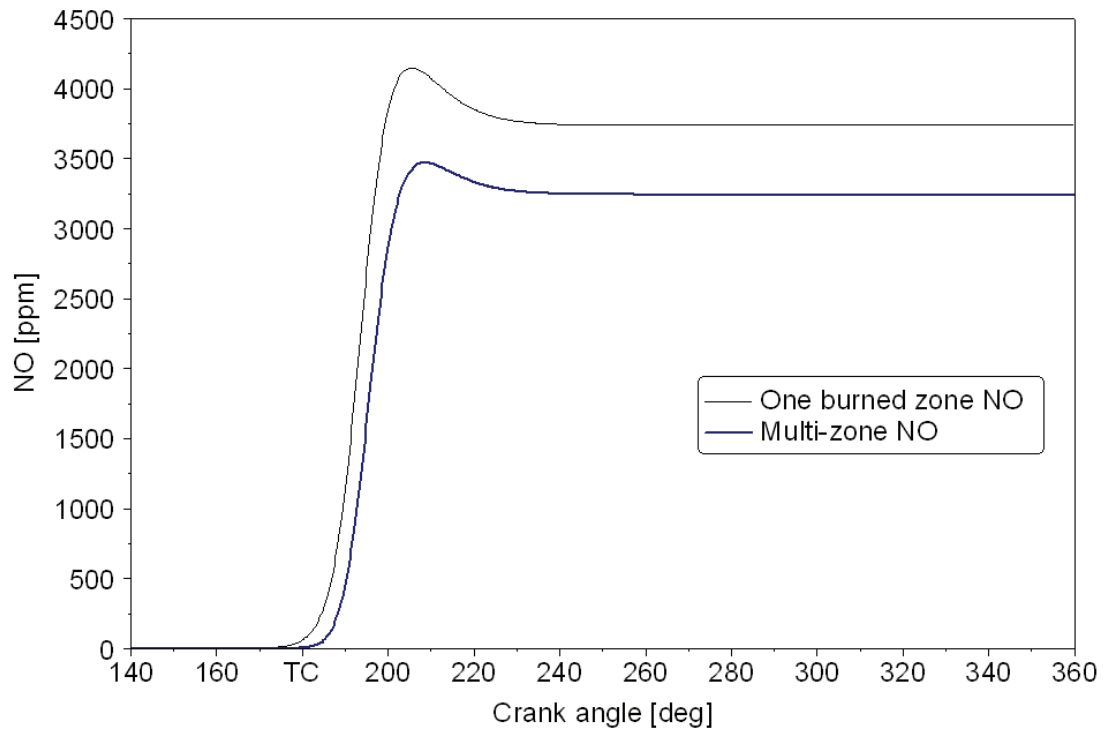


Figure 5.5: NO concentrations of the gas in the cylinder calculated by one burned zone NO compare to multi-zone NO calculation using extended Zeldovich mechanism (Spark at 21.5 deg BTC, engine speed 2500 rpm, load 76 Nm and lambda 0.98).

Results of the multi-zone NO calculation over engine operating map are shown in figure (5.6). It shows percentage error of NO prediction calculated by multi-zone NO calculation using extended Zeldovich mechanism compared to measured value over engine operating map. The average percentage error from figure 5.6 (a) with lambda 0.98 is 15.8 % and from figure 5.6 (b) with lambda 1.02 is 13.8 %. NO prediction errors of medium and high engine load have relatively low variation of error in this area. The errors and their variations are high in low speed area. This may be caused by large variation and a significant amount of residual mass left over from the previous cycle which could not be exactly measured. The amount of intake-air is another reason of high error at low load, amount of intake-air is small and the air-flow measurement has relative high error in the low load area. The sensitivity analysis of the NO model is then necessary and will be described in next part.

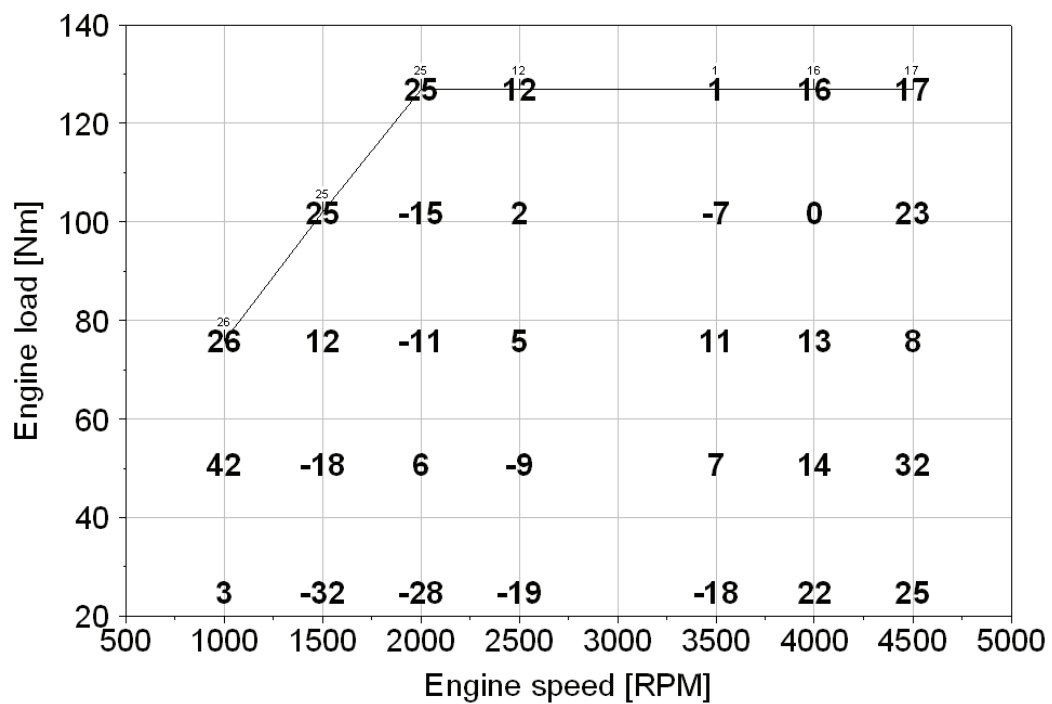
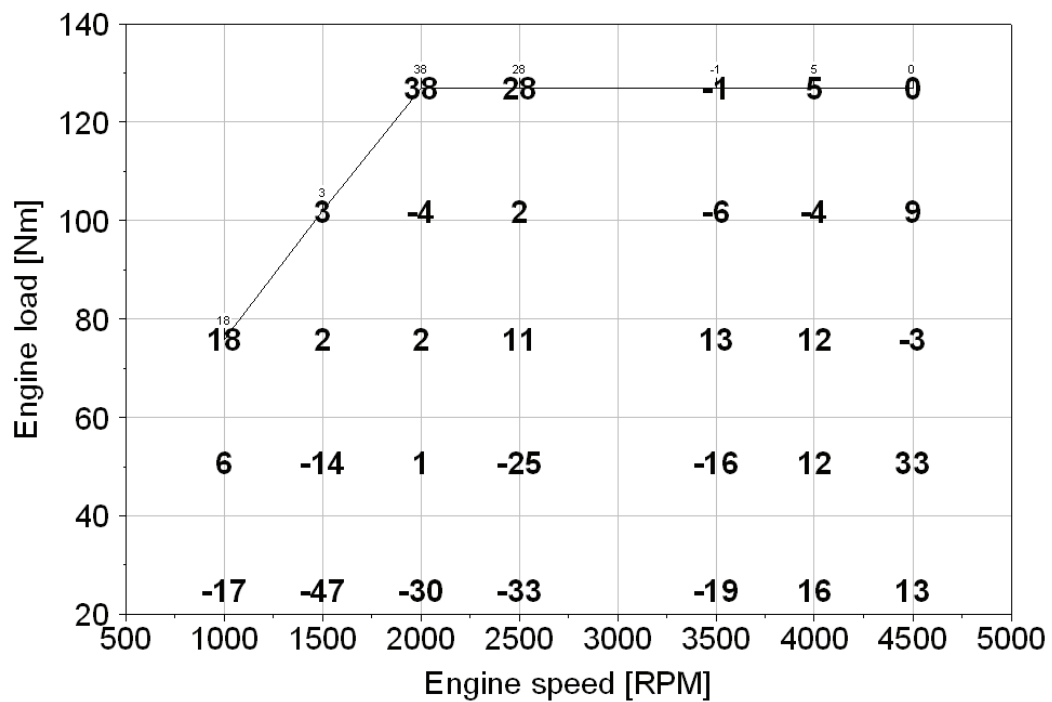
(a) $\Lambda = 0.98$ (b) $\Lambda = 1.02$

Figure 5.6: Percentage error of NO prediction calculated by multi-zone NO calculation using extended Zeldovich mechanism compared to measured value over engine operating map.

Figure (5.7) shows comparison of the multi-zone NO calculation and measured value for all of the operating point (lambda 0.98 and 1.02). The linear trend line show the best fit for $y = 1.044x$ and correlation coefficient (R^2) = 0.742. For high NO measured values, it is clear that the model predictions are satisfactory. For low NO measured values, under the low engine load condition, the model results are lower than measured values. Results from this figure are matched with the figure (5.6) which have relatively high percentage of error in the low engine load area.

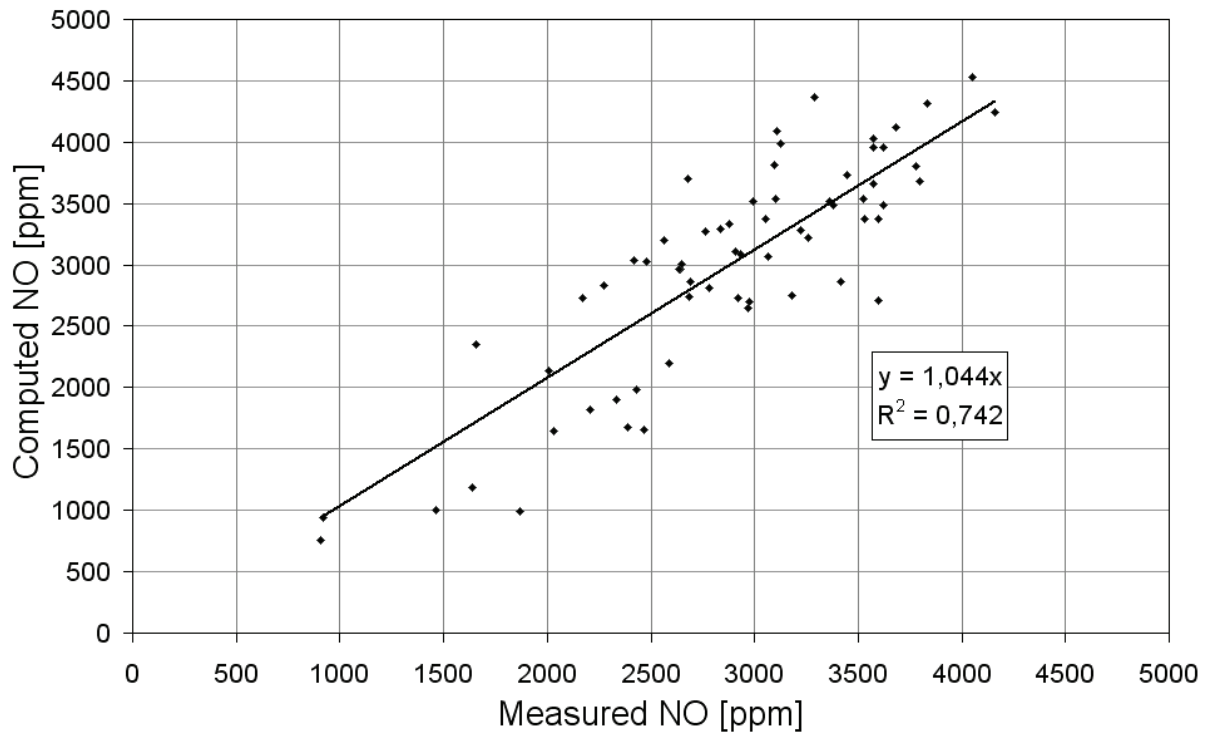


Figure 5.7: Comparison of numerous NO concentrations between multi-zone NO calculation and measured value over engine operating map (lambda 0.98 and 1.02).

An extra measurement has been done to validate the NO model when spark advance has been changed. Engine speed, load and lambda are set to be constants. The spark advanced has been varied from 13.5 deg BTC, which is the optimum point until top dead center (TC). The spark advance cannot be higher than 13.5 degree due to knocking condition. Figure (5.8) shows the variation of measured pressure and calculated burned gas temperature using two-zone model over the crank angle position.

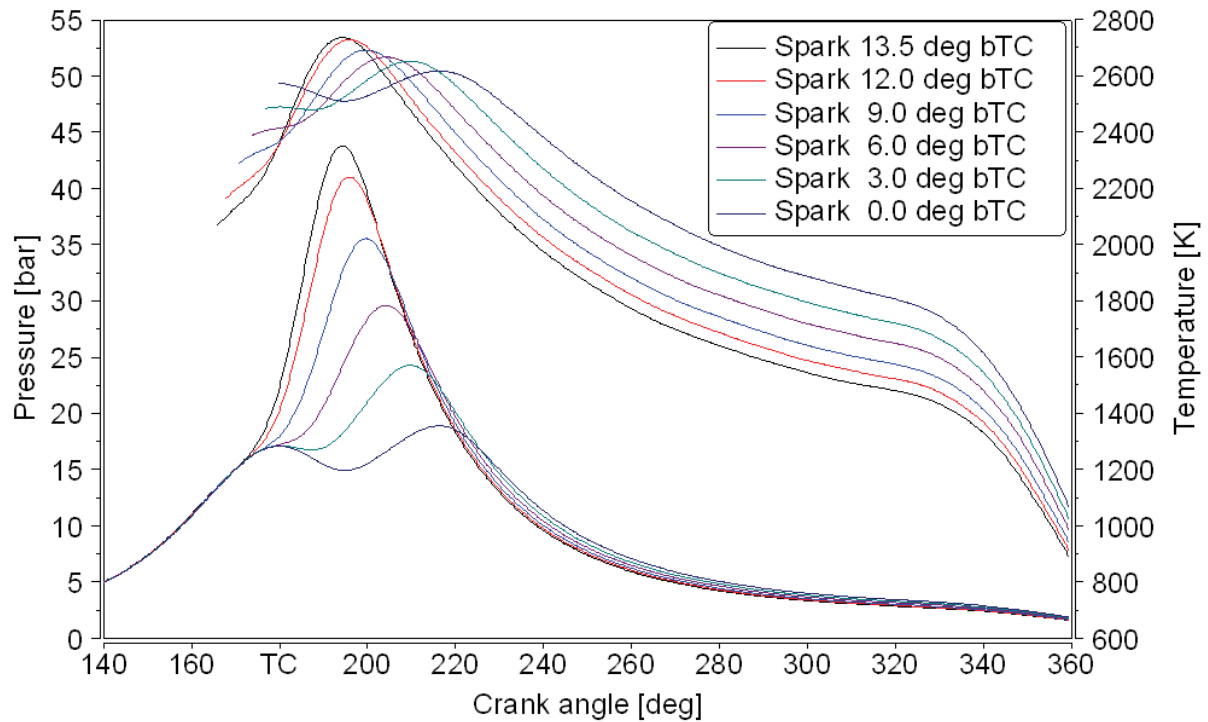


Figure 5.8: Measured pressure and calculated burned gas temperatures with variable spark advance (Engine speed 2500 rpm, load 76 Nm, lambda 1.00).

Figure (5.9) shows the measured NO values, one burned zone NO, multi-zone NO calculation. The measured NO values decrease when spark advance was late. The simple one burned zone NO model predicted only acceptable NO value when spark advance is nearly optimum point (13.5 deg BTC). The multi-zone NO model delivered very good results which have the same trend with measured value, even though the burned gas temperature during late expansion stroke from figure (5.8) are clearly higher when spark lately.

The relative errors of the model are shown in figure (5.10). The one burned zone NO calculation delivered sufficient results compared to the measured value only nearly optimum spark advance. The model result trend line is then moving far apart from the measured value when different spark advances have been reduced. The multi-zone NO calculation delivered very good result compared to the measured value for every spark advance. This is another advantage to use multi-zone NO model.

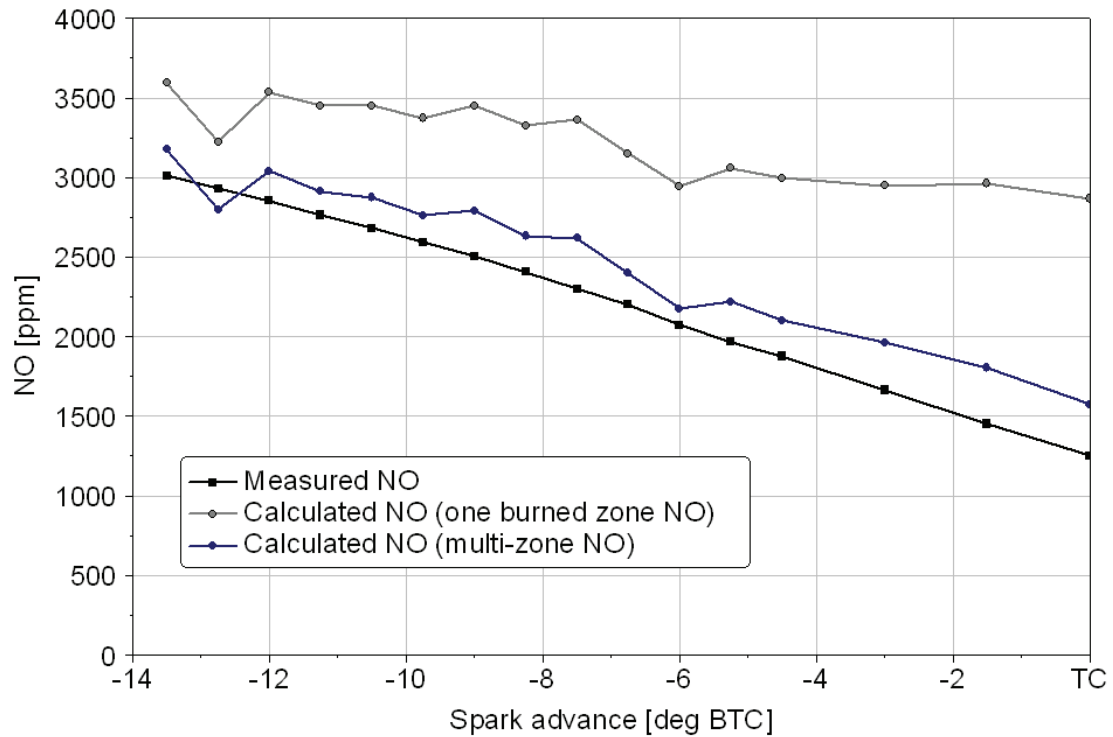


Figure 5.9: Comparison of NO concentrations between one burned zone NO, multi-zone NO calculation and measured NO values with variable spark advance (Engine speed 2500 rpm, load 76 Nm, lambda 1.00).

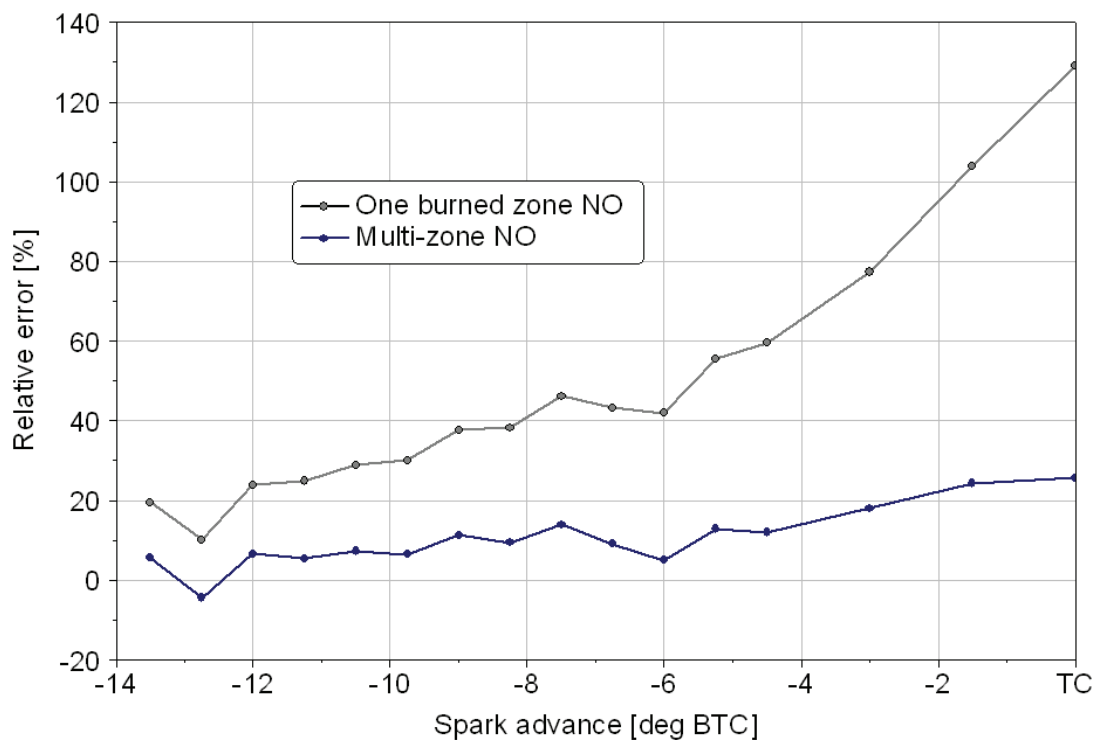


Figure 5.10: Relative error of one burned zone NO and multi-zone NO calculation compared to measured value with variable spark advance (Engine speed 2500 rpm, load 76 Nm, lambda 1.00).

5.3 Sensitivity Analysis of NO Model

Two-zone and NO model need few of input parameters, for example, engine geometry, pressure-time data and boundary conditions. Engine geometry was constant, pressure-time data was measured with high accuracy instrument, which were all reliable input data. Boundary conditions were always changed depending on engine- and surrounding condition. They were mainly taken from the engine control unit which was not a high accuracy instrument. The object to do the sensitivity analysis on the multi-zone NO model was to study effects of variable input value on NO model result. Input parameters being considered were combustion wall temperature, lambda, air-flow rate, exhaust gas recirculation (EGR), burned gas temperature. Furthermore, rate constants of extended Zeldovich mechanism were studied including different rates from other sources. The engine operating condition was at a rotational speed of 2500 rpm, load 76 Nm and lambda 0.98. Remark here that the pressure-time data from pressure sensors were not changed for the studying of sensitivity analysis.

The first parameter to be considered was cylinder wall temperature (T_w). This value was set to be initial value for one- and two-zone model as 393.15 Kelvin. Table (5.1) shows the effect of variations in the wall temperature on NO prediction. From the table, it is clear that the wall temperature is not a sensitive parameter of the model to predict NO.

Table 5.1: Variation of wall temperature and NO prediction

T_w	NO changed [%]
$T_w + 20$ K	0.57
$T_w + 10$ K	0.28
$T_w + 5$ K	0.14
T_w (initial 393.15K)	-
$T_w - 5$ K	-0.14
$T_w - 10$ K	-0.28
$T_w - 20$ K	-0.56

Air flow rate was the main input parameter. It was needed for calculation of the gas temperature at the beginning of compression process. The amount of exhaust gas recirculation, which the value was given in percentage of fresh air mass, depended on air flow rate. Furthermore, air flow

rate was needed for calculation of gas total mass in the cylinder (total mass has an effect on mass burned fraction). Figure (5.11) shows the effect of variation in the air flow rate value on NO prediction. The temperature of burned gas calculated by two-zone model and NO concentration calculated by multi-zone NO model as functions of crank angle position showed in this figure. The burned gas temperature was changed up to 150 K when the air flow rate change -5%. The NO prediction changed in percentage from table (5.2) shows that, one percentage change of air flow rate input value can affect NO prediction up to 19.01 %. It is clear that air flow rate is a very sensitive parameter of the model to predict NO.

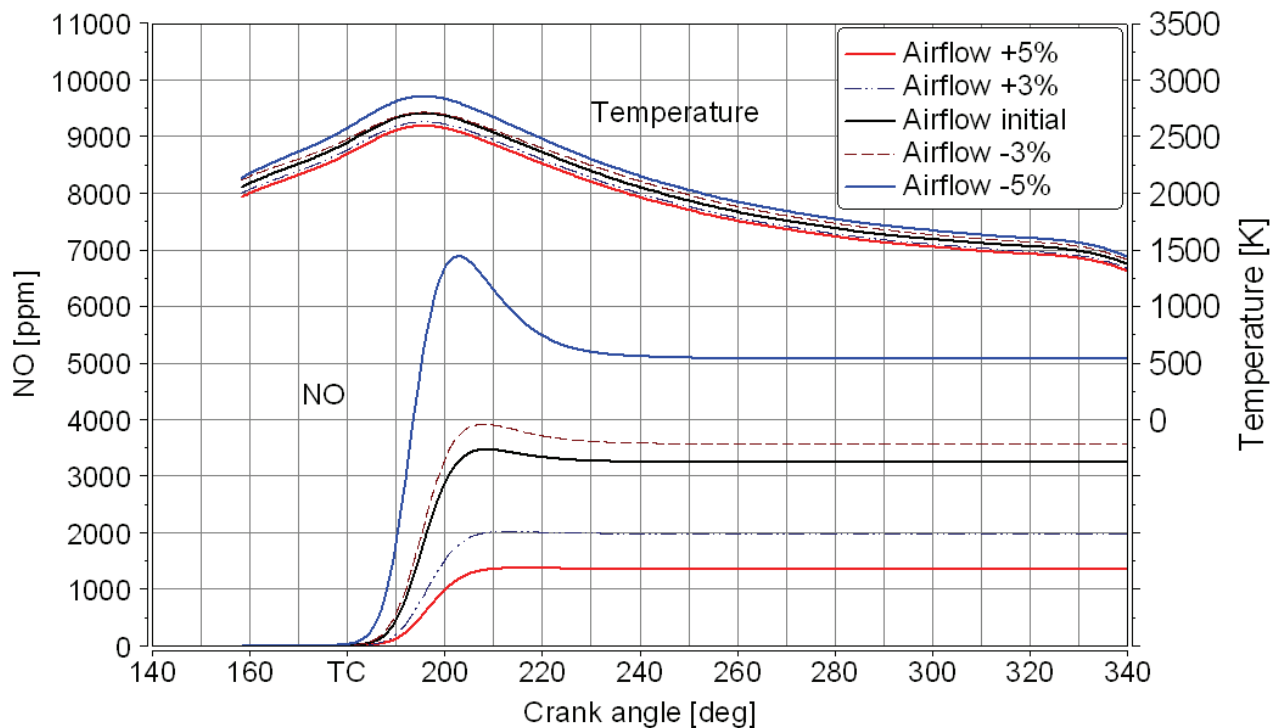


Figure 5.11: Variation of air flow rate and NO prediction.

Table 5.2: Variation of air flow rate and NO prediction.

Air flow rate	NO changed [%]
Air flow rate +5%	-58.36
Air flow rate +4%	-48.16
Air flow rate +3%	-38.01
Air flow rate +2%	-23.92
Air flow rate +1%	-19.01
Air flow rate (initial)	-
Air flow rate -1%	13.12
Air flow rate -2%	18.22
Air flow rate -3%	29.11
Air flow rate -4%	46.96
Air flow rate -5%	54.84

Exhaust gas recirculation (EGR) was one of input parameter needed for calculation of the gas temperature at the beginning of compression process, and then total mass (total mass has an effect on mass burned fraction). The experimental engine was operated with out EGR, EGR valves were closed. Then the engine control unit received information of the zero percent EGR. Actually, there was the internal EGR that remains in the cylinder and intake port. This could affect NO prediction. The internal EGR data from a car research and development company were taken and already included in the two-zone model. The amount of internal EGR was depending on engine speed and load. At the sensitivity analysis condition, there was only a few percentage of internal EGR. For the sensitivity analysis of EGR, the variable percent of EGR were used as input of two-zone model.

Table 5.3 shows the effect of variations in the exhaust gas recirculation value on NO prediction. Note that, EGR+1% means the initial internal EGR value is shifted simply by 1 %, for example, if initial value is 3%, EGR plus+1%* means 4% EGR. One can see that one percentage changed of exhaust gas recirculation input value effects on NO prediction up to 16.08 %. The reason that NO prediction changed relatively high because, for this case, 1% more internal EGR mean 1% more of total mass (only for this case). Then, this effect is nearly the same as changed the air flow rate. Extra care of internal EGR and external EGR rate should be considered.

Table 5.3: Variation of EGR and NO prediction.

EGR	NO changed [%]
EGR +4%*	-52.19
EGR +3%*	-40.56
EGR +2%*	-25.13
EGR +1%*	-16.08
EGR (initial)	-
EGR -1%*	13.23
EGR -2%*	25.35
EGR -3%*	36.01
EGR -4%*	45.27

NO concentration of S.I. engines depended primary on burned gas temperature and lambda. Burned gas temperature variation was done by shifting the temperature predicted from two-zone model by adding or reducing 10, 20, 50 and 100 K. After that, equilibrium concentrations of burned gas, which was main input of multi-zone NO model were recalculated using shifted temperature. Figure (5.12) shows the effect of variations in the burned gas temperature on NO prediction, NO concentrations as functions of crank angle position are shown. From the figure, 10 K change of burned gas temperature can affect NO prediction about 5.5 %.

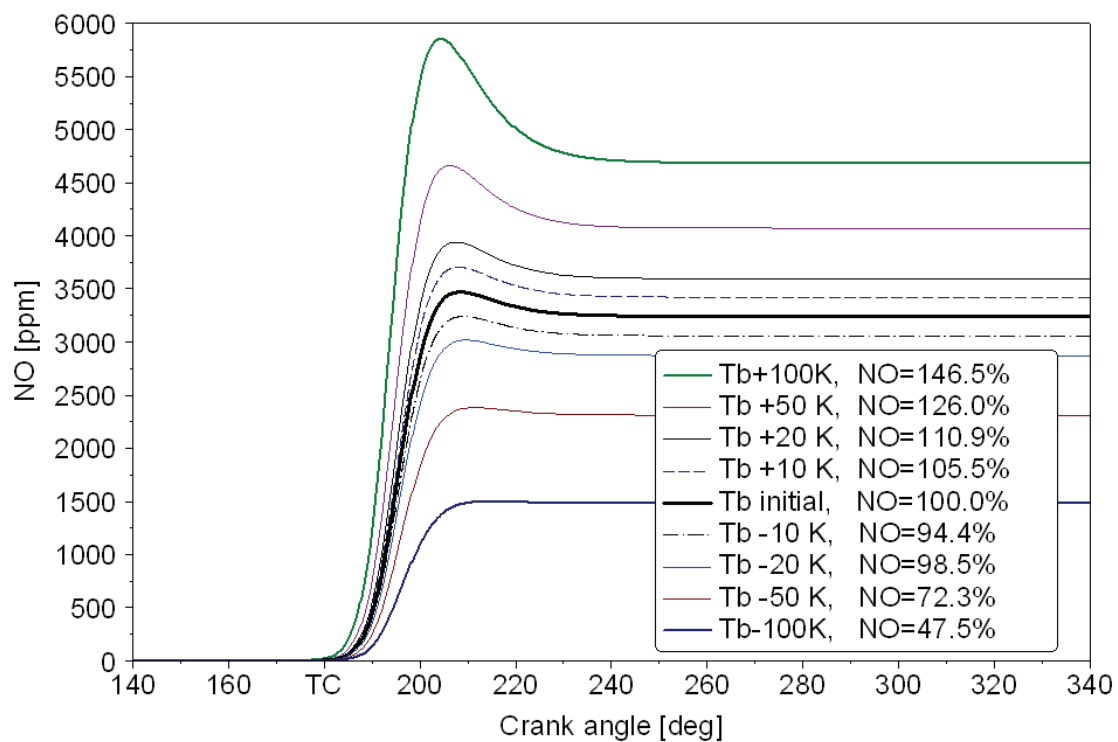


Figure 5.12: Variation of burned gas temperature and NO prediction.

Lambda was a parameter that could indicate amount of oxygen left in burned gas. Since NO formation depended on the remaining oxygen, it is important for the NO model to receive correct value of lambda for equilibrium concentration calculation. Figure 5.13 shows the effect of variations in the lambda value on NO prediction. From the figure, one percentage change of lambda input value can affect NO prediction up to 11.51 %. It is clear that lambda is a very sensitive parameter of the model to predict NO.

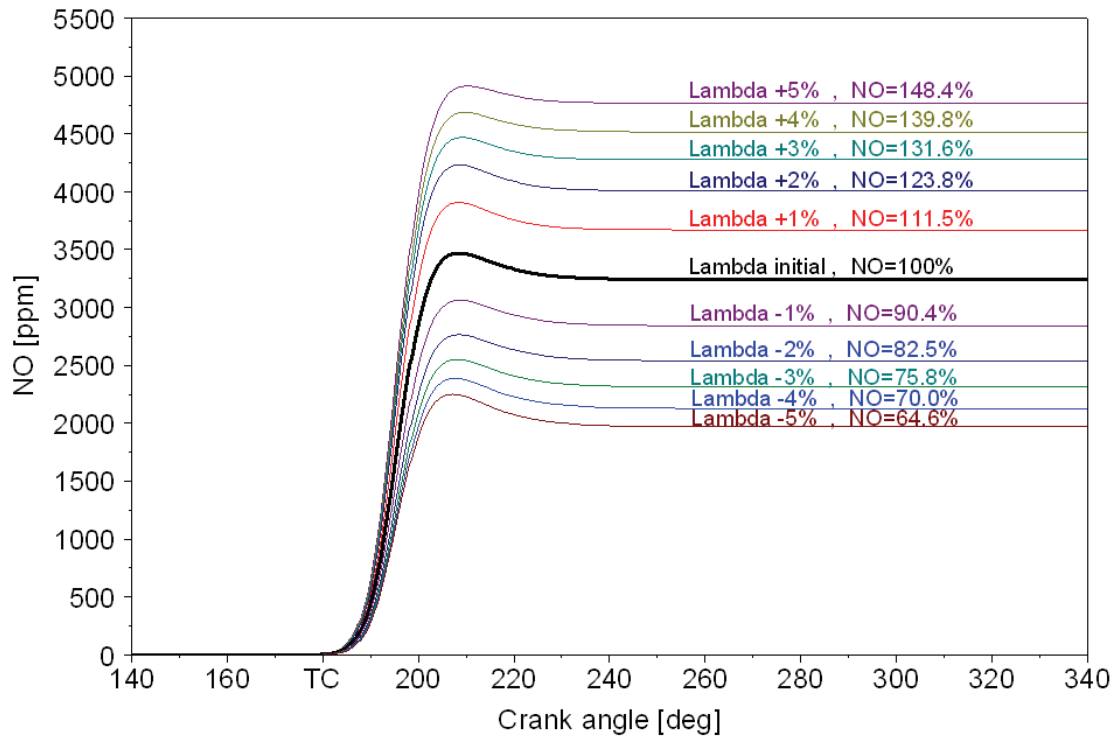


Figure 5.13: Variation of lambda and NO prediction.

There are different published rate coefficients of extended Zeldovich mechanisms. This current NO model used rate coefficients following Heywood [4]. For comparison of NO prediction with another rate coefficient, four published rate coefficients collected by [41] were then used to calculate NO. NO formations with differently rate constant are shown in figure (5.14). Rate constants of Urlaub, Pattas, Blauch/Bracco and Wray/Campbell [41] delivered different NO results compared to Heywood 9.23 %, -3.20 %, 10.65 % and -2.71% respectively.

Extended Zeldovich mechanism contains 3 equations, equation (3.51)-(3.53). The literatures [5, 6, 7, 8, 9] show that, it is needed to adjust the rate constant of extended Zeldovich mechanism to get a good result. The rate constant of equation (3.51), or called k_1 , had been adjusted up to 50% depending on the engine. To study the sensitivity analysis, the rate constants had been adjusted only one equation per time by 5 %, 10%, 20 % and 50 %. Figure (5.15) shows NO results with variation in rate constant of equation (3.51). It was also found that adjusting equation (3.52) or (3.53) have no effect on NO result less than 1%. That's mean; equation (3.51) takes the main role in the extended Zeldovich mechanism.

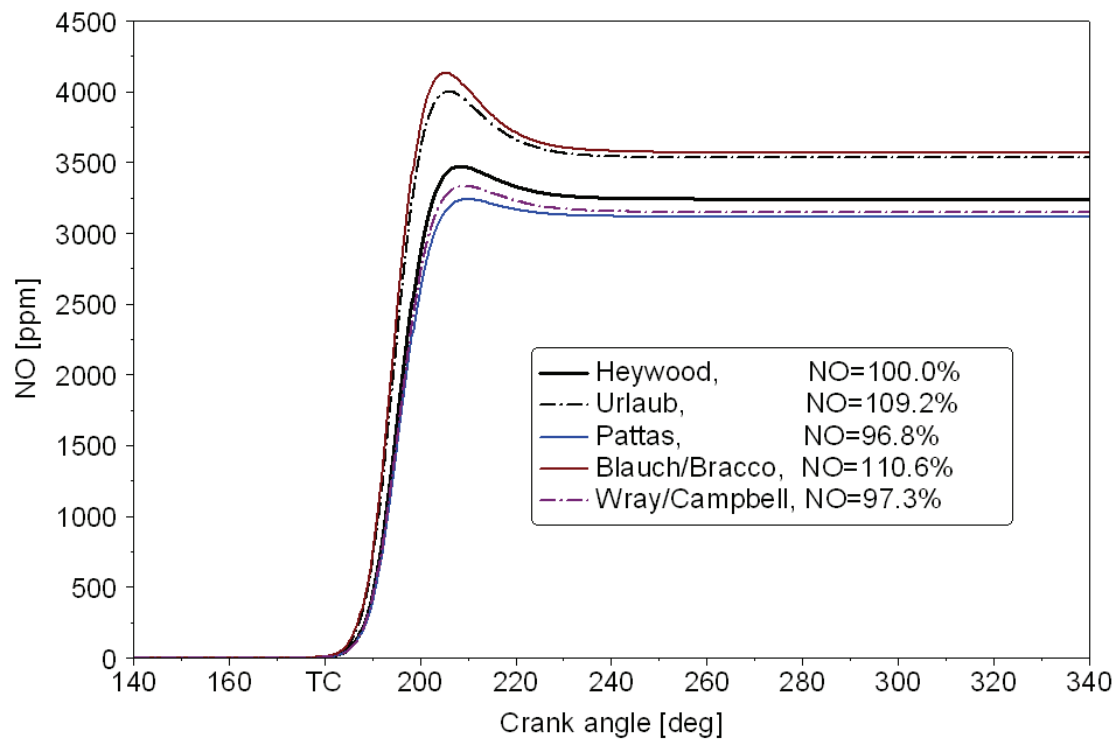


Figure 5.14: Variation of NO rate constant from publications and NO prediction.

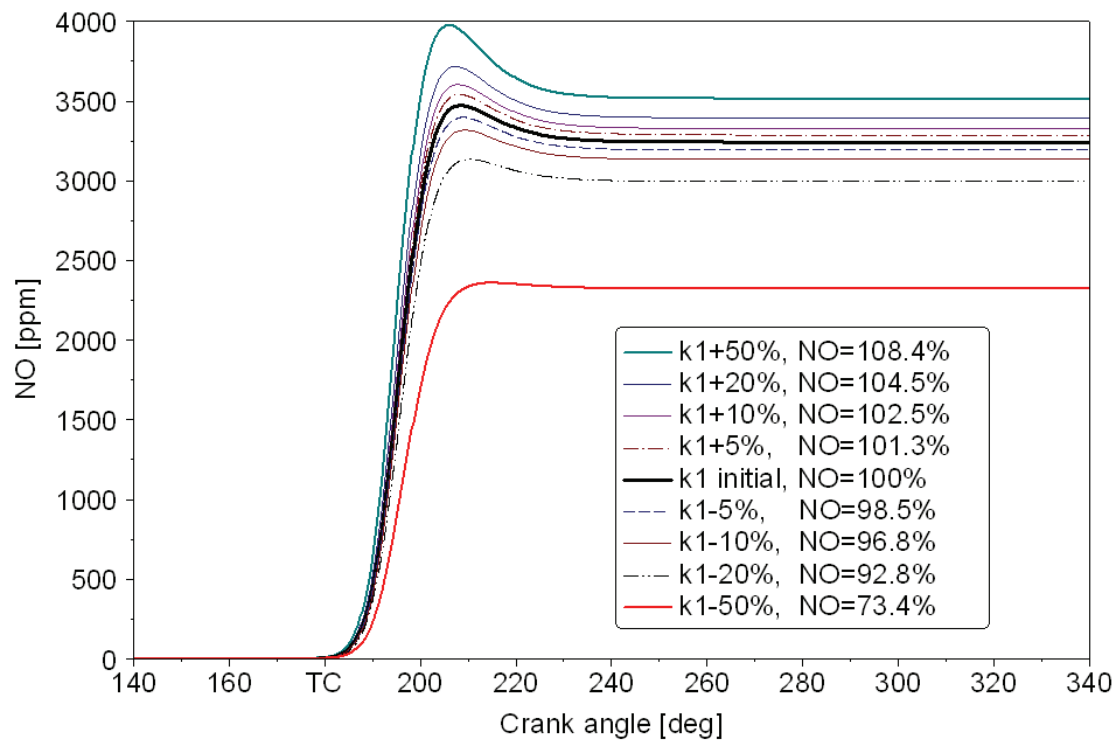


Figure 5.15: Variation of NO rate constant and NO prediction.

5.4 Summary

To predict NO emission from a gasoline directed injection engine, two-zone thermodynamic model was implemented to deliver burned gas temperature and concentration for NO model. After that, NO model using extended Zeldovich mechanism was used to predict NO. Section 5.1 showed unsatisfactory NO calculated result using the simple NO model over the engine operating map.

To achieve a better NO result, without more complex multi-zone thermodynamic model, the method to calculate NO had been modified. The multi-zone NO model had been implemented with minimum calculation time. Two-zone thermodynamic model needed 1.30 minutes for calculation of one operating condition for 4 cylinders engine on 3.2 GHz and 64-bit double CPU computer. For calculation, the simple NO model needed 1.39 seconds while the complex NO multi-zone model needed 4.01 seconds which is considered quite low. Section 5.2 showed satisfactory results of the NO multi-zone model over the engine operating map without any tuning factor. Furthermore, the extra measurement showed the advantage of multi-zone NO model over simple one-burned zone NO model when spark advances are varied.

Because of the two-zone model and NO model input came from the measurement, the value should be accurate. Section 5.3 showed the sensitivity analysis of multi-zone NO model. The NO result depended mainly on burned gas temperature and lambda. Air mass flow rate was the main reason for the changing of burned gas temperature of two-zone model because air flow rate was needed to calculate temperature of gas in cylinder when intake valve closed. Lambda was a parameter that indicated amount of oxygen left in burned gas. It had strong effect on chemical equilibrium concentration of burned gas, which was the main input of the NO model. If the lambda value from the sensor was not accurate, then the model result would not match with the measured value. The model needed accurate input value for a good prediction. The engine measurements were done only without EGR, but internal EGR should be considered.

The rate constants used in the NO model were from Heywood [4]. It is clear that current rate constants delivered NO result which lies in between the other rates showed in the literatures. Miller et al. [7, 8] concluded that it is uncomplicated to tune the reaction constant (k_1) of the

extended Zeldovich mechanism to get the matched result with the experiment of one engine speed or load. However, it is complicate to use one factor to get the matched results for all engine operating map. Rate constants from Heywood used in this model were original values without any tuning factor. In the future, these constants might be tuned depending on engine speed and load to get the better result for all operating conditions. Moreover, the current model used the averaged pressure-time data of 100 cycles to keep the low calculation time, which could contain some errors. The cycle to cycle variations and cylinder to cylinder variations were the main reason of complexity for the calculation of every individual cycle due to measurement tools, such as air flow rate sensor, lambda sensor and EGR sensor which delivered averaged value for all cylinders during the entire period of time. If individual cycle could be calculated, the model result should be improved.

6. CO Model Result

CO predictions by two-zone thermodynamic model and CO model had been validated with the engine measurements. First part shows result of two-zone model which based on chemical equilibrium. The second part shows result of CO kinetic model. The improved CO kinetic model will then be introduced for achieving a better result. The last part shows sensitivity analysis of the model.

6.1 CO Model Result Using Chemical Equilibrium

The two-zone thermodynamic model is mainly used for calculating temperature and combustion products of the gas in cylinder. The combustion product calculation is based on chemical equilibrium. The measured pressure, burned gas temperature, CO equilibrium concentration, CO measured value and burned mass fraction calculated by two-zone model are shown in figure (6.1).

The CO concentration, based on chemical equilibrium at the time of the exhaust valves opening (crank angle degree is 330 grad or 30 grad BBC), is taken as the calculated CO value. Figure (6.1) shows that at this operating point the calculated CO value is only about 50% of measured value. Shown in figure (6.2) is the percentage error of the model compared to measured value over engine operating map. The CO prediction using chemical equilibrium delivered unsatisfactory calculation with about 50 % error with lambda 0.98. Furthermore, for the lean condition with lambda 1.02, the CO prediction using chemical equilibrium delivered more than 98 % error for every operating point. This confirms again that chemical equilibrium is not a good CO prediction. The kinetic model is needed to predict CO from the engine.

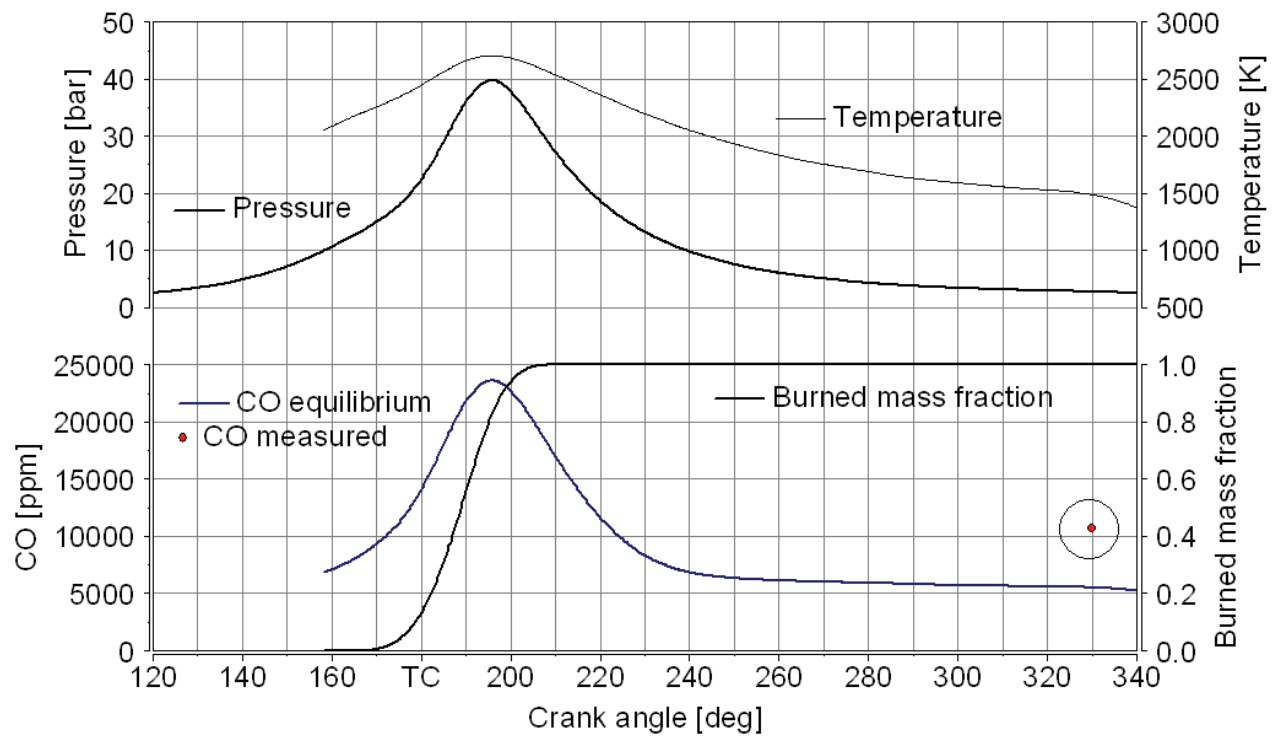


Figure 6.1: Pressure, burned gas temperature, CO concentration of the gas in the cylinder and burned mass fraction (Spark at 21.5 deg BTC, engine speed 2500 rpm, load 76 Nm and lambda 0.98).

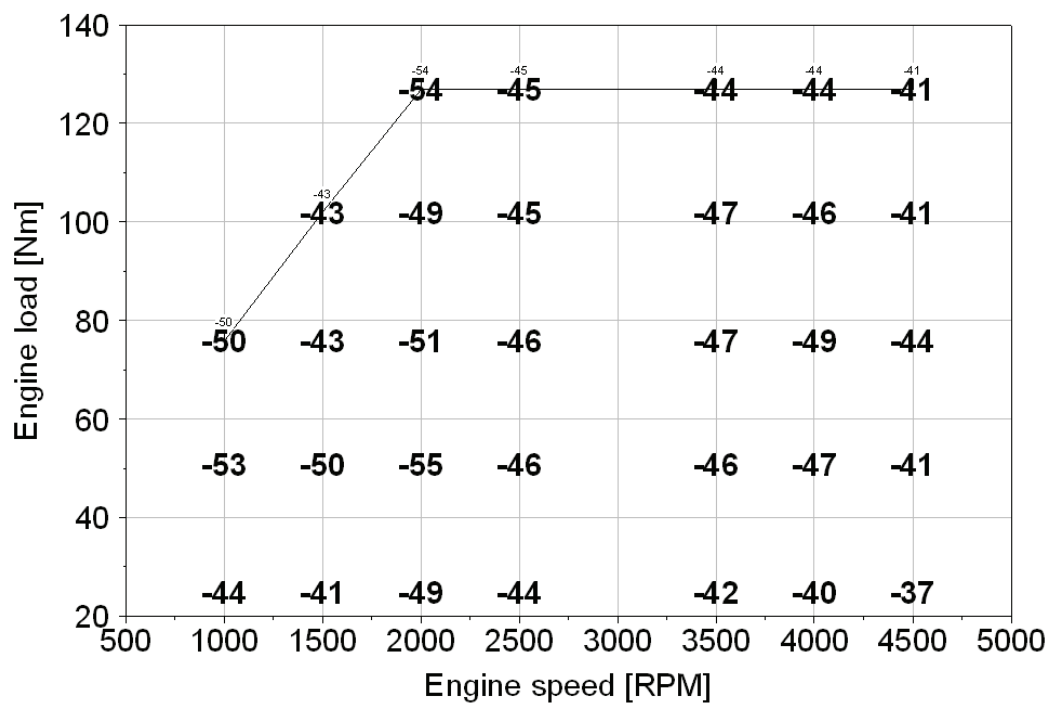


Figure 6.2: Percentage error of CO prediction using chemical equilibrium compared to measured value over engine operating map (lambda 0.98).

6.2 CO Model Result Using Kinetic Model

The prediction of CO concentration in the exhaust gas with the help of the chemical equilibrium delivered disappointing result. During the expansion stroke, the burned gas temperature dropped very strong and fast which was not a condition for chemical equilibrium. It is well known that the CO concentration is determined by kinetics; figure (6.3) shows result of kinetic model described in section 3.4.4 compared to the equilibrium concentration and measured value.

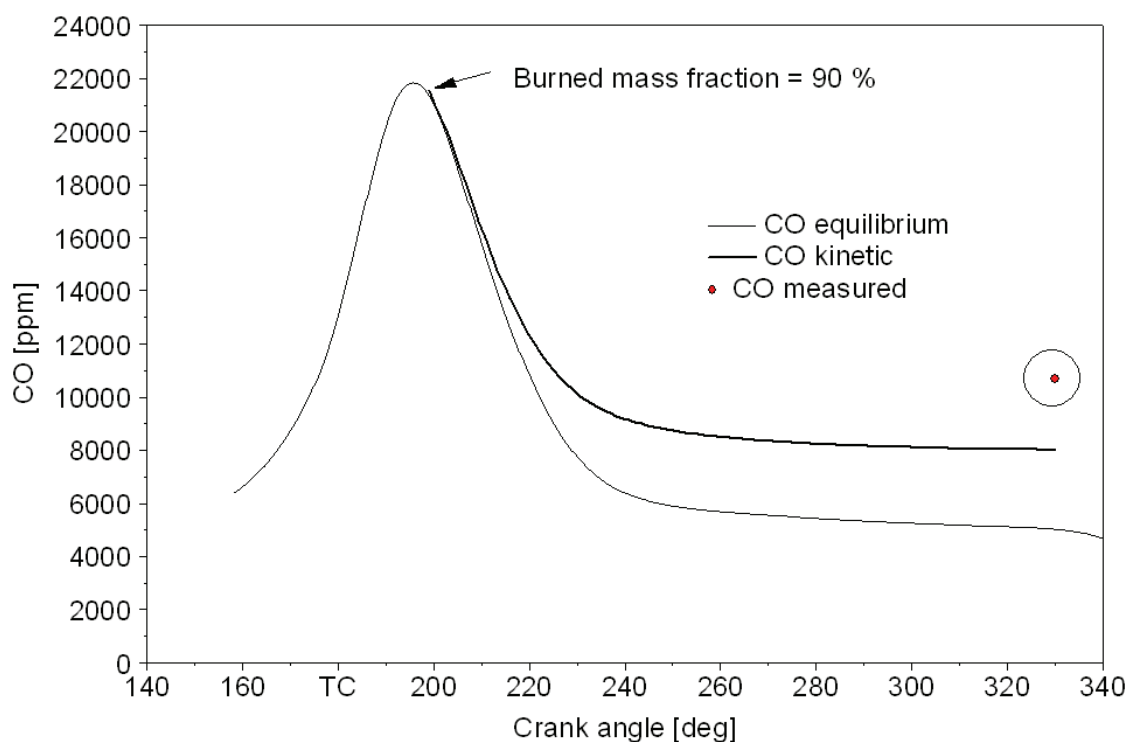


Figure 6.3: CO kinetic versus equilibrium concentration and measured value (Spark at 21.5 deg BTC, engine speed 2500 rpm, load 76 Nm and lambda 0.98).

The CO equilibrium concentration in figure (6.3) calculated by two-zone model is shown one more time. It started from the ignition point until exhaust valves open. The kinetic model started when burned mass fraction was 90% until exhaust valves opened. The reason for choosing this starting point was already described in section 3.4.4.1. Consider figure (6.1), the starting point of kinetic model (burned mass fraction is 90%) was shortly after the maximum pressure and temperature point.

The kinetic model starting point was 90 % burned mass fraction to avoid the complex chemical mechanism of gasoline during combustion. It considered only the post flame gas which contained no fresh mixture. The chemical equilibrium concentration at the starting point was delivered to the kinetic model as the initial concentration. The kinetic model used the measured pressure-time data and calculated temperature-profile from two-zone model to calculate the gas concentration.

Tests of different starting points of kinetic model were done. The same kinetic calculation method was used with new starting point (ignition point), without considering the main combustion process. Figure (6.4) shows CO concentrations calculated by kinetic model with two starting points. The CO concentration of initial starting point with 90 % burned mass fraction was compared with new starting point, at ignition point. It was found that both methods delivered the same result. Therefore, this CO kinetic model calculation could start at 90% burned mass fraction to keep low calculating time.

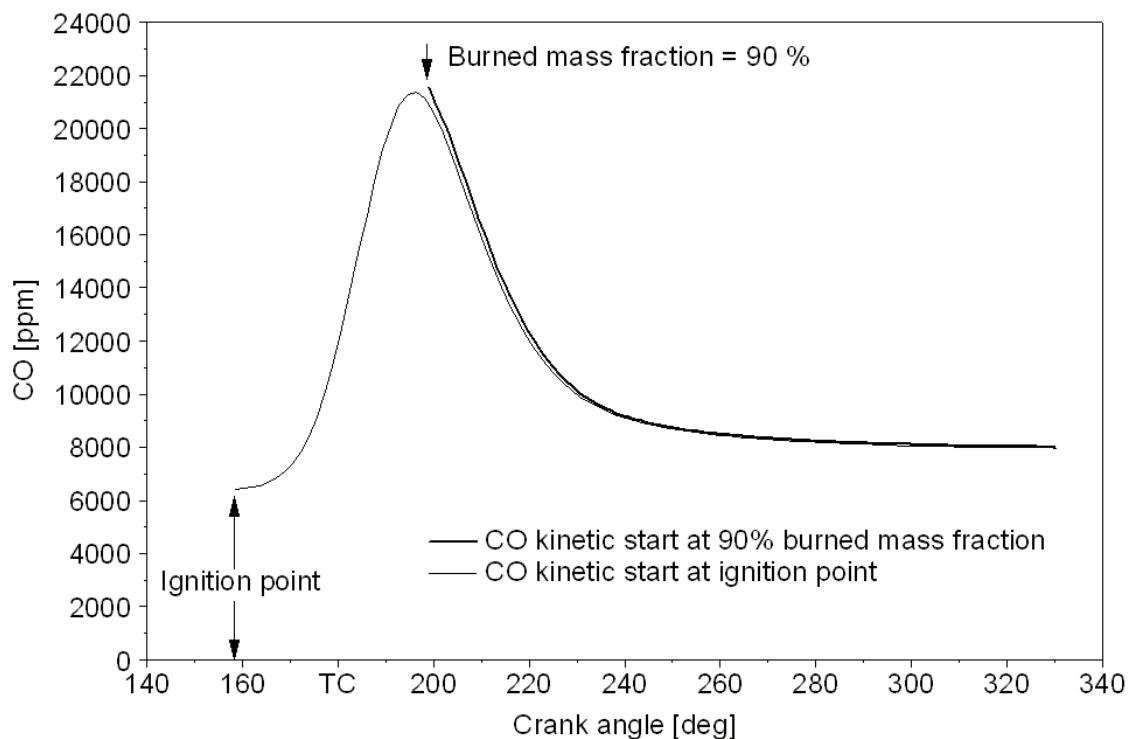
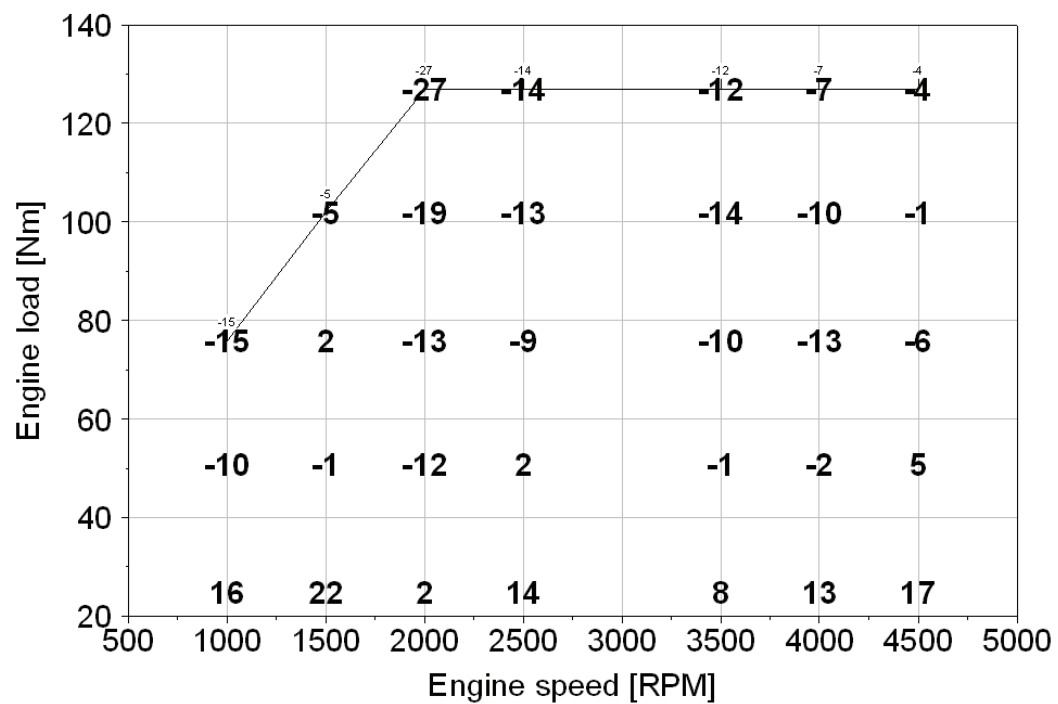
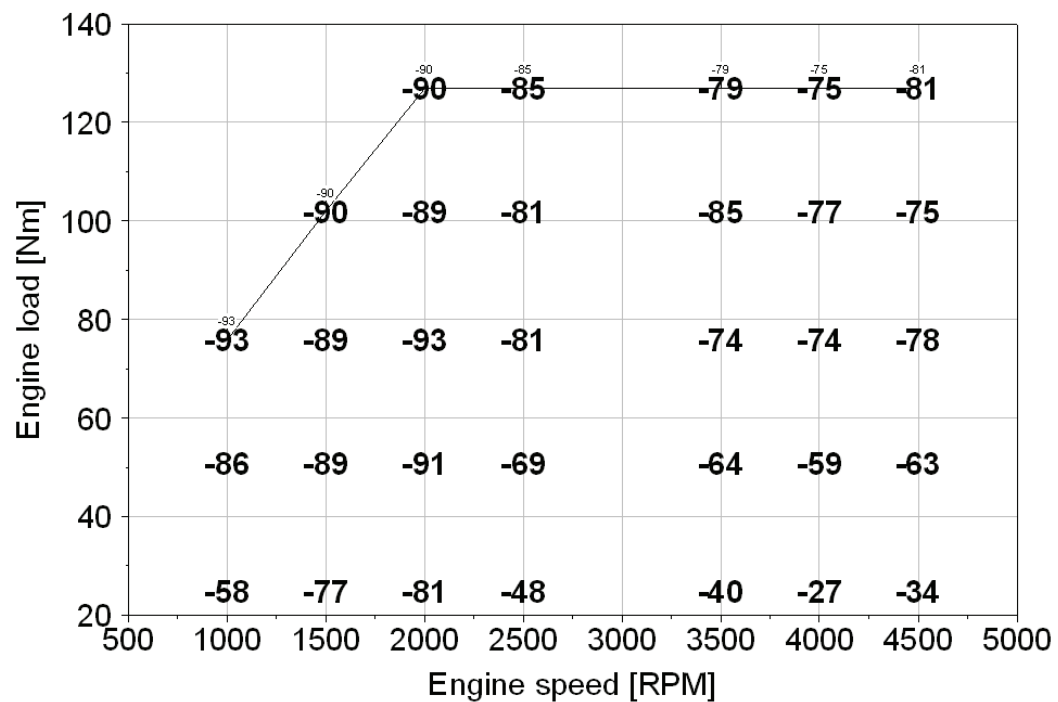


Figure 6.4: Variation of kinetic model starting point (Spark at 21.5 deg BTC, engine speed 2500 rpm, load 76 Nm and lambda 0.98).

The percentage error of the kinetic model compared to measured value over engine operating map is shown as follows:



(a) Lambda = 0.98



(b) Lambda = 1.02

Figure 6.4: Percentage error of CO prediction calculated by chemical kinetic model compared to measured value over engine operating map.

Figure (6.4) shows results of the CO kinetic model, percentage error of CO prediction calculated by chemical kinetic model compared to measured value over engine operating map. The average percentage error from figure 6.4 (a) with lambda 0.98 (rich mixture) is 10.0 %. The CO prediction errors of medium and high loads have relatively low variation in this area. Under the constant engine speed, the variation of error is decreased when engine load becomes higher. Moreover, under the low load, the CO predicted values are higher than measured values. This may be caused by a large variation and a significant amount of residual mass left over from the previous cycle which is hard to measure. The information from the car research and development company reveals that the internal EGR value could be two times the measured value. Under the low load and low speed condition, air flow rate was relatively low but percentage of internal EGR was high due to the engine was strongly throttled. It was hard to get the correct value of internal EGR. This could be the explanation for high variation error under the low speed and low load condition.

The average of percentage error from figure (6.4) (b) with lambda 1.02 (lean mixture) is 74.2 %. This result is not satisfactory and the reason of high error should be investigated. Even though, the overview of the results in figure (6.4) (a) and (b) of kinetic model is much closer to the real CO values from the measurement than using the CO concentration from chemical equilibrium. This is the advantage of the kinetic model over the chemical equilibrium prediction from two-zone model.

It is well known that the CO emission from engine depends primary on lambda. Since the model results were good with rich mixture but poor with lean mixture, the extra measurements had been done on some of operating points in the engine operating field to find the effect of lambda on the CO model. Lambda values had been varied from 0.96-1.20 with constant engine speed, load and spark advance. The measured and predicted CO values are shown in two following figures.

Figure (6.5) and (6.6) show the measured-, calculated- and absolute error of CO concentration with variable lambda. Note that both axes in the figure have the same scale, only the zero point is different. The trend lines of both pictures are similar and also same as other operating points. The CO kinetic model delivered good result with rich mixture. With lambda 0.98, the relative error is about -20%, like another point in figure (6.4) (a). The absolute error reached maximum value when lambda was closer to one or the mixture was slightly lean.

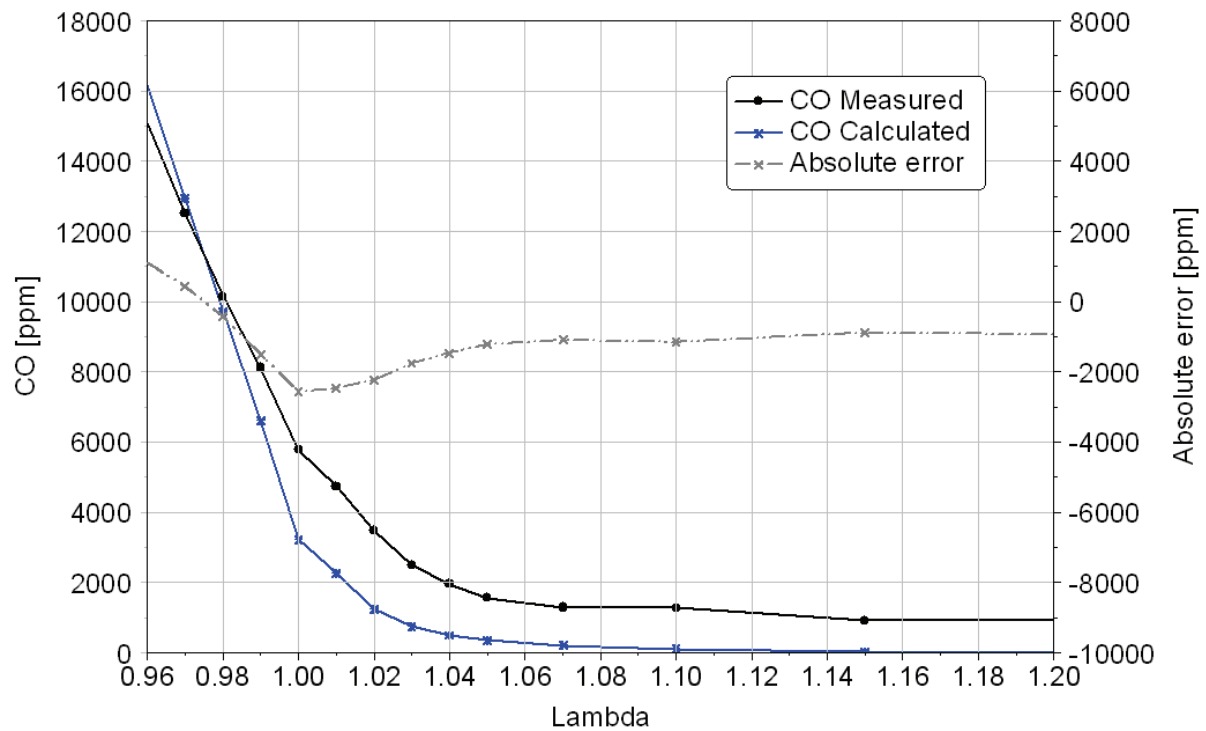


Figure 6.5: Measured versus calculated CO concentration and absolute error with variable lambda (Engine speed 2500 rpm, load 76 Nm).

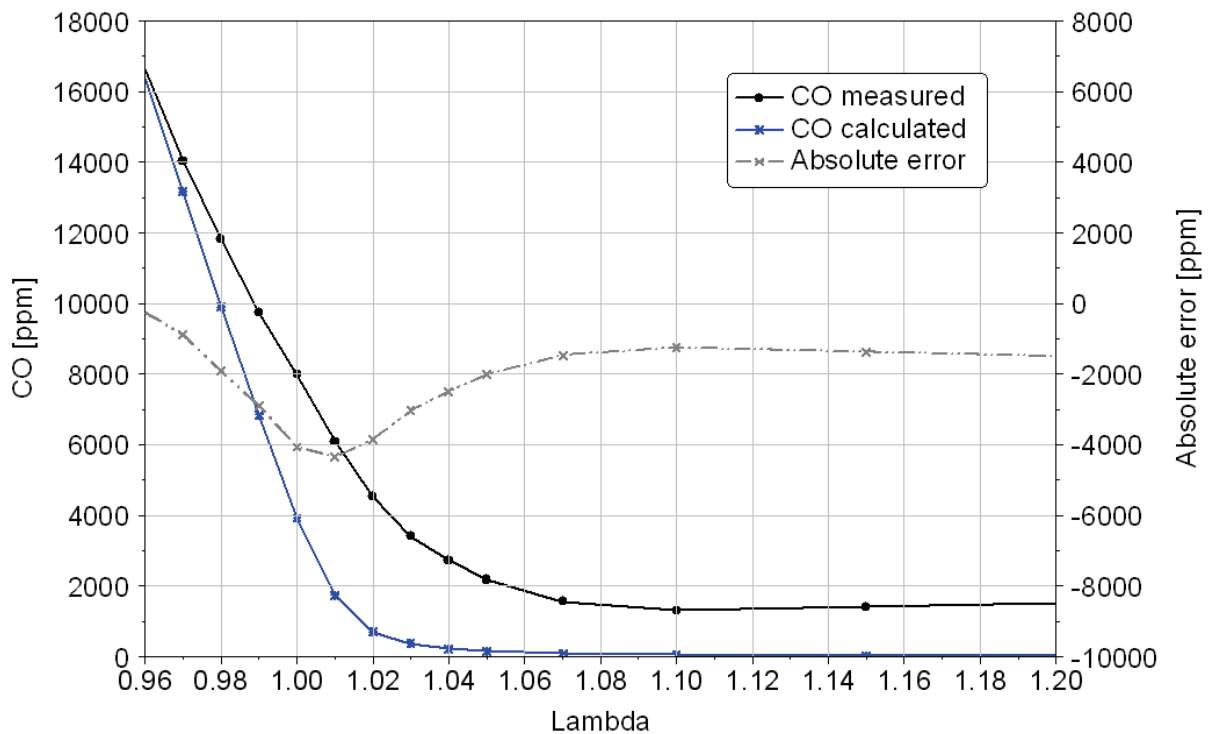


Figure 6.6: Measured versus calculated CO concentration and absolute error with variable lambda (Engine speed 4500 rpm, load 76 Nm).

Under the lean mixture, it is found that the CO model predicted CO values relatively constant and too low compared to measured value. That is because the CO kinetic model considered only CO which is produced in post flame gas. Results from figure (6.5) and (6.6) are then similar and comparable to the complex CFD model of D'Errico et al. [15] and others in [12, 13, 42, 43].

Heywood [4] made the assumption that under the lean mixture, measured CO emissions were higher than any of the model based on kinetically controlled bulk gas phenomena because some of UHC from crevices volume, and oil layers or deposits were only partial oxidized to CO. These CO values were high compared to the CO came from bulk gas under the lean mixture, but low under the rich mixture. Hence, models based on kinetically controlled bulk gas delivered good result under the rich- and nearly stoichiometric mixture. Ferguson [24] made a comment that in lean-running engines there appeared to be an additional source of CO caused by the flame-fuel interaction with the walls, the oil films, and the deposits.

It can be concluded that the UHC is the main reason for under prediction of the CO model in lean mixture area [4, 23, 24] because it is the additional source of CO especially under the lean mixture. The currently CO model could be improved by considering the UHC oxidation. Details of improved model are described in next part.

6.3 Improved CO Model

Section 6.2 shows that the kinetic CO model delivered satisfactory result only in rich mixture area and poor result in lean mixture area. The model should be improved to get a better CO prediction especially in lean mixture area. It has been found that UHC which was oxidized to CO was one of CO source that took an important role when mixture was lean. [4, 24, 44, 45] The current model considered only the post flame gas, which fuel was already burned. It did not include the CO that came from UHC oxidation. Cheng et al. [26] showed that some 9% of the fuel escaped from the burning during the normal combustion process and went into HC mechanisms. Next, 3.7% of total fuel through HC mechanisms was oxidized to CO₂ or CO in combustion chamber and exhaust port, and this value was not included in any CO models. Main HC sources can be described as follows:

- Crevices

Crevices are narrow volumes present around the surface of the combustion chamber which the flame cannot propagate. They occur around the piston, head gasket, spark plug and valve seats, and represent about 1 to 2% of clearance volume [46]. During compression and combustion, these volumes are filled with unburned charge. During expansion, part of the unburned HC-air mixture leaves the crevices and is oxidized in the hot burned gas mixture.

- Quench Layers

Quench layers are regions very close to the cooled engine walls through which a premixed flame can no longer propagate.

- Lubricant Oil Layer

The presence of lubricant oil on the liner walls creates an opportunity for fuel to be absorbed before flame passage.

Unburned HC left in the crevices is oxidized in the hot burned gas mixture. Hence, it is not a main source of CO from HC. Unburned HC from lubricant oil layer is also not a source of CO because it is unburned fuel, and the oxidation occurred only small part. The main CO source from HC came from quench layer because the temperature in this area is low such that flame front cannot reach but it is still high enough that air/fuel mixture can be oxidized at temperature about 1000-1500 K. At this typical temperature, pressure and short time condition in combustion chamber, the fuel is oxidized mainly to CO and unburned HC which is not a complete combustion.

The model could be improved by considering the quench layers. These quench layers are then added into two-zone model as the third-zone which located at the combustion chamber wall. The size of these zones depends on the distance from the wall where the flame cannot reach. This distance is assumed to be the same size as thermal boundary layer thickness. The thermal boundary theory is then introduced to find the thermal boundary layer thickness and temperature in this zone which will be described in next part. After that, the oxidation of mixture in this zone should be considered in order to get the CO from quench layers.

6.3.1 Thermal Boundary Layer Thickness

The thermal boundary layer thickness can be calculated following the method of Eiglmeier's dissertation named "Phänomenologische Modellbildung des gasseitigen Wandwärmeüberganges in Dieselmotoren" or "The phenomenological modelling of the gas-phase heat transfer in diesel engine"[47]. The boundary layer thickness calculation was based on equations of two-dimensional, transient and compressible flow over a flat plate. With assumptions: 1. The pressure in cylinder was homogeneous; 2. The velocity- and temperature gradient in direction of flow (coordinate x , velocity of u) were negligible compared with their gradients perpendicularly to the direction of flow (coordinate y , velocity of v); 3. The development of heat by viscous dissipation within the boundary layer was negligibly small; the model could be reduced to one-dimension. The equation of continuity-, momentum- and energy equation were introduced as the following equations, which could also be found in [48].

$$\frac{\partial \rho}{\partial t} + \frac{\partial}{\partial y}(\rho v) = 0 \quad (6.1)$$

$$\rho \left(\frac{\partial u}{\partial t} + v \frac{\partial u}{\partial y} \right) = \frac{\partial \tau}{\partial y} \quad (6.2)$$

$$\rho c_p \left(\frac{\partial T}{\partial t} + v \frac{\partial T}{\partial y} \right) = \frac{\partial q_{conv,i}}{\partial y} + \frac{\partial p}{\partial t}. \quad (6.3)$$

An integration of the energy equation (6.3) over the boundary layer thickness $\delta_{th,i}$ supplies as follows:

$$\int_0^{\delta_{th,i}} \rho c_p \frac{\partial T}{\partial t} dy + \int_0^{\delta_{th,i}} \rho c_p v \frac{\partial T}{\partial y} dy = \int_0^{\delta_{th,i}} \frac{\partial q_{conv,i}}{\partial y} dy + \int_0^{\delta_{th,i}} \frac{\partial p}{\partial t} dy. \quad (6.4)$$

The application of the reversal of the product rule for the second term and attention to the continuity equation (6.1) results in

$$\int_0^{\delta_{th,i}} \rho c_p \frac{\partial T}{\partial t} dy + \left[\rho v T c_p \right]_0^{\delta_{th,i}} + c_p \int_0^{\delta_{th,i}} T \frac{\partial \rho}{\partial t} dy = -q_{conv,i} + \frac{dp}{dt} \delta_{th,i}. \quad (6.5)$$

The first and the third term on the left side are summarized, continues as follows:

$$c_p \int_0^{\delta_{th,i}} \frac{\partial(\rho T)}{\partial t} dy + [\rho v T c_p]_0^{\delta_{th,i}} = -q_{conv,i} + \frac{dp}{dt} \delta_{th,i}. \quad (6.6)$$

The application of the ideal gas law,

$$\rho T = \frac{p}{R} \quad (6.7)$$

and the reapply of the continuity equation (6.1) for the velocity v in sufficiently large distance from the wall specifies after few transformations, the equation (6.6) can be written as follows:

$$-T_{conv,i} c_p \frac{\partial}{\partial t} \int_0^{\delta_{th,i}} \rho dy = -q_{conv,i} + \frac{dp}{dt} \delta_{th,i} \left(1 - \frac{c_p}{R} \right). \quad (6.8)$$

After introduction of averaged gas density $\rho_{m,i}$ within the thermal boundary layer equation (6.8) becomes

$$-T_{conv,i} c_p \left(\frac{d\rho_{m,i}}{dt} \delta_{th,i} + \frac{d\delta_{th,i}}{dt} \rho_{m,i} \right) = -q_{conv,i} + \frac{dp}{dt} \delta_{th,i} \left(1 - \frac{c_p}{R} \right). \quad (6.9)$$

Further simplifying transformation results in the conditional equation for the thermal boundary layer thickness, which is used in the computation of the convective heat transfer coefficient within the available heat transfer model

$$\frac{d\delta_{th,i}}{dt} = \frac{\rho_g}{\rho_{m,i}} \frac{dp}{dt} \frac{1}{p\kappa} \delta_{th,i} - \frac{1}{\rho_{m,i}} \frac{d\rho_{m,i}}{dt} \delta_{th,i} + \frac{q_{conv,i}}{\rho_{m,i} c_p T_{conv,i}}. \quad (6.10)$$

where ρ_g is density of the bulk gas in cylinder. Eiglmeier defined T_{conv} and q_{conv} as follows:

$$T_{conv,i} = T_u \left(1 - \frac{m_b}{m} \right) + T_b \frac{m_b}{m} \quad (6.11)$$

$$q_{conv} = \alpha_{conv} (T_{conv} - T_{wall}) \quad (6.12)$$

T_{conv} is based on average temperature of bulk gas and is the same as temperature from one-zone model. α_{conv} is calculated using heat transfer model from Woschni.

Baehr and Stephan [49] determined the boundary layer in completely different way, on the basis of equation (6.12) which can be rewritten as follows:

$$\alpha = \frac{q_{wall}}{T_g - T_{wall}} \quad (6.13)$$

In order to calculate heat transfer coefficient α , the immediate point close to the wall (wall distance $y \rightarrow 0$) is considered. Except with extremely thin gas, the fluid sticks to the wall, its speed here are directly zero, and energy can be transported only by thermal conduction. For this case, the law of Fourier applies:

$$q_{wall} = -\lambda \left(\frac{\partial T}{\partial y} \right)_{wall} \quad (6.14)$$

λ is heat conductivity of the fluid at wall temperature. The result of heat transfer rate from the upward gradient of the temperature distribution in the fluid at the wall. Combined equation (6.13) and (6.14), results as follows:

$$\alpha = \frac{-\lambda \left(\frac{\partial T}{\partial y} \right)_{wall}}{T_g - T_{wall}} \quad (6.15)$$

and further transformation

$$\frac{\lambda}{\alpha} = -\frac{T_g - T_{wall}}{\left(\frac{\partial T}{\partial y} \right)_{wall}} \quad (6.16)$$

From this equation, the following figure can be delivered. The following figure (6.7) shows (a) an example of temperature profile in boundary layer, (b) boundary layer determination. From the figure, λ / α is a good approximation for the thermal boundary layer thickness.

$$\delta_{th} = \frac{\lambda_{fluid}}{\alpha} \quad (6.17)$$

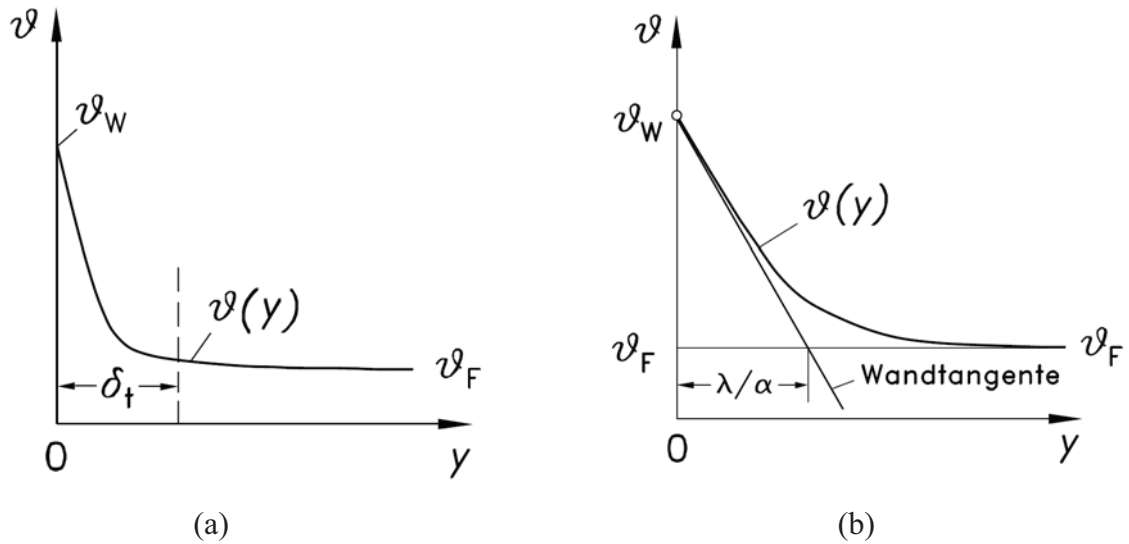


Figure 6.7: Temperature profile and thermal boundary layer thickness [49].

The solution of this equation however generally supplies too small thickness of boundary layer. Therefore, the tangent at height level of the middle temperature of the temperature profile is applied, so that the error becomes smaller. This means that the heat conductivity with the middle temperature of the boundary layer is selected.

Furthermore, the different boundary layer calculation methods had been tested, for example, by Lyford-Pike and Heywood [50], and Merker [51], which determined the boundary thickness over a relationship to the Reynolds number. When the piston was at top dead centre position, the Reynolds number became zero. This did not correspond to the facts. Furthermore; Hajireza et al. proved in [52] that the boundary layer thickness had a minimum value of 0.01 mm. If this value were defined, then calculation of boundary layer thickness would be unnecessary. However, the minimum thickness value during combustion was a crucial factor of the determination of CO emissions through quench layer. Then, both methods of Eiglmeier and Baehr were introduced and compared later in this chapter.

6.3.2 Thermal Boundary Layer Temperature

There are literatures which are based on different concepts for the temperature field of boundary layer. It is important to select the correct method to determine the temperature field with the problem depending on velocity of the flow, turbulence and etc. To maintain simplicity and low calculating time, two methods for determining temperature profile were chosen and introduced as follows:

- Temperature Field using 1/7 Power Law

The 1/7 power law for the velocity profile of fluid is described in the following equation

$$\frac{v(y)}{v_{\infty}} = \left(\frac{y}{\delta_{flow}} \right)^{1/7} \quad (6.18)$$

The temperature field is very similar to the flow field. Thus the temperature profile can be described similar through

$$\frac{T(y) - T_{wall}}{T_{gas} - T_{wall}} = \left(\frac{y}{\delta_{th}} \right)^{1/7} \quad (6.19)$$

Where y is the distance from the wall, $0 \leq y \leq \delta$. δ_{th} is the boundary layer thickness. T_{gas} is the incylinder gas temperature. $T(y)$ is the temperature at y distance. In order to determine an average value for the boundary layer temperature, equation (6.19) is transformed and integrated as follows over the boundary layer thickness, δ_{th} :

$$\bar{T} = \frac{1}{\delta_{th}} \int_0^{\delta_{th}} \left[(T_{gas} - T_{wall}) \left(\frac{y}{\delta_{th}} \right)^{1/7} + T_{wall} \right] dy \quad (6.20)$$

Then

$$\bar{T} = \frac{7}{8} (T_{gas} - T_{wall}) + T_{wall} \quad (6.21)$$

- Temperature Field using Arithmetic Mean

This is the simplest method and also used in [48, 50] to determine not only temperature but also heat conductivity, viscosity and density. It is found that this method can supply quite close results to the reality.

$$\bar{T} = \frac{T_{gas} - T_{wall}}{2} + T_{wall} = \frac{T_{gas} + T_{wall}}{2} \quad (6.22)$$

6.3.3 New Chemical Model for Thermal Boundary Layer

Due to the fact that the gas mixture in the third zone of improved CO model had not reacted directly with flame front and the two reaction mechanisms of Glassman and Newhall are suitable to apply only with the post flame gas, a new chemical mechanism is needed. Reactants in the third zone are gasoline/air mixture and the reaction occurs at temperature range of 1000-1500 K. A simple method to calculate the CO in the third zone is to use the carbon oxidation factor and another method is the chemical kinetic model with gasoline mechanism. Both methods are described as follows:

- CO Calculation by Oxidation Factor

In the literatures of [20, 21, 53], the post oxidation of HC in the exhaust system from exhaust runner to exhaust pipe was investigated accomplishing for different fuels, including isooctane. The exhaust gas temperatures were between 1500 K, when exhaust valves opened and 1300 K at the end of exhaust stroke. Result showed 40 % of HC were oxidized in the exhaust system. Mendillo and Heywood [20] showed that the rate of oxidation depended on lambda which had maximum value when lambda 1.

The complete simplified method was introduced regarding an empirical equation to estimate CO concentration of the gas in the third zone (thermal boundary layer) that oxidized to CO.

$$c_{CO} = c_{isooctane} * Number_of_C(atom) * factor \quad (6.23)$$

$c_{isooctane}$ is isooctane (fuel) concentration, c_{CO} is CO concentration which is a product of isooctane oxidation, $Number_of_C(atom)$ is 8 for isooctane and $factor$ is the percentage of fuel that oxidized to CO and is set to 0.4 for 40% oxidation. Carbon dioxide is not considered and assumed not occur since the temperatures are not high enough. The oxidation temperature is assumed to be the same as thermal boundary layer temperature. With this method, the quantities of CO in the boundary layer can be simple determined.

- CO Calculation by Chemical Kinetic Model

The temperature of thermal boundary layer is around 1000-1500 K. If one assumed that the oxidation temperature is the same as thermal boundary layer temperature, the oxidation mechanism of isooctane at this temperature and pressure range is needed for kinetic calculation. Hasse [54] studied the quenching of laminar premixed isooctane flame at cold wall using detailed kinetics. Different reaction mechanisms were used and compared. The complex mechanism of isooctane which considered 189 reactions and 56 species [55] and its extension [56] were studied. Hasse had modified and reduced these mechanisms to 29 species and 48 reactions and received satisfactory result. This mechanism [54] should be suitable for this work, since Hasse studied on the same problem of flame quenching and the mechanism was small in order to keep minimum calculating time. The reactants, pressure- and temperature time data of the thermal boundary layer were then delivered to kinetic model solving by CHEMKIN.

6.4 Improved CO Model Result

In this part, results of improved CO model are presented step by step. Furthermore, the decision on choosing methods is also described.

6.4.1 Thermal Boundary Layer Temperature Result

The average boundary layer temperatures according to the methods specified in section 6.3.2 are shown in figure (6.8). The bulk gas temperature in the cylinder calculated by one-zone model is shown to compare the difference of temperature between bulk gas- and averaged thermal boundary layer temperature.

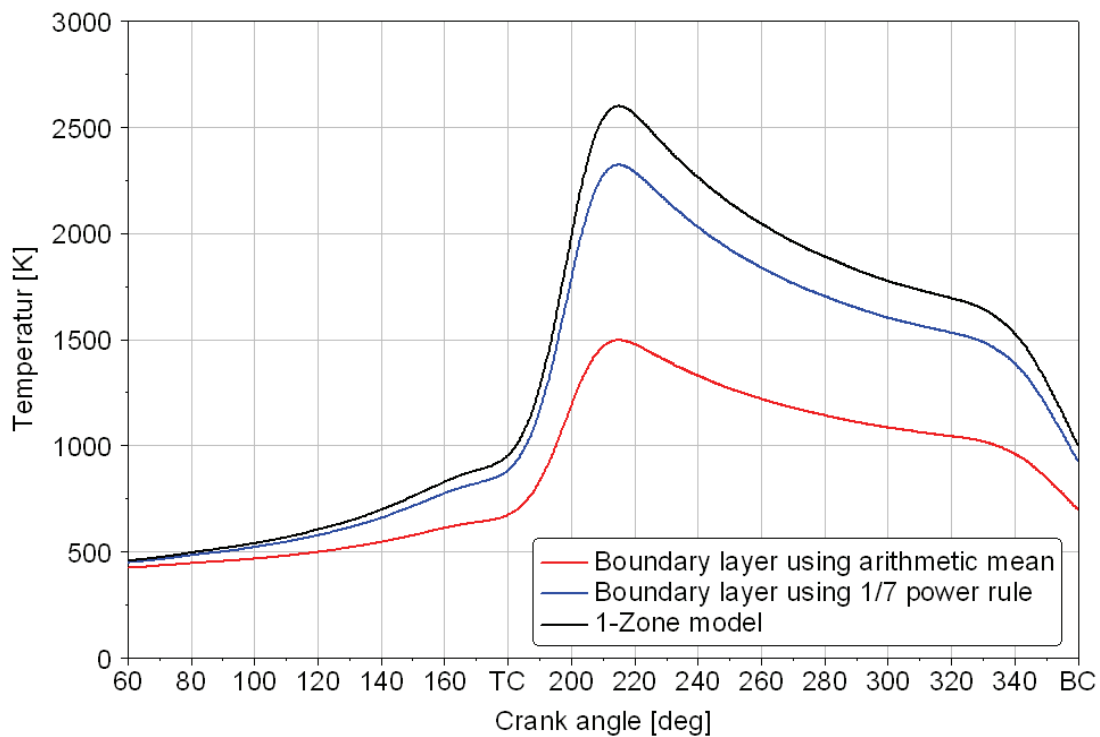


Figure 6.8: Average thermal boundary layer temperature, rotational speed of 3500 rpm, load 102 Nm, lambda 1, ignition timing 16 deg BTC, and intake valve close at 59 deg ABC.

The temperature profiles of both methods are completely different. The maximum temperature calculated by the 1/7 power law is approximately 2250 K while the arithmetic mean method and the bulk gas temperature calculated by one-zone model is about 1500 and 2600 K, respectively.

The temperature of 1/7-power law method appears too high for the thermal boundary layer temperature, since there is no flame front reached and this zone is concerned as an unburned zone. Therefore, the boundary layer temperature should lay in the proximity of the temperature of unburned zone, which is computed by two-zone model.

Comparing these results with the literature presented in [15], the boundary layer temperature profile was shown and it seemed very similar to the temperature obtained by the arithmetic mean of current work. The operating conditions of [15] were engine speed of 3000 rpm and full load. The decision was finally made to choose the arithmetic mean method to calculate average thermal boundary layer temperature.

6.4.2 Thermal Boundary Layer Thickness Result

After the average temperature over the boundary layer was computed, boundary layer thickness can be determined. Results are shown as following figure.

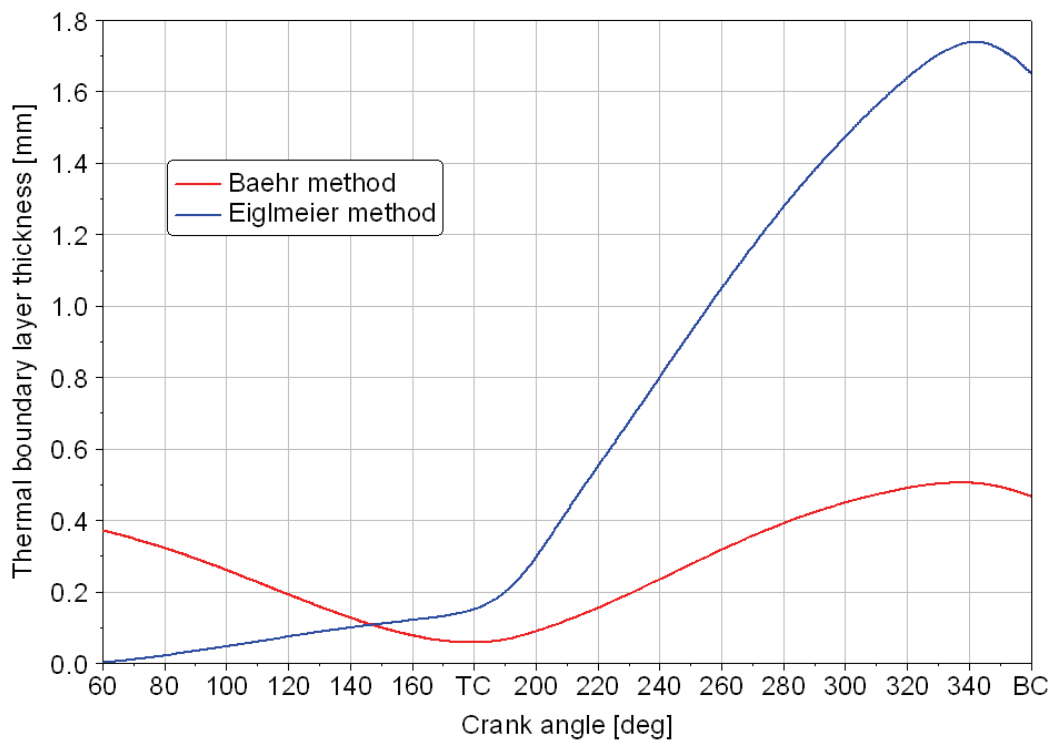


Figure 6.9: Thermal boundary layer thickness, rotational speed of 3500 rpm, load 102 Nm, lambda 1, ignition timing 16 deg BTC, and intake valve close at 59 deg ABC.

The thermal boundary layer thickness profiles of both methods are qualitatively very similar from TC until BC. Their behaviours are the same when parameters were changed. The thermal boundary layer thickness decreased when engine speed or load is increased. Changes of air/fuel ratio have only very small affect on boundary layer thickness. The difference in the thickness before TC is resulted from using different methods. Eiglmeier used an energy equation to determine the boundary layer. The method indicated that there was no thermal boundary layer if no temperature difference between wall and gas was occurred.

The thickness profile according to Eiglmeier method is qualitative and similar to the literature of Lyford-Pike and Heywood [50], which the boundary layers investigated and measured by taking the schlieren photographs. The measured thickness size was 2 mm. at the end of the expansion phase, which is alike to the result using Eiglmeier method. But within the range before TC, the thickness of [50] was about 1 mm. which represented five times bigger than the result computed by Eiglmeier method. This large difference could be because of the differently operating condition and engine.

Lyford-Pike and Heywood fitted their results with an equation which was qualitatively nearly identical to the Baehr method. However, they were quantitative different. Considering figure (6.7), the boundary layer thickness is not exactly defined by Baehr, but rather using an approximation which is generally smaller. This made no significant effect, since the boundary layer thickness in this work is determined only as an approximation of the distance, with which the flame expires (quenching distance). This distance is however not the same value of the thermal boundary layer thickness in any case. That is to be justified with the definition for quench layer, in which the flame expires due to low gas temperature. This can happen only in the case of heat loss is large enough when high temperature difference occurred. The temperature gradient in thermal boundary layer, as shown in figure (6.7), can be recognized that at the border of boundary layer, the temperature is still high and hardly fall. Even then the flame can still continue to spread into a small part of the boundary layer. Therefore, it can be an advantage to consider a smaller thermal boundary layer thickness as the distance between the wall and the flame quench position. This condition is fulfilled by the Baehr method. It can be confirmed by comparing the result with the previous works [54, 57 and 58] in the view of boundary layer thicknesses and quenching distances. The rest of calculation is then based on Baehr method.

6.4.3 CO Result Using Oxidation Factor

It is well known that CO emissions depend on air/fuel ratio or lambda. Section 6.2 showed that the magnitude error on current CO model is also depended on lambda. The computation of the CO emission at some operating points with variation of lambda was tested. Moreover, the temperature in the boundary layer and the exhaust port temperature for an operating point with lambda variation were not extremely different. Therefore, the first method to estimate CO concentration in quench layer using simple oxidation factor is determined and added according to the old calculation. The addition is based on CO concentration and mass fraction of the zones. Results are shown in following figure. Note that both axes in figure have the same scale, only zero point is different.

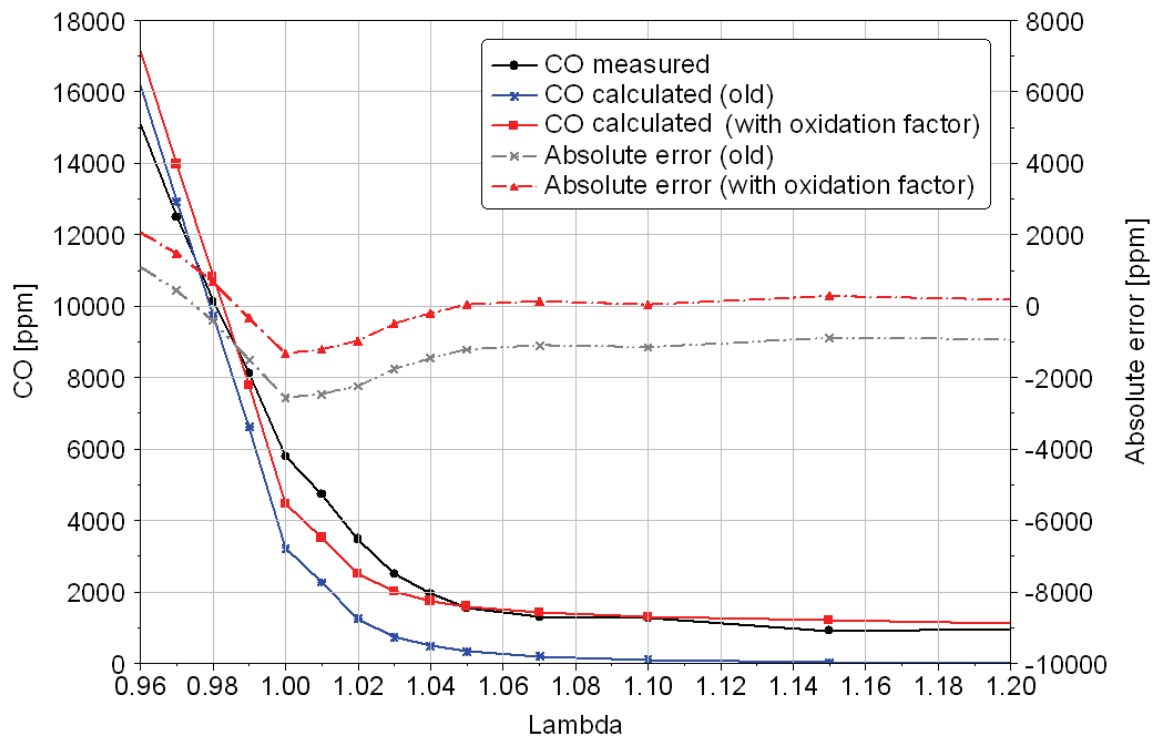


Figure 6.10: Measured versus calculated CO concentrations with and without oxidation factor ($factor = 0.4$) and absolute error with variable lambda (Engine speed 2500 rpm, load 76 Nm).

Figure (6.10) shows that there is no large deviation occurred within the lean mixture area. When lambda is greater than 1.04, the calculated CO values are more than measured values. That is because of the fact that a constant oxidation factor ($factor = 0.4$) is used. Refer to the literature of Mendillo and Heywood [20] the oxidation factor depended on lambda. With lambda equivalent

to 1.2, the oxidation factor value is only about two thirds of the maximum value which is occurred at $1.0 < \lambda < 1.02$ range. If the change of λ affects on oxidation factor were considered, results of the CO concentration in the exhaust gas with variable λ would changed, as shown in figure (6.11).

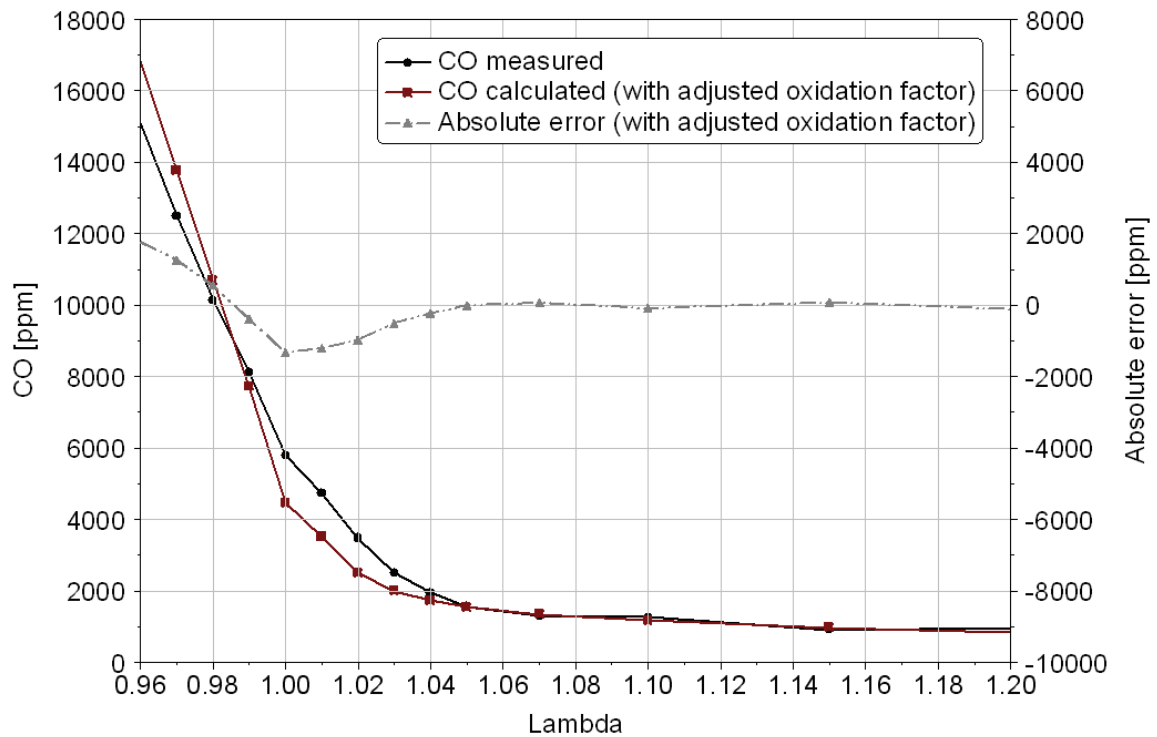


Figure 6.11: Measured versus calculated CO concentration with adjusted oxidation factor and absolute error with variable λ (Engine speed 2500 rpm, load 76 Nm).

Figure (6.11) shows that it is hard to see the deviation within the lean mixture area ($\lambda > 1.04$). In the rich mixture area, the deviations using adjusted oxidation factor are smaller in comparison to the constant oxidation factor. In the range of $1.0 < \lambda < 1.02$ which Mendillo and Heywood showed the strongest oxidation of HC, the proportional errors of CO model are largest. In this range, the NO_x emissions reach maximum value. The formation of nitrogen oxides require oxygen and this can obstruct the oxidation of CO to CO₂, which leads to higher measured CO concentration.

To verify this method, the CO predictions are also calculated at another operating point (different engine speed and load). Results of the model at another operating point are shown in figure (6.12). It is found that the model did not pass at this operating point. The oxidation factor depends on engine speed, load and exhaust gas temperature. The correct oxidation factor finding,

depending on variables, becomes very difficult and then the further determination of oxidation factor is not possible for all ranges of engine map. Hence, this method is a good CO prediction tool only for a specific engine speed and load, not for all operating conditions.

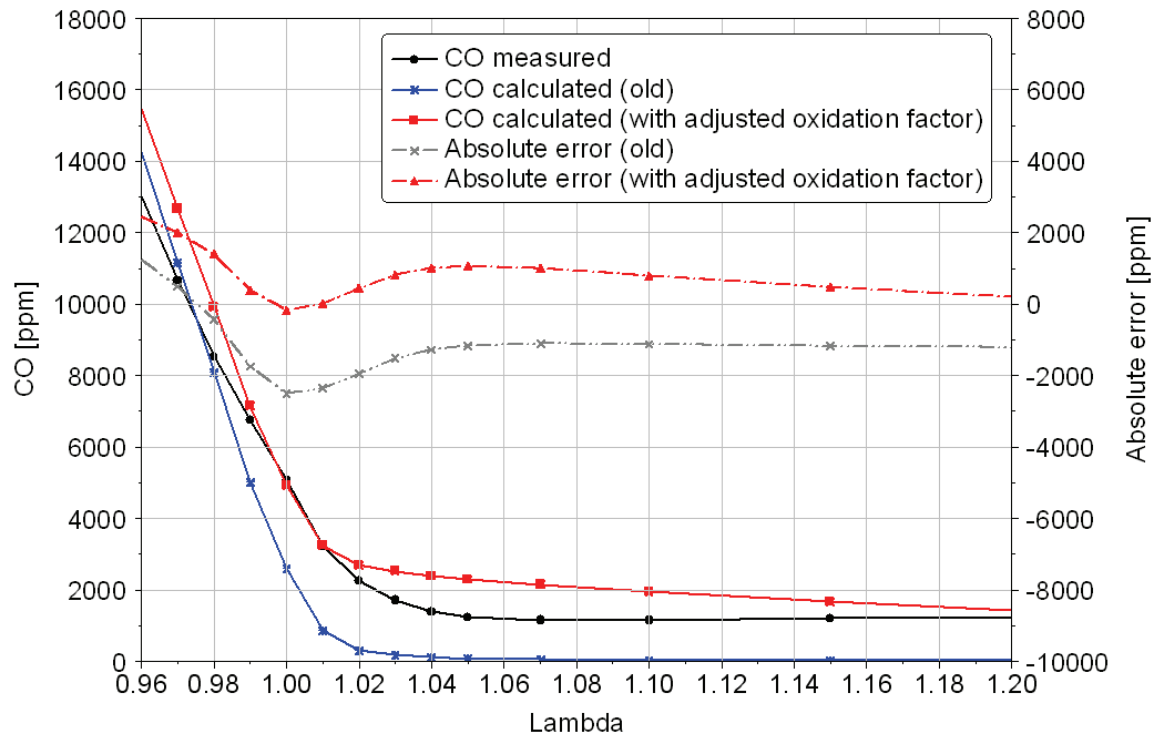


Figure 6.12: Measured versus calculated CO concentration with- and without adjusted oxidation factor and absolute error with variable lambda (Engine speed 1500 rpm, load 25 Nm).

6.4.4 CO Result Using Chemical Kinetic Model

CO emissions in quench layer (thermal boundary layer) are separately calculated from bulk gas in combustion chamber. After the temperature and thickness profile of quench layer are calculated, the CO emission in this zone are then calculated using chemical kinetic model. The kinetic model is based on closed homogeneous system and solved by CHEMKIN. This model was started at ignition point until exhaust valves opened. Thermal boundary temperature profile and measured cylinder pressure profile were main input. The reactants were isooctane/air mixture and EGR. Because of CO emission in quench layer was separately calculated from bulk gas in combustion chamber, the CO quantity from quench layer using kinetic model were mixed with CO quantity of bulk gas on mass fraction basis. The CO results from the old model and improved model with quench layer were shown firstly with lambda variation in three differently engine speeds and loads in figure (6.13), (6.14) and (6.15). Note that both axes in figure have the same scale, only the zero point is different.

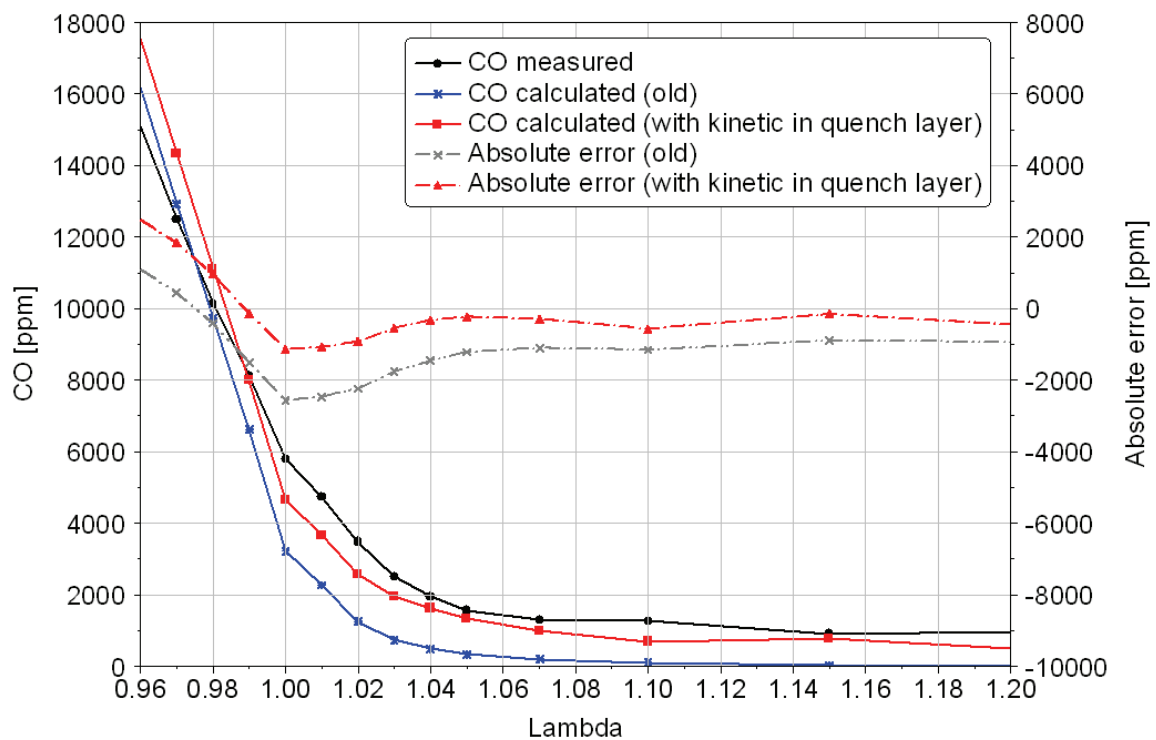


Figure 6.13: Measured versus calculated CO concentration with kinetic model in quench layer and absolute error with variable lambda (Engine speed 2500 rpm, load 76 Nm).

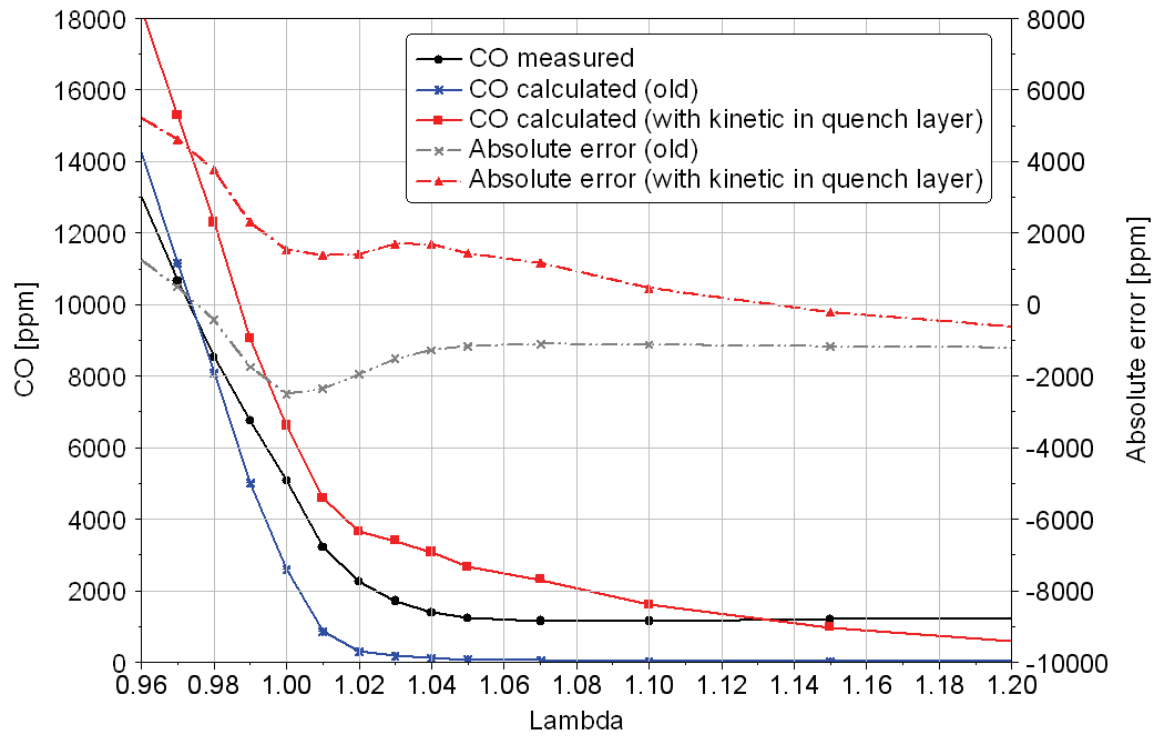


Figure 6.14: Measured versus calculated CO concentration with kinetic model in quench layer and absolute error with variable lambda (Engine speed 1500 rpm, load 25 Nm).

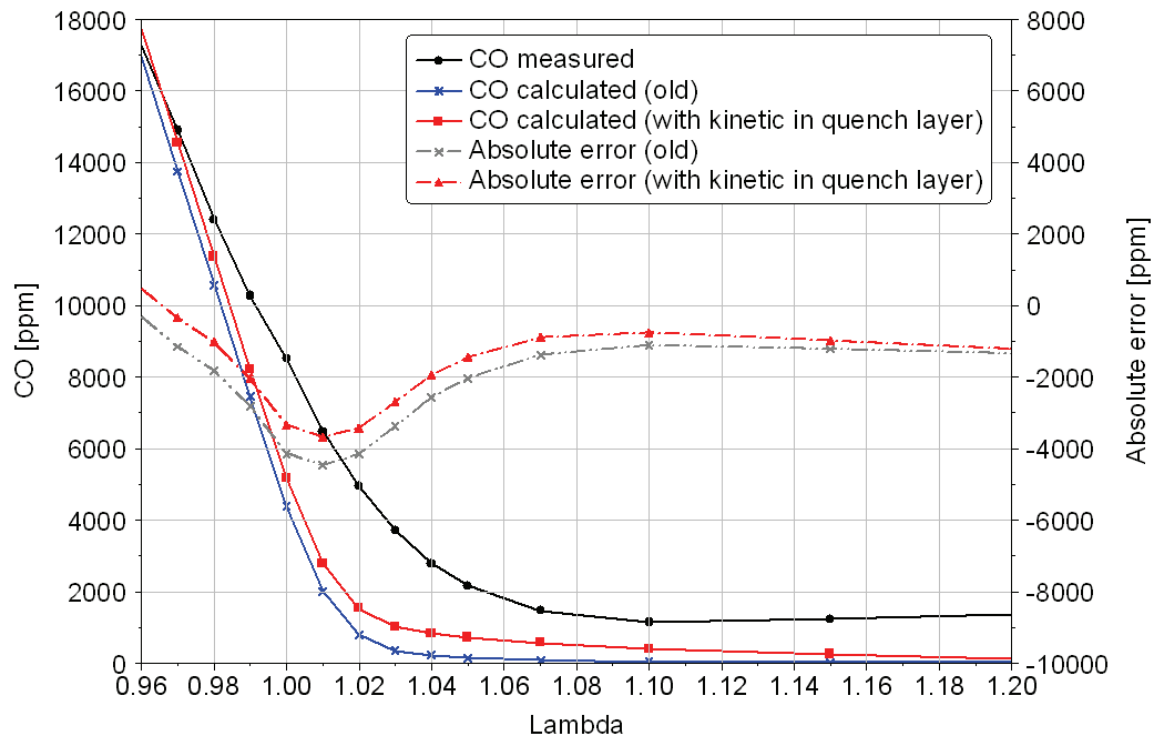


Figure 6.15: Measured versus calculated CO concentration with kinetic model in quench layer and absolute error with variable lambda (Engine speed 3500 rpm, load 102 Nm).

Figure (6.13) shows the positive results of improved CO model along the lambda variation. The absolute errors are very low with lean mixture ($\lambda > 1.03$) and results of lambda range from 0.98 to 1.20 are significantly better than the old model. Nevertheless, results from figure (6.14) which engine speed and load are low, CO prediction shown too high whereas from figure (6.15) which, engine speed and load are high, CO prediction shown too low compared to measured value. It was found that with smaller engine load and speed, the model predicted more amount of CO. This can be described by the boundary layer thickness which decreases with increasing of engine speed or load. Thus, the mass fraction of gas in boundary layer becomes smaller and the predicted CO portion from boundary layer is smaller.

The correct temperature of the boundary layer is extremely crucial for kinetic model with isooctane oxidation. It was found that a temperature difference of 30 K have significant affect on CO quantity in the boundary layer because the temperature range which isooctane oxidizes to CO is very small. The critical temperature of this chemical mechanism is around 1500 K. At maximum temperature below 1450 K, the CO formation is very slow and this result in low CO value. Furthermore, when the maximum temperature is more than 1550 K the CO occurred is further oxidized to CO_2 and this result in low CO value.

The thermal boundary layer temperature was calculated using arithmetic mean, described in section 6.3.2; from equation (6.22), therefore this value would depend on wall temperature. The current model used constant wall temperature at 393.15 K or 120°C, which was a good approximation for two-zone-, NOx- and previous CO model due to the wall temperature was not a sensitive parameter of these models. Furthermore, it was very complicate to measure the exact wall temperature. However, using constant wall temperature was not a good approximation to predict CO emissions from thermal boundary layer for every operating point since the wall temperature had strong effect on CO result. In order to determine the thermal boundary layer temperature more accurately, the constant wall temperature is no longer accepted. The method to estimate wall temperature for every operating point should be taken into account. The simple and low cost method is considering of engine oil and coolant temperature which values are shown in the following figure.

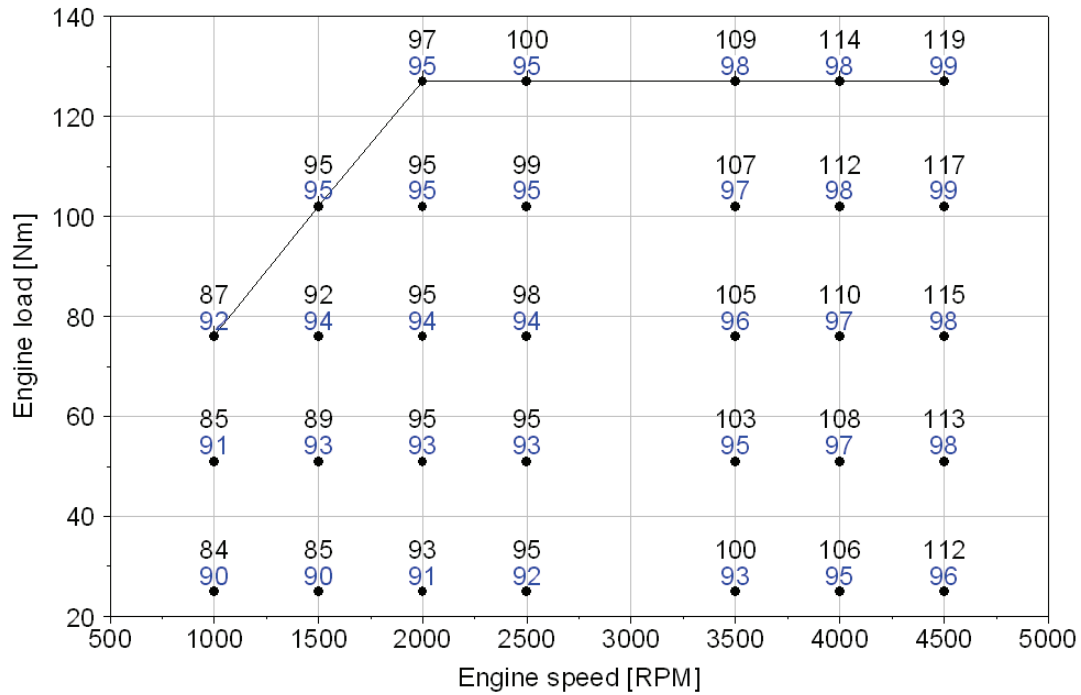


Figure 6.16: Motor oil temperature (black) and cooling water temperature (blue) in Celsius with lambda 0.98.

The cooling water and oil temperature in figure (6.16) depends on engine speed and load. The temperature of cooling water is considered to be used since it has relatively faster response than oil temperature. The method using coolant temperature to estimate wall temperature is also shown in [48]. The current model assumed the wall temperature to be constant at 393.15 K which is about 30 K over the coolant temperature. Two wall temperatures are then chosen and tested, 30 K and 60 K over the coolant temperature. The CO model results with wall temperature and lambda variation on the same operating point as before are shown in figure (6.17), (6.18) and (6.19).

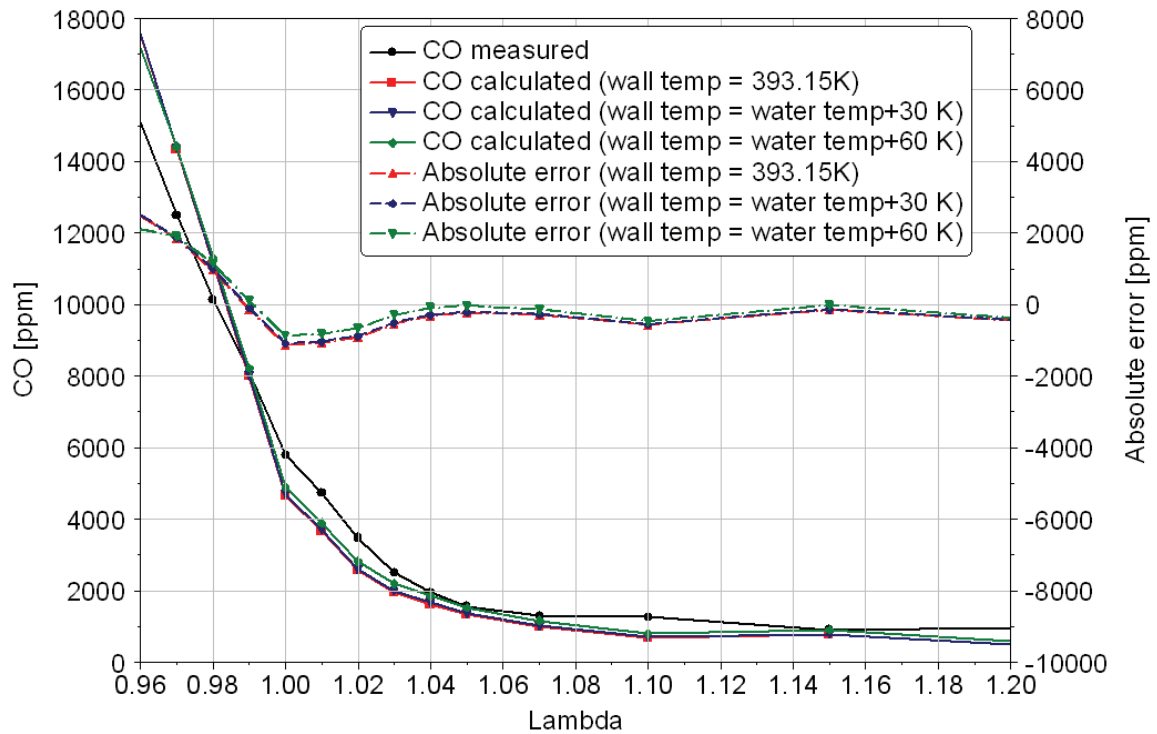


Figure 6.17: Measured versus calculated CO concentrations with kinetic model in quench layer and absolute error with variable wall temperature and lambda (Engine speed 2500 rpm, load 76 Nm).

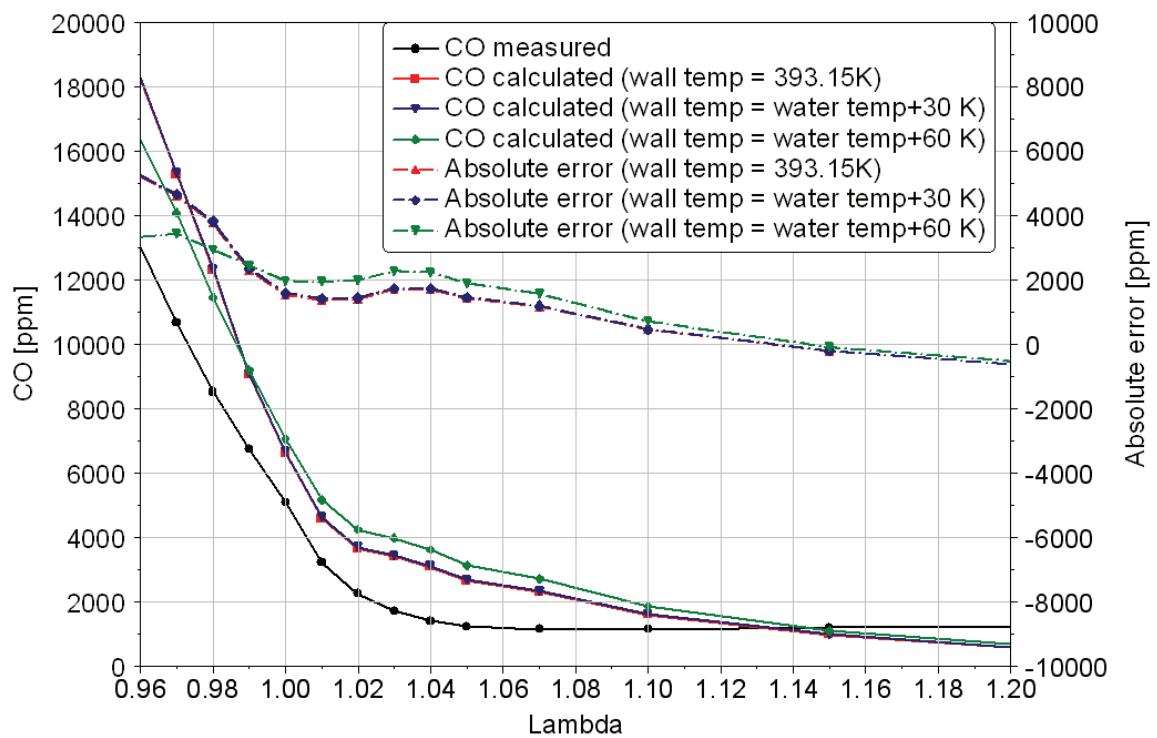


Figure 6.18: Measured versus calculated CO concentrations with kinetic model in quench layer and absolute error with variable wall temperature and lambda (Engine speed 1500 rpm, load 25 Nm).

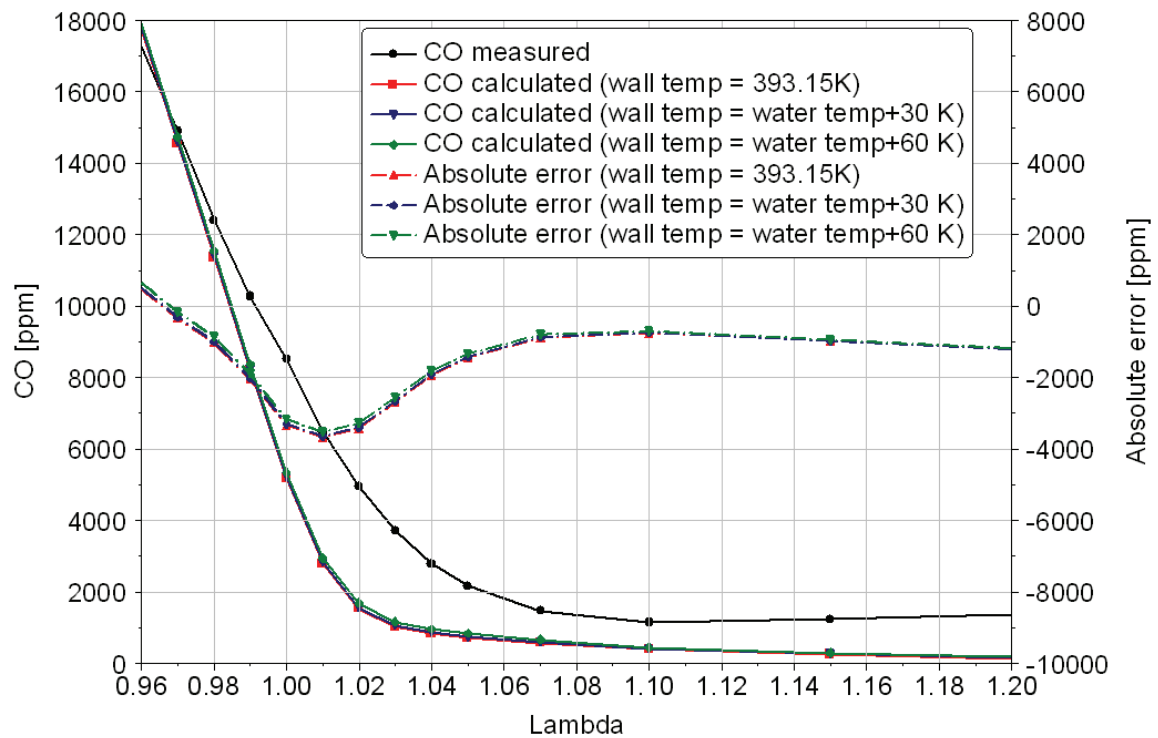


Figure 6.19: Measured versus calculated CO concentrations with kinetic model in quench layer, and absolute error with variable wall temperature and lambda (Engine speed 3500 rpm, load 102 Nm).

Figure (6.17), (6.18) and (6.19) shows that the predicted CO values, by using the coolant temperature plus 30K and 60 K as wall temperature, are higher than using constant wall temperature at 393.15 K. That means the absolute errors of CO prediction are smaller for figure (6.17) and (6.19). It is found that a different wall temperature causes a substantial change of CO prediction only in the low engine load area. This effect is small on high engine load. One explanation is the boundary layer thickness changed due to load changes.

In order to validate the model, the predicted CO emissions over the engine map are calculated and compared with measured values. Figure (6.20) shows results of CO model with lambda 0.98 and 1.02 for the three variants of the wall temperature.

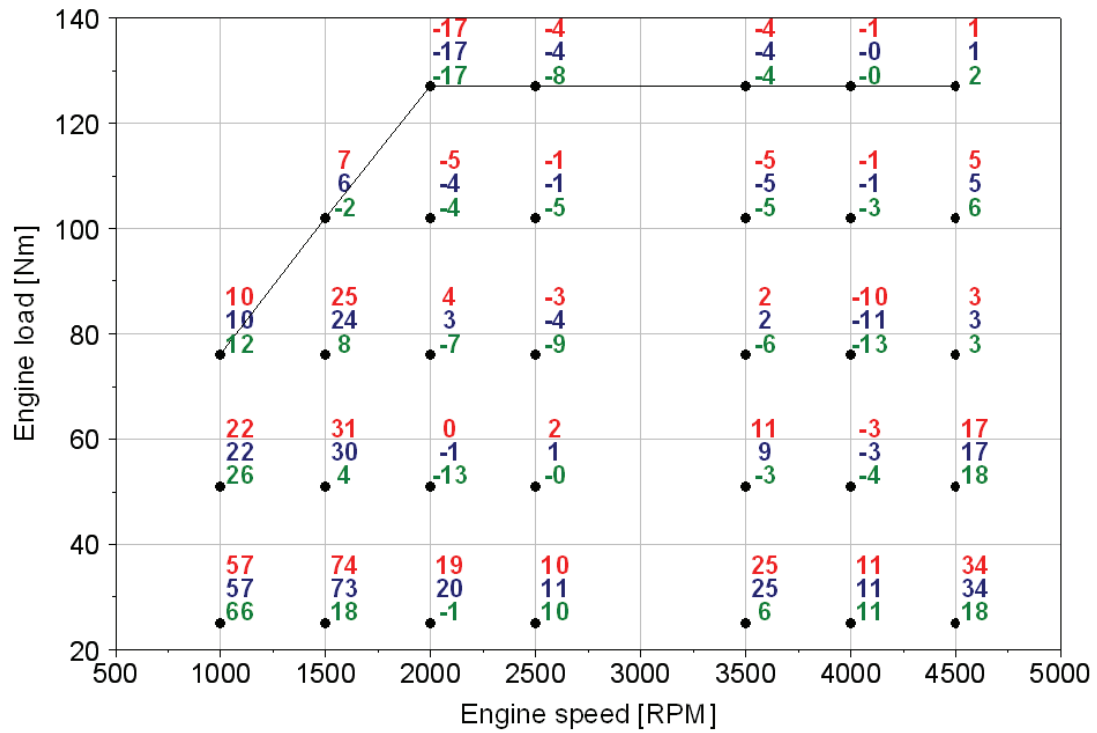
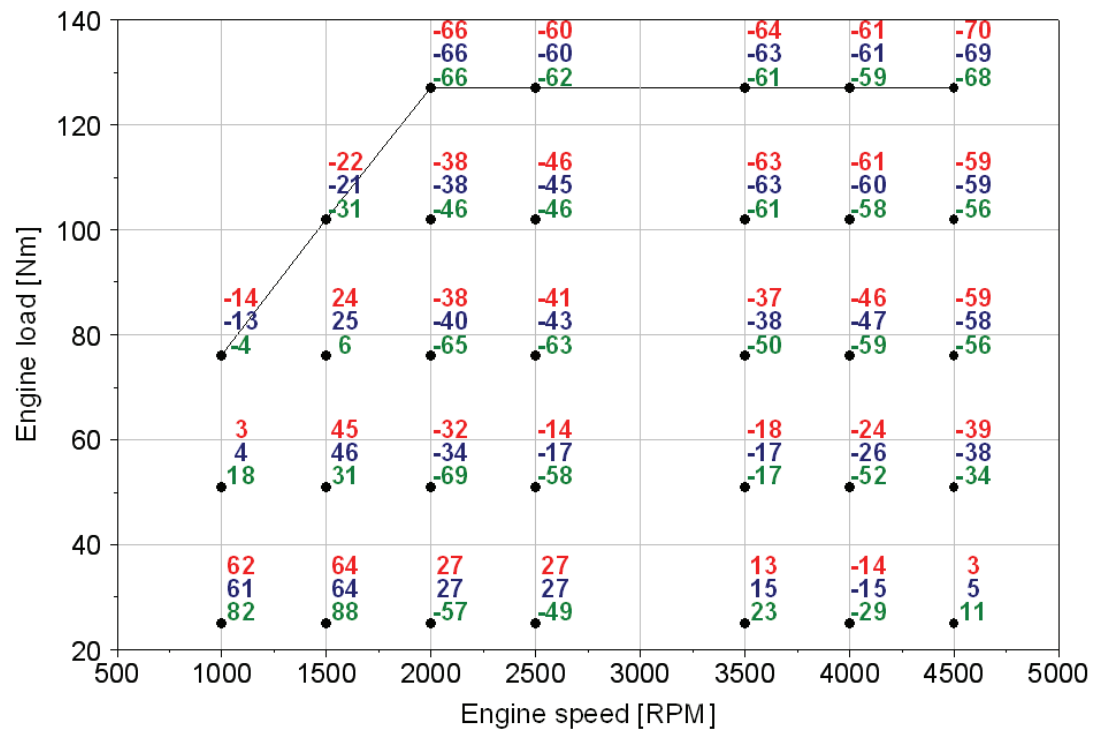
(a) $\Lambda = 0.98$ (b) $\Lambda = 1.02$

Figure 6.20: Percentage error of CO prediction calculated by chemical kinetic model compared to measured value over engine operating map, $T_w = 393.15$ K [red], $T_w + 30$ K [blue], $T_w + 60$ K [green].

Results of CO prediction from figure (6.20) (a), lambda at 0.98 with variable wall temperature shows that the CO prediction using wall temperature equal coolant temperature plus 30 K are slightly better than using constant wall temperature at 393.15 K or 120°C. The CO prediction, using a wall temperature equivalent to the coolant temperature plus 60 K, are generally lower than using other wall temperatures due to the boundary layer temperatures are too high and then the CO occurred in boundary layer is then further oxidized to CO₂. Then, CO results are lower than using another wall temperature and even without boundary layer, for example at 2000 rpm and 51 Nm.

The percentage prediction error of improved CO model with boundary layer are clearly better than the old CO model (without boundary layer), as shown in figure (6.4) (a). This new results are more accurate with smaller deviation between points in the engine map. It is found that the optimum wall temperature is coolant temperature plus 30K and the average percentage error of CO prediction using this wall temperature from figure (6.20) (a) is 13.7 %. This average value is 3.7 % higher than without boundary layer, as shown in figure (6.4) (a), this is because of the result of some points such as 1000 rpm, 25 and 51 Nm shown relatively higher error which will be described later.

Under the lean mixture, lambda at 1.02, results from figure (6.20) (b) show the same trend that using wall temperature equivalent to coolant temperature plus 30 K are slightly better than using constant wall temperature at 393.15 K or 120°C and using the wall temperature equivalent to coolant temperature plus 60 K is too high. Percentage prediction error of the improved CO model with boundary layer are clearly better than the old CO model, as shown in figure (6.4) (b). The optimum wall temperature is coolant temperature plus 30K and the average percentage error of this wall temperature from figure (6.20) (b) is 39.4 % which is much better than 74.2 % from figure (6.4) (b).

However, there are some operating points in figure (6.20) (b), which have different trend with others point in engine map such that CO predicted value increased when wall temperature increased. This can be described as, for example, with the operating point at 1500 rpm, 25Nm, here the average value of the maximum temperature of the boundary layer rises from 1482 K to 1497 K, consequently the CO formation increases. This characteristic also can be found in some points in figure (6.20) (a) where engine speed is low as 1000 rpm but with smaller difference.

Principally, one can conclude that the improved CO model with thermal boundary layer is much better than former model and the result was satisfactory.

The amount of EGR in the cylinder is very important, as discussed in section 6.2. The information from car manufacturer reveals that the internal EGR value can be two times as the measured value, and this could be the reason for the error, especially under the low load and speed which air flow rates were relatively low but percentage of internal EGR were high due to low throttle condition. The current CO model result used the EGR rate from engine control unit, (internal EGR data). Furthermore, there is a list of internal EGR rate of the engine from the company, in which substantially higher EGR rate is specified. The percentage error of the improved model with wall temperature equivalent to coolant temperature plus 30 K compared to measured value is presented in figure (6.21) with lambda 0.98 and (6.22) with lambda 1.02 using internal EGR data from engine control unit and internal EGR data from company.

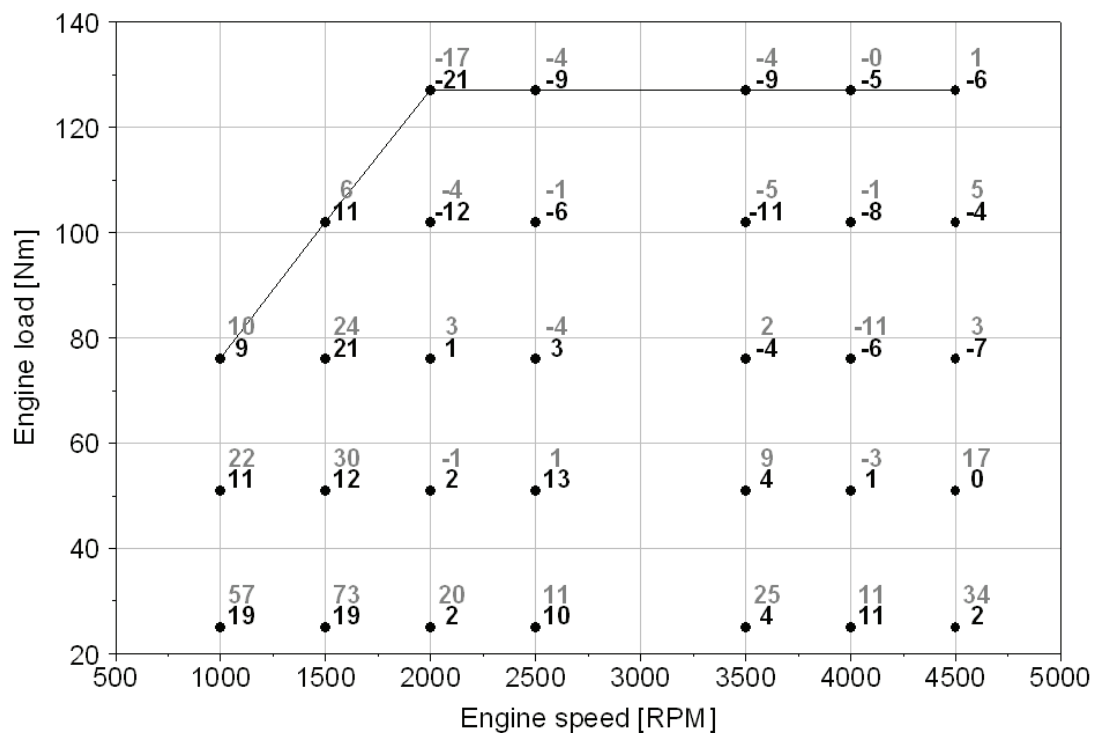


Figure 6.21: Percentage error of CO prediction calculated by improved CO model compared to measured value over engine operating map with lambda 0.98, internal EGR data from engine control unit [grey] and internal EGR data from company [black].

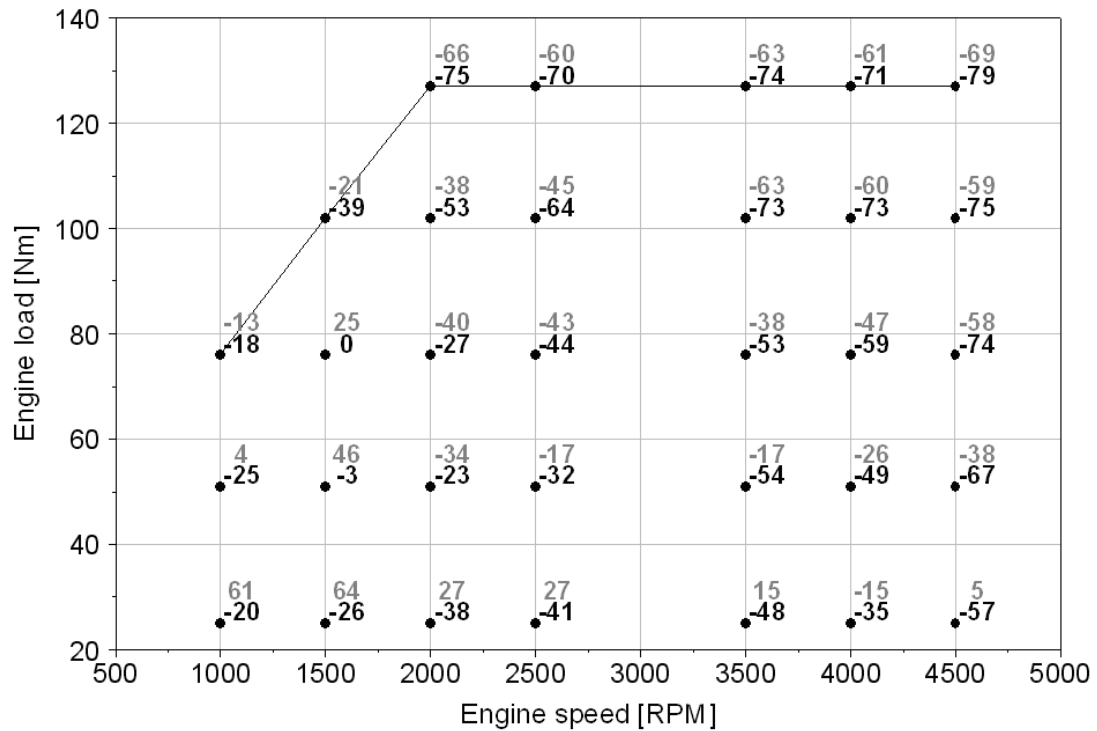


Figure 6.22: Percentage error of CO prediction calculated by improved CO model compared to measured value over engine operating map with lambda 1.02, internal EGR data from engine control unit [grey] and internal EGR data from company [black].

From figure (6.21) and (6.22), one can see clearly that the prediction results using the internal EGR data from company, when EGR rate was higher, are generally lower prediction of CO than using internal EGR rate from engine control unit. The cause for this is the temperature computed by the physical two-zone model sink with higher EGR rates. Furthermore, it can be recognized from figure (6.21) with lambda 0.98, the difference of the CO prediction using different EGR rate data is largest in the low load area. This is because of the fact that the largest differences of internal EGR rate between the data sources occurred in this area. In this range, it is most difficult to determine the exact EGR rate since the engine is strongly throttled and the amount of rest gas in the cylinder from the cycle before is difficult to be determined. In the remaining area of engine map the deviation between various results are not so large, since the EGR rates do not exhibit such large differences there. Similar characteristics are shown in figure (6.22) with lambda 1.02. Differences of CO result between the two data sources of internal EGR rate became smaller with increasing load. They are however substantially larger than that with lambda 0.98.

One of the reasons that the CO model results are generally lower than the measured value can be from the oxidation of UHC which has not been considered in this model. The UHC oxidations took place (1) in the cylinder after main combustion by mixing of UHC and hot bulk gas and (2) in exhaust port and runner where the temperature was still high and there was enough time for oxidation. Because of the exhaust gas sampling probe was neither installed directly after exhaust valves nor in a short distance after exhaust runners in which all the exhaust gases are mixed together, see in figure (4.1). This would have an effect on the measured CO value. The current CO model did not include this UHC oxidation effect because the total HC oxidation mechanisms were complex and needed further study which was not in this study scope. However, the amount of UHC in the boundary layer could be advantage information in future to predict HC emission, oxidation model in exhaust port and runner, and even catalytic converter model. The predicted UHC values which were calculated by improved CO model over engine map are shown in figure (6.23).

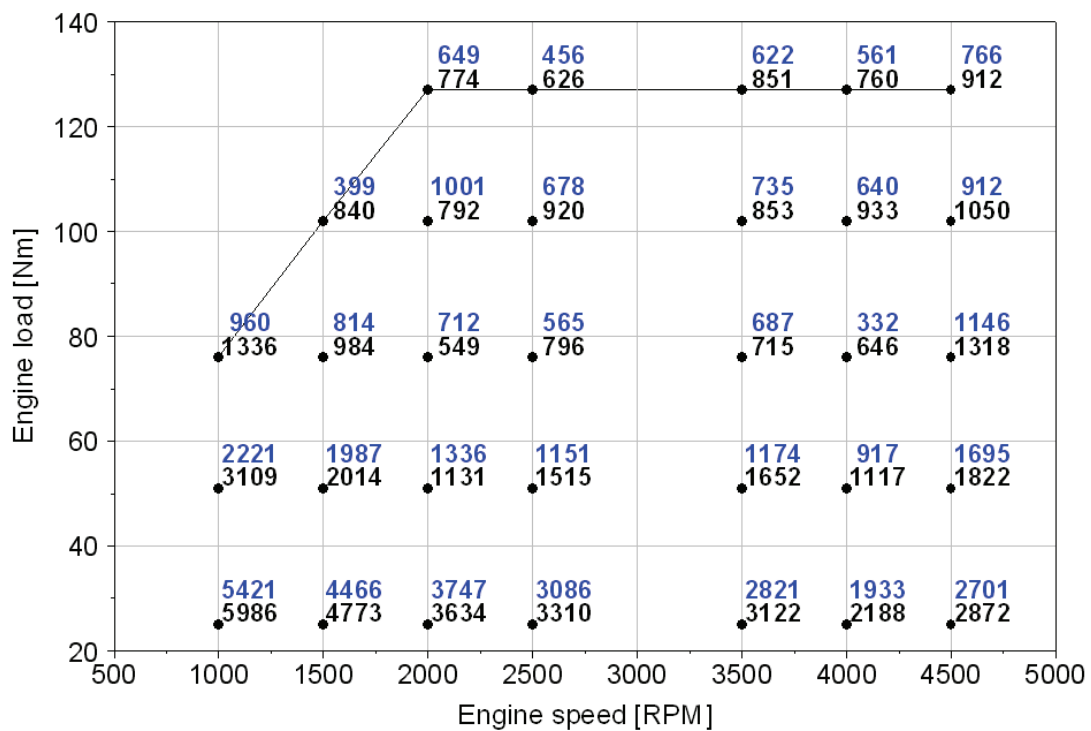


Figure 6.23: Predicted unburned hydrocarbons from improved CO model in ppm, lambda 0.98 [blue], and lambda 1.02 [black] (Using internal EGR data from company).

Results from figure (6.23) show that the predicted UHC decreased with increasing engine speed and load. This is because of the mass fraction of the boundary layer to total mass is high with low engine load and speed. Under the higher load, the boundary layer temperature is higher and

then oxidation of fuel (gasoline) is faster, results in lower prediction of UHC. However, these results cannot directly be compared to the measured HC emission from the engine since they are only one part of UHC that occurred in cylinder and their oxidations are still on going during the exhaust process, but it could be good information for further HC modelling.

Moving back to validate the CO result from another point of view, referring to the own published work with this topic [59], CO concentrations were calculated by the kinetically CO model without boundary layer. The average lambda 1 results were calculated from an averaging of results determined with lambda 0.98 and 1.02. In order to be able to compare these new results, errors from the average value are indicated with- and without boundary layer in figure (6.24).

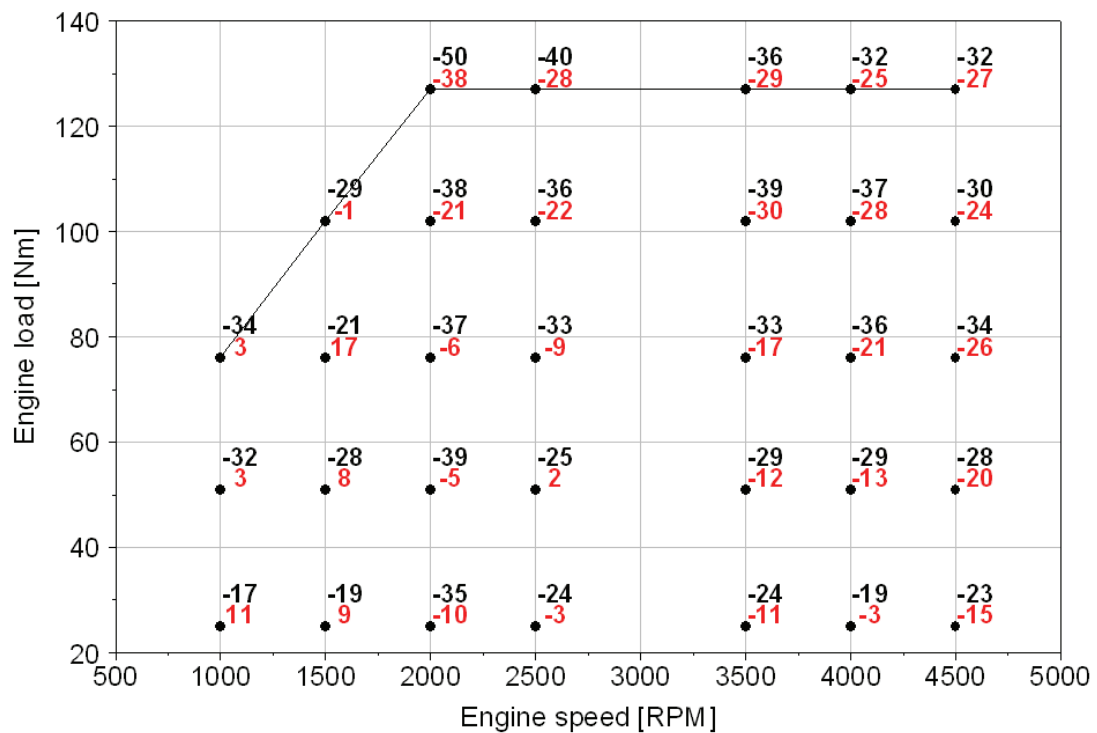


Figure 6.24: Percentage error of CO prediction calculated by old CO model (black) and improved CO model (red) compared to measured value over engine operating map for average lambda 1 (Using internal EGR data from company).

Results of the improved model are clearly closer to the measured values than the old model, which the average percentage error was reduced from 31.1 to 15.4 %. They are mainly lower than measured values due to excluding of the effect from the oxidation in of UHC in exhaust port and runner.

6.5 Sensitivity Analysis of CO Model

This section shows the sensitivity analysis of CO model. Inputs to the model were from measurements which could not exactly be determined. The methods were the same as described in “section 5.3-Sensitivity Analysis of NO Model”. Moreover, the CO model result of bulk gas and thermal boundary layer will be separately described and then the total predicted CO concentration will also be shown. The engine operating condition is speed 2500 rpm, load 76 Nm and lambda 0.98. It should remark again here that the pressure-time data from pressure sensor was not changed for the study of this sensitivity analysis.

The first parameter to be considered is cylinder wall temperature (T_w). This value, 393.15 Kelvin, was set to be initial value for one- and two-zone model. Table (6.1) shows the effect of variations in the wall temperature on CO prediction. It was found that wall temperature was not a sensitive parameter of the bulk gas CO model but it affected on boundary layer CO model to some degree. The total predicted CO changed only by a small percentage, thus one can conclude that the wall temperature is not a sensitive parameter of the model to predict CO.

Table 6.1: Variation of wall temperature and CO prediction.

T_w	CO-bulk gas changed [%]	CO-b. layer changed [%]	Total CO changed [%]
$T_w +20$ K	0.03	4.25	0.86
$T_w +10$ K	-0.12	1.73	0.25
$T_w +5$ K	-0.60	0.12	-0.46
T_w (initial 393.15K)	-	-	-
$T_w -5$ K	-0.02	-3.24	-0.66
$T_w -10$ K	-0.07	-5.11	-1.08
$T_w -20$ K	-0.48	-9.00	-2.19

Air flow rate was a main input parameter because burned gas temperature was changed up to 150 K when the air flow rate change -5% (as described in section 5.3). Table (6.2) shows the effect of variations in the air flow rate value on CO prediction. Unlike NO model, air flow rate was not a strong sensitive parameter for the bulk gas CO model. However, it was a sensitive parameter on boundary layer CO model. Hence, the total predicted CO result changed up to -14.2% with increasing air flow rate by +5%.

Table 6.2: Variation of air flow rate and CO prediction.

Air flow rate	CO-bulk gas changed [%]	CO-b. layer changed [%]	Total CO changed [%]
Air flow rate +5%	-6.85	-40.13	-14.27
Air flow rate +4%	-5.24	-33.55	-11.58
Air flow rate +3%	-3.93	-26.08	-8.94
Air flow rate +2%	-2.34	-17.45	-5.78
Air flow rate +1%	-1.92	-8.82	-3.54
Air flow rate (initial)	-	-	-
Air flow rate -1%	1.20	5.35	2.28
Air flow rate -2%	1.60	-0.72	1.55
Air flow rate -3%	2.62	-23.22	-2.21
Air flow rate -4%	4.59	-61.35	-8.68
Air flow rate -5%	5.54	-86.80	-13.42

Exhaust gas recirculation (EGR) was one of a sensitive input since it strongly affected the total mass and then predicted temperature. It is important to remark here again that the engine was operated without EGR mode but there was the internal EGR that remained in the cylinder and intake port. In conducting the sensitivity analysis of EGR, the variable percentages of EGR were taken as input of two-zone model. Table 6.3 shows the effect of variations in the exhaust gas recirculation value on CO prediction. Note that, EGR+1% means the initial internal EGR value was shifted simply by 1 %, for example, if initial value is 3%, EGR plus+1%* means 4% EGR.

Table 6.3: Variation of EGR rate and CO prediction.

EGR	CO-bulk gas changed [%]	CO-b. layer changed [%]	Total CO changed [%]
EGR +4%*	-5.80	-36.36	-12.63
EGR +3%*	-4.23	-28.17	-9.62
EGR +2%*	-2.45	-18.78	-6.16
EGR +1%*	-1.57	-9.35	-3.38
EGR (initial)	-	-	-
EGR -1%*	1.21	5.39	2.31
EGR -2%*	2.32	-2.30	1.81
EGR -3%*	3.36	-26.53	-2.31
EGR -4%*	4.34	-62.35	-9.10

One can see that EGR rate was a sensitive parameter on CO model especially boundary layer CO model. The reason that CO prediction results changed relatively high because, for this case, 1% more internal EGR mean 1% more of total mass (only for this case) and this affected the temperature. Then, the effect is nearly the same to the change of air flow rate. Extra care of internal EGR and EGR rate should be considered.

A lambda can indicate amount of oxygen left in burned gas. Since CO oxidation rate depends on the amount of oxygen left, it is important for the CO model to receive correct value of lambda for equilibrium concentration calculation. Table 6.4 shows the effect of variations in the lambda value on CO prediction. It is clearly shown that lambda was the strongest parameter of the model to predict CO. The change in the boundary layer CO model results were relatively small because this artificial lambda value had small effects on temperature calculation since the pressure profile was not changed.

Table 6.4: Variation of Lambda and CO prediction.

Lambda	CO-bulk gas changed [%]	CO-b. layer changed [%]	Total CO changed [%]
Lambda +5% (lean)	-98.31	-4.32	-79.02
Lambda +4%	-96.55	-3.47	-77.45
Lambda +3%	-88.29	-2.62	-70.70
Lambda +2%	-63.13	-1.76	-50.53
Lambda +1%	-32.29	-0.88	-25.84
Lambda 0.98 (initial)	-	-	-
Lambda -1%	33.25	0.89	26.61
Lambda -2%	67.29	1.80	53.84
Lambda -3%	102.02	2.71	81.62
Lambda -4%	137.40	3.64	109.93
Lambda -5% (rich)	173.34	4.57	138.67

The last investigated parameter was bulk gas temperature. To check the effect of the change in bulk gas temperature of thermodynamic model, the variation was done by shifting the temperature predicted by one- and two-zone model by 10, 20, 50 and 100 K. Table (6.5) shows the effect of variations in the bulk gas temperature on CO prediction. It was found that increasing gas temperature up to 50 K, the total CO predictions changed only a few percentages. The change in bulk gas temperature up to 100 K strongly affects boundary layer CO model and thus made the total CO prediction results moved up to 11.93 %.

Table 6.5: Variation of bulk gas temperature and CO prediction.

T	CO-bulk gas changed [%]	CO-b. layer changed [%]	Total CO changed [%]
T+100K	4.70	-62.53	-9.18
T+50K	2.44	-1.81	1.46
T+20K	1.00	4.96	1.78
T+10K	0.51	2.95	0.99
T (initial)	-	-	-
T-10K	-0.53	-3.48	-1.11
T-20K	-1.06	-7.24	-2.29
T-50K	-2.76	-18.78	-5.97
T-100K	-5.89	-35.87	-11.93

6.6 Summary

The CO emission model was implemented to predict CO emission from a gasoline direct injection engine. The one-zone thermodynamic model was used to calculate bulk gas temperature in cylinder and the two-zone thermodynamic model was then implemented to predict burned gas temperature and exhaust gas concentration. Because of the equilibrium concentration was not a good tool to predict CO emission; kinetic model was then needed to achieve the goal.

The kinetic CO model was then introduced. The pressure- and temperature-time data were delivered into kinetic model. The equilibrium concentration of gas mixture was used as initial concentration of kinetic model to avoid the complex mechanism of gasoline. The chemical mechanisms introduced by Glassman were chosen and the chemical model was solved by CHEMKIN program. With this method, the kinetic model could start when the burned mass fraction equals 0.90 to keep minimum calculation time with the same output. Results from CO kinetic model were relatively acceptable compared to the literatures [12, 13, 15, 42, 60, 61]. However, the CO model should be improved to achieve a satisfactory result.

The improvement of CO kinetic model was completed through modifying the physical and the chemical model. In order to arrange the physical model more realistic, a third zone in the

combustion chamber due to quench layer was introduced because the quench layer was one of the CO source in combustion chamber. The flame was assumed that it could not go through the new zone, hence the main combustion could not take place but the oxidation of fuel in the zone was still important. The quench layer temperature and pressure were assumed to be the same as thermal boundary layer. Next, considering oxidation of fuel in boundary layer, a chemical kinetic model was then introduced using boundary layer temperature and measured pressure-time data. A reaction mechanism for isooctane was used in order to determine the quantity of carbon monoxide which developed in the boundary layer. Furthermore, the boundary layer CO model also delivered the amount of UHC. But the complexity of UHC oxidation during exhaust stroke and in the exhaust system, and the rate of their oxidation to be CO and CO₂ were not identified; so the oxidation of UHC to be CO from this source was not considered. However, this could be an advantage to include it in an UHC model in the future.

CO models calculation time was 7 minutes (for bulk gas CO kinetic model) and 2 minutes (for boundary layer CO kinetic model) per one operating condition of 4 cylinders engine on 3.2 GHz and 64-bit double CPU computer. Including 1.30 minutes for two-zone model, the total calculation time was 10.30 minutes. Results obtained from both bulk gas CO kinetic model and boundary layer CO kinetic model (called improved model) showed a clear improvement for all range of lambda. Also, the CO prediction results over engine map were very satisfactory. Results were mainly lower than measured values due to the UHC oxidation in exhaust port and runner which was not considered in this model. It could be a great advantage to do the model in the exhaust gas system to achieve a better CO result. Another reason explaining low CO prediction could be the formation of nitrogen oxides, which needed oxygen; and this can obstruct the oxidation of CO to CO₂, which lead to higher measured CO concentration especially when lambda value was about 1.02, a level where the maximum NO_x occurred.

The sensitivity analysis showed that lambda was the most important parameter in the CO model. Hence, the cylinder to cylinder variation was critical for the CO model, if one cylinder runs with rich mixture and the other run with lean mixture, then the CO model would not deliver good result since there was only one lambda sensor shortly after exhaust manifolds. Air flow rate and EGR were sensitive parameter because they affected the total mass and then the temperature. The model result could be improved if the cylinder to cylinder variations were reduced or the air flow, EGR rate and lambda for every cylinder could be measured individually.

7. Summary and Conclusion

7.1 Summary

The purpose of this work was to predict NO_x and CO emissions from a gasoline direct injection engine combustion chamber with low calculation time. Model should be small and fast to allow embedding in the engine control unit. To achieve the purpose of this study, a two-zone thermodynamic model was developed to predict the exhaust gas temperature and combustion product under a wide range of operating condition. Successfully, the studied model was efficient, small and requires low calculation time.

The NO model using extended Zeldovich mechanism delivered too high NO prediction value then the NO model was improved. The improved NO model was done by dividing a small new amount of burned gas into a new zone. Each zone was assumed to have the same temperature and pressure, and then NO calculation using extended Zeldovich mechanism was done separately for each zone. Lastly, the NO emission from each zone was mixed together on mass fraction basis.

The CO emission from two-zone thermodynamic model combustion product based on chemical equilibrium is known to be an insufficient CO predictor. To achieve good CO prediction, a kinetic CO model was introduced. The model was a homogeneous chemical model which used temperature and pressure profiles from two-zone model. Chemical equilibrium products were introduced as the initial reactants of CO kinetic model in order to avoid the complexity of combustion mechanisms. The chemical mechanisms and start point of CO kinetic model had been studied to keep the best result and low calculation time.

The CO prediction quality from the kinetic model was comparable to the results available in international literatures using complex models for constant engine speed and load conditions. However, they were not satisfactory for every operating point in the engine map which was the goal of this work. It was found that the model delivered good prediction in rich mixture area and poor prediction in stoichiometric and lean mixture area. To overcome this problem, the CO

model was improved by introducing a new CO model which additionally calculated CO emission from another source in cylinder, the quench layer. Quench layer characteristics were assumed to be the same as thermal boundary layer characteristics, then the boundary layer temperature and thickness had been calculated. The oxidation of fuel (gasoline) in the layer needed a new chemical mechanism. The reduced mechanism for isooctane oxidation at this temperature range and boundary condition had been chosen and used in the kinetic model. The improved CO model result reached satisfactory result for the complete engine map.

7.2 Conclusion

Important conclusions based on the results of the NO and CO model are as follows:

The improved NO model results over the engine operating map, and especially when spark advance changed were much better than simple NO model.

The improved CO model results over the engine operating map were very satisfactory, on the other hand, the CO results with lambda variation were matched with measured values but not for every engine load and speed.

Reasons of model error were mainly from the amount of internal EGR which was not exact, and cylinder to cylinder variations which were, for example, lambda and air flow rate variation.

Sensitivity analysis showed that lambda was the most sensitive parameter of NO and CO model. The air flow rate and the amount of EGR were sensitive parameters of NO and CO model because these parameters strongly affected the temperature calculation of two-zone thermodynamic model.

To improve the model results, cylinder to cylinder variations should be reduced or the lambda and air flow sensors should be individually installed; and the amount of EGR left should be exactly determined.

References

- [1] Zeldovich, Y., “The Oxidation of Nitrogen in Combustion Explosions”, Acta Physicochimica USSR, 1946, via Ferguson C.R. and Kirkpatrick, A.T., Internal Combustion Engines, Second Edition, John Wiley & Sons, 2001.
- [2] Lavoie, G.A., Heywood J.B. and Keck J.C., “Experimental and Theoretical Study of Nitric Oxide Formation in Internal Combustion Engines”, Combustion Science and Technology, vol. 1, pp. 313-326, 1970.
- [3] Heywood, J.B., “Pollutant Formation and Control in Spark-Ignition Engines”, Prog. Energy Combust. Sci., vol. 1, pp. 135-164, 1975.
- [4] Heywood, J.B., Internal Combustion Engine Fundamentals, McGraw-Hill, Singapore, 1988.
- [5] Raine, R.R., Stone, C.R. and Gould, J., “Modelling of Nitric Oxide Formation in Spark Ignition Engines with a Multizone Burned Gas”, Combustion and Flame, vol. 102, pp. 241-255, 1995.
- [6] Rublewski, M. and Heywood, J.B., “Modeling NO Formation in Spark Ignition Engines with a Layered Adiabatic Core and Combustion Inefficiency Routine”, SAE paper No. 2001-01-1011, 2001.
- [7] Miller, R., Davis, G., Lavoie, G., Newman, C. and Gardner, T., “A Super-Extended Zel'dovich Mechanism for NO_x Modeling and Engine Calibration”, SAE paper No. 980781, 1998.
- [8] Miller, R., Russ, S., Weaver, C., Kaiser, E., Newman, C., Davis, G. and Lavoie, G., “Comparison of Analytically and Experimentally Obtained Residual Fractions and NO_x Emissions in Spark-Ignited Engines”, SAE paper No. 982562, 1998.

-
- [9] Stone, C.R., Wyszynski, L.P. and Raine, R.R., "Prediction of NO Emissions from Stratified Charge Spark Ignition Engines, SAE paper No. 2002-01-1139, 2002.
- [10] Bowman, C.T., "Kinetics of Pollutant Formation and Destruction in Combustion", *Prog. Energy Combust. Science*, vol. 1, pp. 33-45, 1975.
- [11] Newhall, H.K., "Kinetics of engine-generated nitrogen oxides and carbon monoxide", *Proceedings of Twelfth International Symposium on Combustion*, pp. 603-613, 1968.
- [12] Arsie, I., Pianese, C. and Rizzo, G., "Models for the Prediction of Performance and Emissions in a Spark Ignition Engine A Sequentially Structured Approach", SAE Paper No. 980779, 1998.
- [13] Raggi, M.K. and Sodr , J.R., "Model for Kinetic Formation of CO Emissions in Internal Combustion Engines", SAE Paper No. 2003-01-3138, 2003.
- [14] D'Errico, G., Ferrari, G., Onorati, A. and Cerri, T., "Modeling the Pollutant Emissions from a S.I. Engine", SAE Paper No. 2002-01-0006, 2002.
- [15] D'Errico, G., Cerri, T. and Lucchini, C., "Development and Application of S.I. Combustion Models for Emissions Prediction", SAE Paper No. 2006-01-1108, 2006.
- [16] Tinaut, F.V., Melgar, A. and Horrillo, A.J., "Utilization of a Quasi-Dimensional Model for Predicting Pollutant Emissions in SI Engines", SAE Paper No. 1999-01-0223, 1999.
- [17] Wu, K.C. and Hochgreb, S., "Numerical Simulation of Post-Flame Oxidation of Hydrocarbons in Spark Ignition Engines", SAE Paper No. 970886, 1997.
- [18] Hamrin, D.A. and Heywood, J.B., "Modeling of Engine-Out Hydrocarbon Emissions for Prototype Production Engines", SAE Paper No. 950984, 1995.
- [19] Trinker, F.H., Cheng, J. and Davis, G.C., "A Feedgas HC Emissions Model for SI Engines Including Partial Burned Effects", SAE Paper No. 932702, 1993.

- [20] Mendillo, J.V. and Heywood, J.B., “Hydrocarbon Oxidation in the Exhaust Port of a Spark Ignition Engine”, SAE Paper No. 810019, 1981.
- [21] Drobot, K., Cheng, W.K., Trinker, F.H., Kaiser, E.W., Siegl, W.O., Cotton, F.C., and Underwood, J., “Hydrocarbon Oxidation in the Exhaust Port and Runner of a Spark Ignition Engine”, *Combustion and Flame*, vol. 99, pp. 422-430, 1994.
- [22] Wu, K.C. and Hochgreb, S., “Chemical Kinetic Simulation of Hydrocarbon Oxidation Through the Exhaust Port of a Spark Ignition Engine”, *Combustion and Flame*, vol. 107, pp. 383-400, 1996.
- [23] Onorati, A., Ferrari, G. and D’Errico, G., “1D Unsteady Flows with Chemical Reactions in the Exhaust Duct-System of S.I. Engines: Prediction and Experiment”, SAE Paper No. 2001-01-0939, 2001.
- [24] Ferguson, C.R., Internal Combustion Engines, John Wiley & Sons, 1986.
- [25] Roethlisberger, R.P., Favrat, D., Raine, R.R. and Kleemann, R., “Experimental Results and Modelling of Carbon Monoxide Emissions from a Natural Gas Fuelled Spark-Ignition Cogeneration Engine”, *Computational & Experimental Methods in Reciprocating Engines*, num. C587/029/2000, p. 127-140, IMechE (Institute of Mechanical Engineers), London, UK., 2000.
- [26] Cheng, W.K., Hamrin, D., Heywood, J.B., Hochgreb, S., Min, K. and Norris, M., “An Overview of Hydrocarbon Emissions Mechanisms in Spark-Ignition Engines”, SAE Paper No. 932708, 1993.
- [27] Zacharias, F., “Analytische Darstellung der thermodynamischen Eigenschaften von Verbrennungsmotoren”, Dissertation, TU Berlin, 1966.
- [28] Al-Himyary, T.J. and Karim, G.A., “A diagnostic two-zone combustion model for spark-ignition engines based on pressure-time data”, SAE Paper No. 880199, 1988.

- [29] Warnatz, J., Maas, U. and Dibble, R.W., Combustion, Physical and Chemical Fundamentals, Modeling and Simulation, Experiments, Pollution Formation, Springer, Berlin, 1996.
- [30] Olikara, C. and Borman G.L., “A Computer Program for Calculating Properties of Equilibrium Combustion Products with some Application to I.C. Engines”, SAE Paper No. 750468, 1975.
- [31] Turns, S.R., An introduction to Combustion, McGraw-Hill, 1996.
- [32] Warnatz, J., “Hydrocarbon oxidation high-temperature chemistry”, Pure Appl. Chem., Vol. 72, No. 11, pp. 2101–2110, 2000.
- [33] Westbrook, C. and Dryer, F., “Chemical Kinetic Modelling of Hydrocarbon Combustion”, Prog. Energy Combust. Sci., vol. 10, pp. 1-57, 1984.
- [34] Keck, J.C. and Gillespie, D., “Rate-Controlled Partial-Equilibrium Method for Treating Reacting Gas Mixtures”, Combustion and Flame, vol. 17, pp. 237-241, 1971.
- [35] Lapuerta, M., Hernández, J.J. and Armas, O., “Kinetic Modelling of Gaseous Emissions in a Diesel Engine”, SAE Paper No. 2000-01-2939, 2000.
- [36] CHEMKIN[®] User’s manual, release 4.0.2, Reaction Design, 2005.
- [37] Serauskas, B., <http://www.me.berkeley.edu/gri-mech/>, University of California, Berkeley, Gas Research Institute, 2006.
- [38] Lawrence Livermore National Laboratory (LLNL), California, USA, http://www-cmls.llnl.gov/?url_science_and_technology-chemistry-combustion-prf/, 2006.
- [39] Glassman, I., Combustion, Third Edition, Academic Press, San Diego, 1996.

- [40] Kim, T.J., Yetter, A. and Dryer, F.L., “New Results on Moist CO Oxidation: High Pressure, High Temperature Experiments and Comprehensive Modeling”, Proceedings of Twenty-Fifth International Symposium on Combustion, vol. 17, pp. 759-766, 1994.
- [41] Weberbauer, F., “Thermodynamische Analyse von Ottomotoren mit Benzindirekteinspritzung”, Dissertation, TU München, 2002.
- [42] D’Errico, G. and Luccihini, T., “A Combustio Model with Reduced Kinetic Schemes for S.I. Engines Fuelled with Compressed Natural Gas”, SAE Paper No. 2005-01-1123, 2005.
- [43] Ogink, R. and Golocitchev, V., “Gasoline HCCI Modeling: An Engine Cycle Simulation Code with a Multi-Zone Combustion Model”, SAE Paper No. 2002-01-1745, 2002.
- [44] Tamura, T. and Hochgreb, S., “Chemical Kinetic Modelling of the Oxidation of Unburned Hydrocarbons”, SAE Paper No. 922235, 1992.
- [45] Sher E., Handbook of air pollution from internal combustion engines: pollutant formation and control, Chapter 6: Combustion-related emissions in SI Engines: by Hochgreb S., Academic Press, San Diego, 1998.
- [46] Ferguson, C.R. and Kirkpatrick, A.T., Internal Combustion Engines, Second Edition, John Wiley & Sons, 2001.
- [47] Eiglmeier, C. “ Phänomenologische Modellbildung des gaseitigen Wandwärmeüberganges in Dieselmotoren”, Dissertation, Universität Hannover, 2000.
- [48] Merker, G.P. and Schwarz, C., Technische Verbrennung : Simulation verbrennungsmotorischer Prozesse, Stuttgart/Leipzig/Wiesbaden, B. G. Teubner, 2001.
- [49] Baehr, H.D. and Stephan, K., Wärme- und Stoffübertragung, 5. Aufl., Springer, Berlin Heidelberg New York, 2006.

- [50] Lyford-Pike, E.J. and Heywood, J.B., “Thermal Boundary Layer Thickness in the Cylinder of a Spark-Ignition Engine”, International Journal Heat Mass Transfer, Vol. 27, No. 10, pp. 1873–1878, 1984.
- [51] Merker, G.P., Konvektive Wärmeübertragung, Springer-Verlag, Heidelberg, 1987.
- [52] Hajireza, S., Sundén, B. and Mauss F., “A Three-Zone Model for Investigation of Gas Behavior in the Combustion Chamber of SI Engines in Relation to Knock”, SAE Paper No. 1999-01-0219, 1999.
- [53] Wu, K.C., Hochgreb, S. and Norris, M.G., “Chemical Kinetic Modelling of Exhaust Hydrocarbon Oxidation”, Combustion and Flame, vol. 100, issues 1-2, pp. 193-201, 1995.
- [54] Hasse, C., Bollig, M., Peters, N. and Dwer, H.A., “Quenching of Laminar Iso-Octane Flames at Cold Walls”, Combustion and Flame, vol. 122, issues 1-2, pp. 117-129, 2000.
- [55] Peters, N., “Abschlußbericht zum DFG Forschungsvorhaben”, Pe 241/9-2, RWTH-Aachen, 1994.
- [56] Peters, N., Pitsch, H. and Seshadri, K., “Numerical and Asymptotic Studies of the Structure of premixed iso-Octane Flames”, Proceedings of Twenty-Sixth International Symposium on Combustion, pp. 763-771, 1996.
- [57] Jenkin, R.J., James, E.H. and Malalasekera W., “Thermal Boundary Layer Modelling in ‘Motored’ Spark Ignition Engines”, SAE Paper No. 961965, 1996.
- [58] Ezekoye, O.A. and Greif R., “A Comparison of One and Two Dimensional Flame Quenching: Heat Transfer Results”, ASME National Heat Transfer Conference, Atlanta, Georgia, 1993.
- [59] Chindaprasert, N., Hassel, E., Nocke, J., Janssen, C., Schultalbers, M. and Magnor O., “Prediction of CO Emissions from a Gasoline Direct Injection Engine Using CHEMKIN[®]”, SAE Paper No. 2006-01-3240, 2006.

-
- [60] Flowers, D., Aceves, S., Frias, J.M., Hessel, R. and Dibble, R., “Effect of Mixing on Hydrocarbon and Carbon Monoxide Emissions Prediction for Isooctane HCCI Engine Combustion Using a Multi-zone Detailed Kinetic Solver”, SAE Paper No. 2003-01-1821, 2003.
- [61] Arsie, I., Pianese, C. and Rizzo, G., “Identification of Emission Models in a Spark Ignition Engine for Control Applications”, 5th IEEE Mediterranean Conference on Control Systems, Cyprus, 1997.

Appendix A

A1. Zacharias Parameter

Table A1: Constants for calculate internal energy from Zacharias

C_1^u	1.0330121	$\cdot 10^{-6}$
C_2^u	2.3048741	
C_3^u	3.0171634	$\cdot 10^{+3}$
C_4^u	1.6073400	$\cdot 10^{-3}$
C_5^u	5.5410000	$\cdot 10^{-9}$
C_6^u	1.5607340	$\cdot 10^{-6}$
C_7^u	2.3913710	
C_8^u	2.3710740	$\cdot 10^{+3}$
C_9^u	4.4000000	$\cdot 10^{-5}$
C_{10}^u	1.2404000	$\cdot 10^{-8}$

A2. Temperature Calculation Parameter

Table A2: Constants for calculate temperature

C_1^T	1.933	$\cdot 10^{+01}$
C_2^T	3.297	$\cdot 10^{-03}$
C_3^T	2.029	$\cdot 10^{-10}$
C_4^T	3.660	$\cdot 10^{-06}$
C_5^T	3.440	$\cdot 10^{-11}$
C_6^T	3.565	$\cdot 10^{-17}$
C_7^T	4.091	$\cdot 10^{+01}$
C_8^T	3.181	$\cdot 10^{-03}$
C_9^T	3.222	$\cdot 10^{-10}$
C_{10}^T	7.834	$\cdot 10^{-06}$
C_{11}^T	5.420	$\cdot 10^{-11}$
C_{12}^T	5.630	$\cdot 10^{-17}$

Erklärung

Ich erkläre,
die Arbeit

„Thermodynamic based prediction Model for NO_x and CO Emissions from a Gasoline
Direct Injection Engine“

selbstständig angefertigt und die benutzten Unterlagen vollständig angegeben zu haben.

Rostock, 12. August 2007

Curriculum Vitae

Personal data

Name: Nataporn Chindaprasert

Date of birth: 22.11.1977

Place of birth: Bangkok, Thailand

Education

1983-1989	Primary school, Bangkok, Thailand
1989-1995	Secondary school, Bangkok, Thailand
1995-1999	Studies in King Mongkut's University of Technology Thonburi, Bangkok, Thailand Bachelor of Engineering (Mechanical engineering), B.Eng
1999-2002	Studies in King Mongkut's University of Technology Thonburi, Bangkok, Thailand Master of Engineering (Mechanical engineering), M.Eng
2002	Studies Language in Goethe Institut, Bangkok, Thailand Zertifikat Deutsch
2003-2007	Doctoral student, research and graduate assistant at Lehrstuhl für Technische Thermodynamik Fakultät für Maschinenbau und Schiffstechnik Universität Rostock

List of Publications

- [1] Chindaprasert, N., Hassel E., Nocke, J., Janssen, C., Rabba, H. and Köller, M., “Two-Zone combustion model in S.I. engine using polytropic index”, ARGESIM Report No. 27, 2004.

- [2] Janssen C., Hassel, E., Nocke, J., Schulze, A., Chindaprasert, N., Schultalbers, M. and Gottschalk, W., “Modellierung und Simulation des ottomotorischen Verbrennungsprozesses mittels Ein- und Zweizonenmodell”, ARGESIM Report No. 27, 2004.

- [3] Chindaprasert, N., Hassel, E., Nocke, J., Janssen, C., Schultalbers, M. and Magnor O., “Prediction of CO Emissions from a Gasoline Direct Injection engine using CHEMKIN[®]”, ARGESIM Report No. 31, 2006.

- [4] Chindaprasert, N., Hassel, E., Nocke, J., Janssen, C., Schultalbers, M. and Magnor O., “Prediction of CO Emissions from a Gasoline Direct Injection Engine Using CHEMKIN[®]”, SAE Paper No. 2006-01-3240, 2006.

- [5] Chindaprasert, N., Hassel, E., Nocke, J., Janssen, C., Schultalbers, M. and Magnor O., “Combination of two-zone thermodynamic model and chemical kinetic model using CHEMKIN[®] to predict CO Emissions from a Gasoline Direct Injection engine”, Motorische Verbrennung: Aktuelle Probleme und moderne Lösungsansätze (VIII. Tagung), Haus der Technik, 2007.